

INFORMATION TO USERS

This manuscript has been reproduced from the microfilm master. UMI films the text directly from the original or copy submitted. Thus, some thesis and dissertation copies are in typewriter face, while others may be from any type of computer printer.

The quality of this reproduction is dependent upon the quality of the copy submitted. Broken or indistinct print, colored or poor quality illustrations and photographs, print bleedthrough, substandard margins, and improper alignment can adversely affect reproduction.

In the unlikely event that the author did not send UMI a complete manuscript and there are missing pages, these will be noted. Also, if unauthorized copyright material had to be removed, a note will indicate the deletion.

Oversize materials (e.g., maps, drawings, charts) are reproduced by sectioning the original, beginning at the upper left-hand corner and continuing from left to right in equal sections with small overlaps. Each original is also photographed in one exposure and is included in reduced form at the back of the book.

Photographs included in the original manuscript have been reproduced xerographically in this copy. Higher quality 6" x 9" black and white photographic prints are available for any photographs or illustrations appearing in this copy for an additional charge. Contact UMI directly to order.

UMI

A Bell & Howell Information Company
300 North Zeeb Road, Ann Arbor, MI 48106-1346 USA
313/761-4700 800/521-0600

INFERRING AQUIFER PROPERTIES USING
SEISMIC TRAVEL TIMES AND TRACER CONCENTRATIONS

A DISSERTATION
SUBMITTED TO THE DEPARTMENT OF
GEOLOGICAL AND ENVIRONMENTAL SCIENCES
AND THE COMMITTEE ON GRADUATE STUDIES
OF STANFORD UNIVERSITY
IN PARTIAL FULFILLMENT OF THE REQUIREMENTS
FOR THE DEGREE OF DOCTOR OF PHILOSOPHY

David William Hyndman
June 1995

UMI Number: 9535604

UMI Microform 9535604
Copyright 1995, by UMI Company. All rights reserved.


**This microform edition is protected against unauthorized
copying under Title 17, United States Code.**

UMI

**300 North Zeeb Road
Ann Arbor, MI 48103**

© Copyright by David William Hyndman 1995
All Rights Reserved

I certify that I have read this dissertation and that in my opinion it is fully adequate, in scope and quality, as a dissertation for the degree of Doctor of Philosophy.



Steven Gorelick (Principal Adviser)

I certify that I have read this dissertation and that in my opinion it is fully adequate, in scope and quality, as a dissertation for the degree of Doctor of Philosophy.




Jerry Harris

I certify that I have read this dissertation and that in my opinion it is fully adequate, in scope and quality, as a dissertation for the degree of Doctor of Philosophy.



Keith Loague

Approved for the University Committee on Graduate Studies: _____



*To
Ena*

ABSTRACT

The identification of aquifer heterogeneities, particularly flow paths and barriers, has become a critical research topic in hydrology. Traditional estimation methods that rely on sparsely sampled hydrologic data do not provide the needed spatial resolution of aquifer properties. Geophysical methods, such as cross-well seismic tomography, provide high resolution estimates but the relation between seismic parameters and hydrologic parameters is unknown. By combining seismic and tracer-test data, we obtain higher resolution estimates of aquifer properties than could be obtained from either data set alone.

This dissertation presents two approaches to integrate seismic, hydraulic, and tracer data for aquifer property estimates. The first approach estimates the geometry of large-scale lithologic zones, the effective hydraulic conductivities and seismic velocities for these zones, and the effective small-scale dispersivity. The second approach estimates the relation between seismic slowness and log conductivity, and in the process also develops likely three-dimensional hydraulic conductivity estimates. In addition, I present a new seismic estimation algorithm that co-inverts multiple cross-well seismic travel time surveys for the regional zonation of aquifer lithologies. I also test these methods with both synthetic and field data.

The heart of the zonal approach is the split inversion method (SIM), which extracts the geometry of lithologic zones from an estimated seismic velocity field. The zonation can be adjusted to best match multiple types of data, such as seismic travel times, tracer concentrations, and drawdowns. The SIM can also be used with seismic data alone, as I illustrate with the data from the Savannah River site. At this site the SIM maps the dominant clay zones identified in well cores, and images a high slowness zone a few meters above the water table.

For the Kesterson aquifer in the central valley of California, I developed the multiple population inversion (MPI) to co-invert travel times between six well pairs to identify the spatial distribution of a small number of slowness populations. I then use conditional simulation to provide three-dimensional slowness realizations. Next, I used the SIM to split several slowness realizations into three lithologic zones and assign hydraulic properties to the zones to best

match the measured drawdown and concentration histories for a multiple-well tracer test with an injection/withdrawal well pair.

The slowness realizations are also used in the approach that estimates the relation between slowness and log conductivity from field scale measurements. This relation is generally derived from laboratory measurements, but slowness values measured with very high frequencies in the lab are often poorly correlated to lower frequency cross-well and surface seismic slowness values. First, an a-priori relation is determined by correlating conductivity measurements from cores and pump tests to cross-well slowness estimates at the same locations. The slope and intercept of the slowness to log conductivity relation is then adjusted, and for each possible relation I map a slowness realization into a conductivity field. I then simulate groundwater flow and tracer transport through the potential three-dimensional conductivity fields and calculate the residuals between measured and simulated drawdown and concentration arrival time quantiles. The sum of squared residuals is minimized to find the optimal relation between slowness and log hydraulic conductivity. This approach provides valuable information about the relation between slowness and log conductivity, in addition to generating reasonable conductivity estimates.

The SIM and the estimated relation approach both provide conductivity fields that result in reasonable matches between simulated and observed drawdown during a tracer test and tracer concentration histories from two tracer tests, one of which was not used in the inversion. The match to the tracer histories is slightly better using the SIM relative to the approach that estimates the relation, which is expected since the SIM uses more parameters.

Although the current implementation of the algorithms uses only cross-well seismic travel times, tracer concentrations, and a drawdown measurement, the algorithms could incorporate other data types that are sensitive to changes in large-scale lithology. Other attributes of the measured seismic wavefield, such as amplitudes, could be used in a similar manner as the travel times to estimate additional geophysical properties that may correlate to hydraulic properties. The approaches in this dissertation could also be modified to use ground penetrating radar data, which may provide higher resolution estimates for some geological environments.

ACKNOWLEDGMENTS

I am greatly indebted to many people for their roles in this work. First and foremost, I thank Steve Gorelick for his advice and guidance throughout my time at Stanford, and for his careful review of this dissertation. He has taught me many things including how to be a successful research scientist, how to effectively present my research in both oral and written forms, and how to successfully write research grants. I especially appreciate the flexibility that he allowed me to explore this interdisciplinary research topic.

The input of my research committee has been invaluable for this work. Jerry Harris has served as my co-advisor from the Geophysics Department and his input has been critical to many aspects of this work. He has taught me a great deal about geophysics and has consistently challenged me to think about my research in new ways. Jerry Harris and Mark Van Schaack developed the seismic tomography codes which served as the basis for many of my algorithms. Keith Loague has graciously accepted the task of participating in my committee and reviewing this dissertation despite his hectic schedule.

I thank my fellow graduate students in both the Hydrogeology and Seismic Tomography groups for their insight, for their patience of my recent excess computer usage, and for making my experience at Stanford enjoyable.

I also thank Sally Benson, Ernie Majer, John Peterson, and Jill Geller of Lawrence Berkeley Laboratory for the Kesterson field data. Ernie Majer led me to the Kesterson data after a discussion of sites with both seismic and tracer data. I thank Greg Elbring for the cross-well seismic travel times and geologic cross-section from the Savannah River Site, and Carol Eddy-Dilec and Brian Looney for the hydraulic and tracer data from this site.

I am grateful for the financial support from National Science Foundation Grant EAR-9316040, and for the Hewlett Packard Company's grant of computer resources used for this project. Additional computer resources were provided by the Stanford Tomography Project.

Finally, I am most indebted to my family. My parents, Don and Shirley Hyndman, have served as role models in all aspects of their lives. I especially thank my loving wife Ena who has provided immeasurable support throughout my long hours at Stanford, making this work possible.

TABLE OF CONTENTS

Abstract.....	v
Acknowledgments	vii
Table of Contents.....	viii
List of Tables	xi
List of Figures	xii
Chapter 1: Introduction.....	1
Motivation	1
Background	2
Spatial Variability.....	2
Seismic Characterization of Subsurface Properties.....	3
Seismic Data for Hydraulic Property Estimation	4
Scope of the Dissertation.....	6
Chapter 2: Coupled Seismic and Tracer-test Inversion for Aquifer	
Property Characterization.....	8
Abstract.....	9
Introduction	10
Development of Synthetic Seismic and Tracer Data	12
Seismic Travel time Generation	20
Synthetic Concentration Data.....	21
Inversion Algorithm and Results.....	22
1) Cross-well Seismic Tomography	22
2) Split Inversion Method (SIM) with Seismic Data.....	25
3) Tracer-test Inversion.....	30
4) Split Inversion Method (SIM) with Tracer and Seismic	
Data	33
Discussion	38
Assumptions and Limitations	38
Conclusions	39

Chapter 3: Travel time inversion for the geometry of aquifer lithologies	41
Abstract	42
Introduction	43
The MPI Method	45
The Split Inversion Method (SIM): Comparison to MPI	51
Results for a Synthetic Aquifer.....	52
Results for the Kesterson Field Site	57
Discussion	65
Chapter 4: Mapping Lithologic and Transport Properties in Three Dimensions	
Using Seismic and Tracer Data: The Kesterson Aquifer	67
Abstract.....	68
Introduction	69
Hydrogeologic Setting.....	71
Seismic Inversion.....	75
Extension From Multiple 2D Images to 3D Using Conditional	
Geostatistics	78
Tracer Inversion.....	82
Results.....	87
Sensitivity Analysis.....	93
Summary and Conclusions.....	96
Chapter 5: Inferring the Relation Between Seismic Slowness and	
Hydraulic Conductivity in Heterogeneous Aquifers	98
Abstract.....	99
Introduction	100
Overview of the Kesterson site	102
Inversion Method	106
Kesterson Results	117
Independent tracer test comparison.....	120
Incorporation of hydraulic conductivity measurements.....	123
Sequential gaussian simulation of conductivity data alone	123
Co-simulation of conductivity and slowness data	125
Conclusions	126

References	128
Appendix A: Sensitivity of the split inversion method to sand/clay zonation.....	137
Appendix B: Savannah River Site — Seismic Inversion and Core Data	140
Overview of the Savannah River Site.....	140
Inversion Method and Results - Savannah River Case.....	143
Hydrogeologic Interpretation of Zonal Tomograms	147

LIST OF TABLES

2-1 Effective parameter estimates for synthetic aquifers.....	15
3-1 Comparison of zonal estimation methods for a synthetic data set.	56
4-1 Kesterson well locations and conductivity estimates.....	74
4-2 Kesterson aquifer parameter estimates using SIM	83
5-1 Slowness and conductivity measurements in a core near well ST5	109
5-2 Optimal parameter estimates for the tracer and drawdown data	116
5-3 Minimum squared concentration and drawdown residuals	118
5-4 Well locations and hydraulic conductivity values at Kesterson.....	121

LIST OF FIGURES

Chapter 2

2-1. Synthetic hydraulic and seismic cross-sections.....	13
2-2. Map of estimated lithologic zones.....	14
2-3. Scatter plot of seismic velocity vs. log hydraulic conductivity	18
2-4. Seismic and tracer forward simulations.	19
2-5. Flow chart of the split inversion method (SIM).	23
2-6. Estimated seismic velocity fields (tomograms) using SIM.	26
2-7. Histograms of seismic velocity in estimated tomograms.	29
2-8. "Measured" and simulated tracer concentration histories.....	31
2-9. Weighted mean square residuals for different aquifer zonations	35

Chapter 3

3-1. Flow chart of the multiple population inversion (MPI) algorithm.	48
3-2. Estimates from three algorithms for a synthetic	53
3-3. Travel time residuals for inversion of synthetic data sets.	55
3-4. Location map for the Kesterson site.....	58
3-5. Residuals from MPI and unconstrained tomography at Kesterson	59
3-6. 2D layout of estimated Kesterson tomograms.	61
3-7. Histograms of spatially distributed slowness perturbations.	62
3-8. 3D layout of estimated Kesterson tomograms.	64

Chapter 4

4-1. Site map for the Kesterson Aquifer.	73
4-2. Estimated Kesterson tomograms in three dimensions.....	77
4-3. Variograms fit to the tomographic slowness estimates.	79
4-4. 3D slowness realization conditioned to tomograms.	81
4-5. Concentrations for 3D simulations of solute transport.	88
4-6. Estimate of subsurface geology from SIM.	91
4-7. Measured and simulated tracer concentration histories.	92
4-8. Sensitivity of the objective value to slowness splits.	95

Chapter 5

5-1. Site map for the Kesterson aquifer	103
5-2. Relation between the slowness and log conductivity from SIM.....	105
5-3. Estimated Kesterson tomograms in three dimensions.	107
5-4. A-priori linear relation between slowness and log conductivity	110
5-5. Lab derived slowness verses log hydraulic conductivity values	111
5-6. Realizations with simulated and observed concentration histories	113
5-7. Simulated and observed concentration histories for the 1988 test	122
5-8. Estimates from conductivity data alone and all available data	124

Appendix A

A-1. Concentration histories for different sand/clay zonations 138
A-2. Tracer concentration residuals for different zonations 139

Appendix B

B-1. Savannah River Site (SRS) map 141
B-2. Estimated seismic tomograms for the SRS 144
B-3. Objective value surfaces using the SIM 146
B-4. Hydrogeologic interpretation of the estimated tomogram 148

CHAPTER 1: INTRODUCTION

MOTIVATION

The identification of aquifer heterogeneities has become a critical research area in hydrogeology as indicated by *Eagleson et al.* [1991]. This is of particular interest because groundwater flows preferentially along high hydraulic conductivity paths within the three-dimensional structure of an aquifer. Accurate estimation of heterogeneous aquifer properties is thus critical for prediction of solute transport. However, estimating the values of subsurface hydraulic properties and the geometry of lithologies is difficult because the environment is largely inaccessible and common measurements used to deduce subsurface architecture are sparse. Additional wells are expensive and disturb the system being measured.

Aquifer properties must be inferred using an understanding of geology and spatial statistics. These can be combined to estimate parameters using inverse methods. These methods have limited resolution because the interpolated region is large and the variability of aquifer properties is great. Furthermore, when multiple data sources are available, they are often analyzed separately and thus may not provide a coherent and unified image of aquifer architecture.

This dissertation presents a method to estimate aquifer properties and delineate the geometry of aquifer lithologies through the combined analysis of seismic travel times and tracer concentrations. The methods I present could also incorporate other types of information such as hydraulic heads, local values of hydraulic conductivity, lithologic logs, and cross-well seismic amplitudes. By jointly analyzing multiple data sources, each of which contains a particular type of information about aquifer properties, we should be able to more accurately estimate these properties. This dissertation also provides insight into the relation between seismic velocity and hydraulic conductivity.

BACKGROUND

Spatial Variability

Aquifer properties vary spatially due to the complex processes which create and alter geologic formations. Field studies have shown that this variability in aquifer properties has a tremendous influence on groundwater flow and solute transport. At the extensively studied Cape Cod, Massachusetts site the migration pattern of injected tracers was dramatically influenced by aquifer heterogeneity even though this aquifer is relatively homogeneous [Hess *et al.*, 1992; LeBlanc *et al.*, 1991]. At the Bordon, Ontario site, a solute plume appeared to split into two separate plumes as a result of heterogeneity in aquifer material [Freyberg *et al.*, 1987]. At the MAcro Dispersion Experiment (MADE) site in Mississippi, a tracer plume was "lost" because no sampling wells were placed in an unidentified channel deposit, which later studies proved to be the dominant zone of solute transport [Adams and Gelhar, 1992; Boggs *et al.*, 1992; Rehfeldt *et al.*, 1992]. Many other studies have shown that the large-scale structure of hydraulic conductivity controls the path of groundwater flow and solute transport, and the smaller scales control the rate of solute spreading or dispersion [Bakr *et al.*, 1978; Byers and Stephens, 1983; Dagan, 1986; Delhomme, 1979; Gelhar, 1986; Gelhar, 1992; Hoeksema and Kitanidis, 1985; Macmillian and Gutjar, 1986; Peck *et al.*, 1980; Pryor, 1973; Smith, 1981]. Therefore, the primary emphasis in this work is on the determination of large-scale hydraulic conductivity features with a secondary emphasis on smaller scale variability that controls dispersivities.

Different types of geophysical and hydrogeologic data can be combined to estimate aquifer properties. Each type of data gathered from the subsurface, such as seismic travel times and tracer concentrations, contains different information about the geometry of aquifer heterogeneities, the value of hydraulic properties over a particular volumetric scale, or the variability of hydraulic properties within a region. For example, lithologic logs provide point values, well test data provide at least local information around a well, tracer test data provide some averaged measure of the properties between a source and measurement locations, and cross-well seismic travel times provide densely sampled spatial information for a region between wells.

Analysis of each type of data by itself leads to a non-unique and highly uncertain map of aquifer properties, yet each type of measurement sampled the same physical environment. The volumetric scale measured by seismic and tracer data are different but overlapping, and thus provide information about spatial variability that could not be fully obtained using any single data set. By combining all the available data types in a unified analysis, aquifer properties can be determined with greater certainty.

Seismic Characterization of Subsurface Properties

Cross-well seismic tomography is a relatively new technique that shows great promise for estimating small-scale inter-well heterogeneities, thus I will focus on this technique. Cross-well seismic tomography is similar to the Computer Aided Tomography (CAT) scan developed for medical imaging [Dines and Lytle, 1979]. The measured data for travel time tomography are the times for seismic waves to travel from source to receiver locations. For a cross-well test, a seismic source generates sound waves at specified depth intervals in one well, while hydrophones or geophones measure the propagated wave field at multiple depths in nearby wells. The received wave field is analyzed for key events, such as the compressional- and shear-wave arrival times at each receiver [Telford *et al.*, 1990] or reflections [Lazaratos *et al.*, 1993]. In addition there are other geophysical methods that have been developed to characterize subsurface materials in regions where direct measurements are not available.

Cross-well travel time tomography is the inversion of measured travel times to provide a two-dimensional seismic velocity image between wells. This is accomplished by estimating both the path of seismic energy propagation and the seismic velocity at points in the plane between a source well and receiver well. The simultaneous iterative reconstruction technique, which is a robust seismic velocity estimation method [Dines and Lytle, 1979; Harris *et al.*, 1990; McMechan *et al.*, 1987], is used for the seismic inversion algorithms in this dissertation. This technique iteratively updates the seismic velocity field to minimize the total residual travel times. Iteration is necessary because the travel time equations are non-linear since both the slowness values and the ray paths, which depend on variability in slowness, are unknown. These ray paths are determined through the estimated velocity field from the previous iteration using a numerical approximation of Snell's law [Telford *et al.*, 1990].

SEISMIC DATA FOR HYDRAULIC PROPERTY ESTIMATION

Estimation of hydraulic properties using seismic and hydrologic data is a relatively new field, thus few techniques have been presented in the literature on this topic. *Copty* [1994] presented a few approaches to this problem including a stochastic method that combines surface seismic data and lithologic logs to identify subsurface lithologies. [*Araktingi and Bashore*, 1992] explored the effects of adding seismic information to well logs for petroleum reservoir characterization, in which they invert seismic reflection images to obtain synthetic seismic impedance (velocity * bulk density) logs between the wells. Sequential indicator simulation was then used to estimate porosity throughout a three-dimensional reservoir using the soft information provided by the synthetic logs and hard information provided by core measurements. Finally, porosity values were transformed into permeabilities using a lognormal porosity-permeability transform that provided a permeability map which is a rescaled version of the porosity map. A significant limitation of these methods is the large uncertainty in the transformation of porosity to permeability.

Several authors have presented geostatistical methods that estimate porosity or conductivity fields based on seismic and well log information. *Lucet and Mavko* [1990] estimated a two-dimensional porosity field between wells by cokriging a cross-well seismic velocity image with borehole measurements of porosity. The cross-correlation for this approach was determined from laboratory analysis of cores. *Journel and Zhu* [1990] and *Zhu and Journel* [1991] introduced the Markov-Bayes method which simplifies the cokriging algorithm by relating seismic velocity measurements to conductivity only in the same block. *Deutsch* [1991] discusses the use of simulated annealing with multiple data sets, including seismic information and measured hydraulic conductivity values, to generate realizations of conductivity that better capture the continuity of high and low values.

A few methods have also been presented that estimate hydraulic properties using seismic velocity estimates and hydraulic head data, as discussed by *Copty* [1994]. *Rubin et al.* [1992] presented a method that estimates a two-dimensional hypothetical hydraulic conductivity field (horizontal plane) given head and conductivity measurements at several wells, and perfect knowledge of the seismic velocity field. This method was then extended by *Copty et al.* [1993]

to estimate the spatial distribution of permeability given a seismic velocity field with spatially uncorrelated errors. The relation between seismic velocity and hydraulic conductivity was assumed to be perfectly described by the relation given by *Marion et al.* [1992]. These studies indicate that incorporating seismic information can lead to improved conductivity estimates.

One significant difficulty with the implementation of any of these methods has been the generally poorly understood relation between seismic velocity and hydraulic conductivity. This relation is usually derived by laboratory analysis of core samples, which are often disturbed and may not reflect the properties of field-scale heterogeneous formations. Several ideas about this relation have been presented in the literature. The relation is likely to be nonlinear, and in some cases non-unique [*Han et al.*, 1986; *Marion*, 1990; *Marion et al.*, 1992]. However, seismic data can still provide a significant amount of information because the spatial density is great [*Journal et al.*, 1992; *Journal and Zhu*, 1990; *Zhu and Journal*, 1991].

SCOPE OF THE DISSERTATION

This dissertation presents two approaches to integrate seismic, hydraulic, and tracer data for aquifer property estimates. The first approach estimates the geometry of large-scale lithologic zones, the effective hydraulic conductivities and seismic velocities for these zones, and the effective small-scale dispersivity. The second approach estimates the relation between seismic slowness and log conductivity, and in the process develops likely hydraulic conductivity realizations. In addition, I present a new seismic estimation algorithm that co-inverts multiple cross-well seismic travel time surveys for the regional zonation of aquifer lithologies. I also test these methods with both synthetic and field data. The developed algorithms attempt to determine the most representative set of aquifer parameters using the available data since there is only a single underlying geologic reality.

This dissertation is subdivided as a series of four papers that discuss development of the new inversion algorithms, testing of these algorithms with synthetic data sets, application of these algorithms to field sites, and inference of the relation between seismic and hydraulic parameters. These papers are arranged in chronological order, and the later papers build upon the developments in earlier papers. Although these papers are co-authored with Steve Gorelick and Jerry Harris, I am the primary author and contributor.

Chapter 2 presents the theoretical development of the split inversion method (SIM) and the testing of the SIM for two synthetic data sets. The SIM co-inverts seismic travel times and tracer concentrations for the zonation of aquifer lithologies, the value of hydraulic conductivity for each zone, and a value of dispersivity for the estimated region. I demonstrate the approach for two synthetic sandy aquifers, one with interbedded clay lenses and another with interbedded silt and gravel lenses. These examples differ in the uniqueness of the relationship between seismic velocity and hydraulic conductivity. For these examples, the SIM successfully maps inter-well heterogeneities and accurately estimates hydraulic and seismic parameters.

Chapter 3 introduces the multiple population inversion (MPI) to co-invert travel times between multiple well pairs for the spatial distribution of a small number of seismic slowness ($1/Seismic\ Velocity$) populations. By constraining

the number of slowness values, this method is less susceptible than the SIM to inversion artifacts and can resolve finer scale sedimentary structures than unconstrained tomographic methods that smooth the slowness field. The MPI is compared to the SIM with seismic data alone using the synthetic aquifer from Chapter 2. The MPI is then demonstrated in three dimensions with data from the Kesterson aquifer in the central valley of California. In both of these cases, the MPI converged to an equal or smaller average travel time residual than obtained with an unconstrained tomographic inversion.

Chapter 4 extends the SIM to three dimensions and applies it to the Kesterson site to estimate the zonation of aquifer properties along with the hydraulic properties for these zones. I use conditional simulation to provide three-dimensional slowness realizations, conditioned to the tomograms from Chapter 3. The SIM is then used to split several realizations into three lithologic zones and assign hydraulic properties to the zones. Assignment is based on the best match to six concentration histories for a multiple-well tracer test involving an injection/withdrawal well pair.

Finally, Chapter 5 describes an approach to combine field scale seismic and hydrologic data to derive the relation for a particular depositional environment. This approach does not rely on the scale independence assumption that is required to use lab derived relations at the field scale. I demonstrate this method using the Kesterson field data. At this site, I demonstrate the combined use of seismic tomography, core measurements, pump tests, and a multiple-well tracer test to infer the relation between hydraulic conductivity and seismic slowness, and provide three-dimensional estimates of hydraulic conductivity. In addition, I estimate the relation between seismic slowness and log hydraulic conductivity using field scale measurements.

CHAPTER 2:

COUPLED SEISMIC AND TRACER-TEST INVERSION FOR AQUIFER PROPERTY CHARACTERIZATION

ABSTRACT

Seismic and tracer-test data can be combined to estimate the spatial patterns of aquifer properties. We present an algorithm that estimates the geometry of large-scale lithologic zones, the effective hydraulic conductivities and seismic velocities for these zones, and the effective small-scale dispersivity. The heart of this algorithm is our Split Inversion Method (SIM) which extracts the geometry of lithologic zones from an estimated seismic velocity field. This method determines the zonation that best matches multiple types of data, such as seismic travel times and tracer concentrations. Although the current implementation of the algorithm uses only cross-well seismic travel times and tracer concentrations, the algorithm could incorporate other data types that are sensitive to changes in large-scale lithology. We demonstrate the approach for two synthetic sandy aquifers, one with interbedded clay lenses and another with interbedded silt and gravel lenses. These examples differ in the uniqueness of the relationship between seismic velocities and hydraulic conductivities. For these examples, our algorithm successfully maps inter-well heterogeneities and accurately estimates hydraulic and seismic parameters.

INTRODUCTION

Groundwater flow, and thus advective transport, is often predominantly controlled by large-scale heterogeneity in hydraulic conductivity. Reliable solute transport predictions depend on accurate estimates of such spatially variable aquifer properties. The values of hydraulic properties are commonly developed using geostatistical interpolation between a limited number of direct estimates at wells. Unfortunately, such methods often result in smoothed maps of parameter estimates that do not reflect the dominant lithologic structures.

Geophysical methods provide alternatives to expensive drilling programs for aquifer characterization. For example, cross-well seismic tomography provides densely sampled spatial information that complements the spatially averaged information obtained from traditional groundwater methods such as pump tests and tracer tests. However, to estimate the hydraulic conductivity field using seismic information alone, the highly uncertain relationship between seismic and hydraulic properties must also be known. We will demonstrate a method of combining geophysical and hydrogeologic data to accurately characterize aquifer properties.

A limited amount of work has focused on combining seismic and hydraulic data to estimate aquifer properties. *Rubin et al.* [1992] presented the first method to estimate a two-dimensional hypothetical hydraulic conductivity field by combining head and conductivity measurements at several wells, and perfect knowledge of the seismic velocity field. *Coptly et al.* [1993] extended this method and analyzed the effect of uniformly distributed, spatially uncorrelated, random errors added to the seismic velocity values. These authors indicate that incorporating seismic information can lead to improved hydraulic conductivity estimates, even in the presence of significant errors in an estimated seismic velocity field. The methods of *Rubin et al.* [1992] and *Coptly et al.* [1993] rely on accurate knowledge of the relationship between seismic velocity and hydraulic conductivity. This relationship is complex and may be described, under certain circumstances, by empirical approximations [*Han et al.*, 1986; *Marion et al.*, 1992].

We have developed a new parameter estimation algorithm that combines cross-well seismic travel times and solute tracer concentrations to estimate the location and shape of large-scale lithologic zones, the effective hydraulic conductivity and seismic velocity of each zone, and the effective small-scale

dispersivity. Cross-well seismic tomography uses travel times to estimate the two-dimensional seismic velocity field between wells [McMechan *et al.*, 1987; Harris, 1990]. The heart of the algorithm developed for our work is the Split Inversion Method (SIM). It extracts the geometry of lithologic zones from the estimated velocity field for use in seismic and tracer simulations. Aquifer property values within these zones are estimated by minimizing the sum of squared residuals between the measured and simulated tracer concentration histories [Wagner and Gorelick, 1987; Sun and Yeh, 1990]. The algorithm iteratively updates the lithologic zonation and the values of seismic and hydraulic parameters. Updated zonation is based on feedback from seismic and tracer-test simulations.

The primary assumption in this implementation of SIM is that large contrasts in lithology should be manifested as changes in seismic velocity. The SIM is used to extract this information about lithologic zonation. A specified relationship between seismic velocity and hydraulic conductivity is not required. This unknown relationship can be highly nonlinear, and multiple hydraulic conductivities can exist at different spatial locations that have the same seismic velocity.

Our approach is the first that we know of that estimates the geometry of lithologic zones and effective hydraulic and seismic parameters based only on cross-well seismic and tracer-test data. No direct "measurements" of hydraulic conductivity, seismic velocity, or lithologic zonation are used in the method; however, the method would produce more accurate results if such "measurements" were available. In addition, the method incorporates feedback between solute transport simulations and the lithologic zonation, thus allowing the solute data to influence the estimates of lithologic zonation. Combining two sets of independent measurements in the estimation algorithm improves estimates of lithologic zonation.

DEVELOPMENT OF SYNTHETIC SEISMIC AND TRACER DATA

We illustrate the method with a hypothetical, yet realistic, lithologic cross-section based on a fluviodeltaic reservoir in the San Joaquin Valley, California [Miller *et al.*, 1990]. This vertical cross-section represents an inter-well region of a sandy aquifer containing interbedded lenses of clay, silt, and gravel (Figure 2-1). This lithologic geometry could develop in a meandering stream environment or in regions that have experienced marine transgression and regression [Miall, 1984]. For example, Holocene deposits in the San Francisco Bay area are largely interbedded sands and clays that may fit this conceptual model [Koltermann and Gorelick, 1992]. We also designed the shapes of zones to test the algorithm's ability to determine different degrees of stratigraphic continuity between wells.

We created two example geologic images by placing a grid over the large-scale lithologic structure, and assigning lithologies to each grid cell. For example 1 (Figure 2-1a) the lithologies are sand and clay, while for example 2 (Figure 2-1b), the lithologies are sand, gravel, and silt. We then assigned the mean seismic and hydraulic properties in Table 2-1 to the lithologic zones shown in Figure 2-2, based on published parameter ranges for saturated sediments [McLamore *et al.*, 1978; Freeze and Cherry, 1979; Bourbie *et al.*, 1987; Lankston, 1990].

To better represent the range of heterogeneity that occurs in geologic media, we added a field of spatially correlated deviates to each mean parameter field. We generated each field of deviates by multiplying the Cholesky decomposition of a three parameter (mean, variance, and correlation length) exponential covariance matrix by a vector of standard normal deviates [Clifton and Neuman, 1982; Alabert, 1987; Johnson, 1987]. This operation produces random fields with specified correlation statistics that can then be added to the natural log of the mean zonal values from Table 2-1.

Synthetic Hydraulic Cross-Sections

Synthetic Seismic Cross-Section

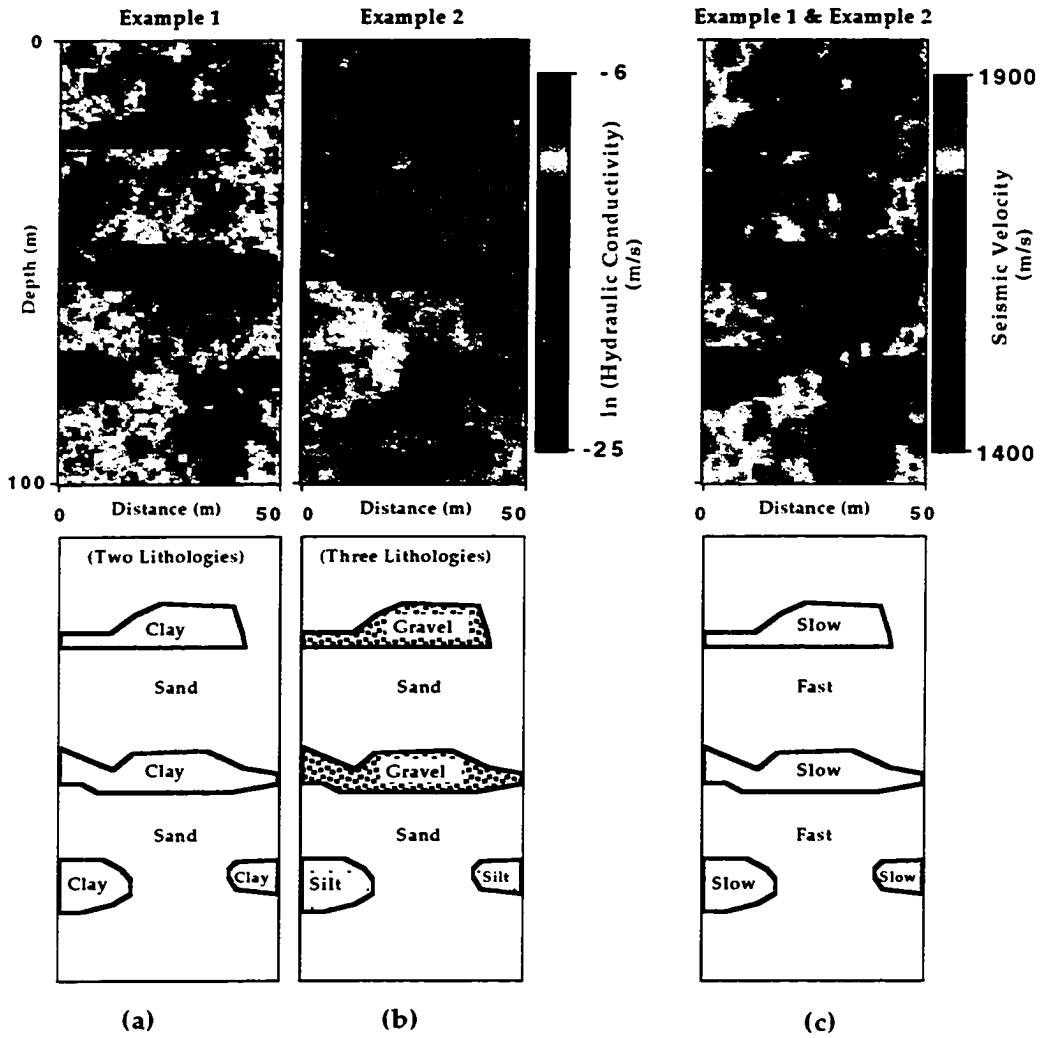


Fig. 2-1. Synthetic hydraulic conductivity and seismic velocity fields used to create synthetic tracer concentrations and seismic traveltimes for examples 1 & 2. In example 1 seismic velocity is highly correlated to hydraulic conductivity. In example 2 seismic velocity and hydraulic conductivity are poorly correlated (See Figure 2-2). Example 2 illustrates the case in which multiple hydraulic conductivities correspond to a single seismic velocity.

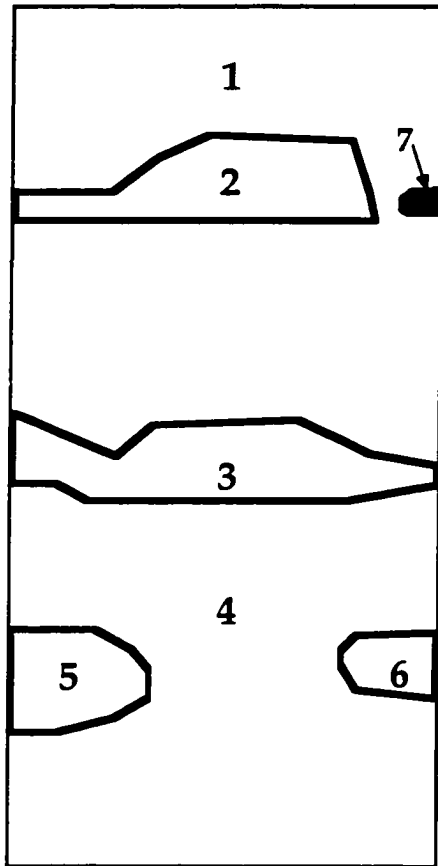


Fig. 2-2. Map of estimated lithologic zones. Zones 1 through 6 are found in the synthetic cross sections of Figure 2-1. Zone 7 is erroneously estimated during the implementation of SIM with seismic data alone. The numbers in this figure correspond to those listed in Table 2-1.

Table 2-1. Effective parameter estimates.

Example 1

Zone*	Parameter†	Mean* Synthetic Value	Effective parameter estimates for zones developed with	
			(Seismic)	(Seismic & Tracer)
1 & 4 2,3,5&6	ln(K) {m/s}	-9.21	-9.37	-9.36
		-20.72	-11.68	-11.29
all	α_ℓ {m}	1.0	2.65	2.58
1 & 4 2,3,5&6	V {m/s}	1830.	1805.	1817.
		1520.	1571.	1520.

Example 2

Zone*	Parameter†	Mean* Synthetic Value	Effective parameter estimates for zones developed with	
			(Seismic)	(Seismic & Tracer)
1	ln(K) {m/s}	-8.52	-9.06	-8.96
2		-6.91	-7.34	-7.45
3		-6.91	-7.15	-7.10
4		-9.21	-9.60	-9.28
5		-11.51	-6.29	-9.48
6		-11.51	-10.73	-9.53
7		¥	-9.44	¥
all	α_ℓ {m}	1.0	2.25	2.25
1 & 4 2,3,5&6	V {m/s}	1830.	1805.	1817.
		1520.	1571.	1520.

* Zone numbers correspond to those illustrated in Figure 2-2.

† α_ℓ is dispersivity, K is hydraulic conductivity, and V is seismic velocity

* The mean synthetic values are used to represent the homogeneous zones before spatially correlated variability was added. However, the effective parameter estimates (shown in the next two columns) better represent the travel time and concentration data than do the mean synthetic values. The effective porosity was fixed at 0.25 and the transverse dispersivity was fixed at half the value of the longitudinal dispersivity.

¥ Zone 7 not estimated using SIM with seismic and tracer data. This zone is not in the "true" image, thus the synthetic value would be similar to that of Zone 1.

Both examples use the same seismic velocity field. The synthetic seismic velocity field (Figure 2-1c) was developed by adding a field of deviates (mean = 0.0, variance = 3.0 E-4, correlation length = 5.0 meters) to the mean natural log seismic velocity values and smoothing the resulting field. We used a log normal model of the small-scale variability in seismic velocity. Although a log normal model is reasonable, it has not been fully resolved in the geophysics literature. The seismic velocity field is smoothed for accurate simulation of travel times.

The two examples have different hydraulic conductivity fields, in terms of both the mean parameter values and the uniqueness of the relationship between hydraulic conductivity deviates and seismic velocity deviates. Example 1 presents the case in which the seismic velocity and hydraulic conductivity fields have closely correlated mean values and deviates. The hydraulic conductivity field for example 1 was generated by adding a scaled field of the seismic deviates (mean = 0.0, variance = 1.15, correlation length = 5.0 meters) to the mean natural-log hydraulic conductivity values (Figure 2-1a). This assumes that for each lithologic type, hydraulic conductivity can be represented as a second-order stationary log-normally distributed random variable [Freeze, 1975; Hoeksema and Kitanidis, 1985]. The range of hydraulic conductivity in porous media is several orders of magnitude larger than the range in seismic velocity, therefore the variance of the hydraulic conductivity deviates were scaled up according to equation (2.1). For this example, the scaling of the variance is equivalent to scaling each log seismic velocity deviate by the square root of the scaling term in (2.1).

$$\sigma_{\ln(K) \text{ deviates}}^2 = \sigma_{\ln(V) \text{ deviates}}^2 \left(\frac{\ln \bar{K}_{\max} - \ln \bar{K}_{\min}}{\ln \bar{V}_{\max} - \ln \bar{V}_{\min}} \right)^2 \quad (2.1)$$

where

- \bar{K}_{\max} mean hydraulic conductivity of the sand zones for example 1
or the gravel zones for example 2, {m/s};
- \bar{K}_{\min} mean hydraulic conductivity of the clay zones for example 1
or the least conductive silt zone for example 2, {m/s};
- \bar{V}_{\max} mean seismic velocity of sand zones for examples 1 and 2 {m/s};
- \bar{V}_{\min} mean seismic velocity of the clay zones for example 1
or the silt and gravel zones for example 2, {m/s};

Example 2 presents the case of poorly correlated mean values and deviates (Figure 2-3). In terms of mean values, gravel and silt have low seismic velocities while their hydraulic conductivities differ by two orders of magnitude. In terms of the deviates, we add a different field of deviates to the hydraulic conductivity field than we add to the seismic velocity field. In fact, we add two different deviate fields with the same statistics (mean = 0.0, variance = 0.25, correlation length = 5.0 meters) to the conductivity field, one for the sand zones and another for the interbedded silt and gravel zones (Figure 2-1b). This accounts for the expected shift in depositional environment across the boundaries of lithologic zones. We used (2.1) to determine the variance for these fields of conductivity deviates.

Two synthetic data sets, seismic travel times and tracer concentrations, were developed for each example by simulating the physics of sound wave propagation and solute transport through these parameter fields (Figure 2-4). We assume our synthetic values represent measurements from field tests conducted with limited resources. Field methods can be designed to gather more information about subsurface heterogeneity than provided by the simulated tests in this study, but such methods are more expensive to use.

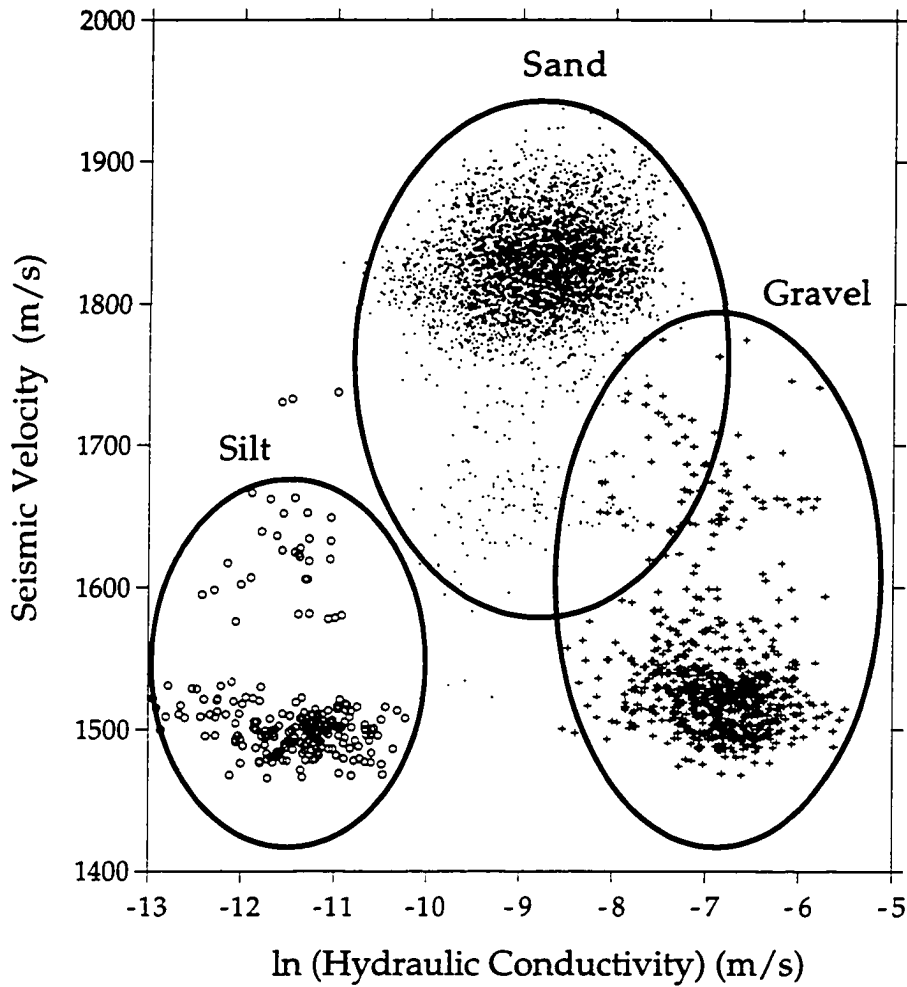


Fig. 2-3. Scatterplot of seismic velocity versus natural log hydraulic conductivity for each grid cell of the synthetic parameter fields used in example 2 (See Figures 2-1b and 2-1c). The points are delineated by lithologic type to illustrate that the correlation between seismic velocity and log hydraulic conductivity is small for each lithologic type.

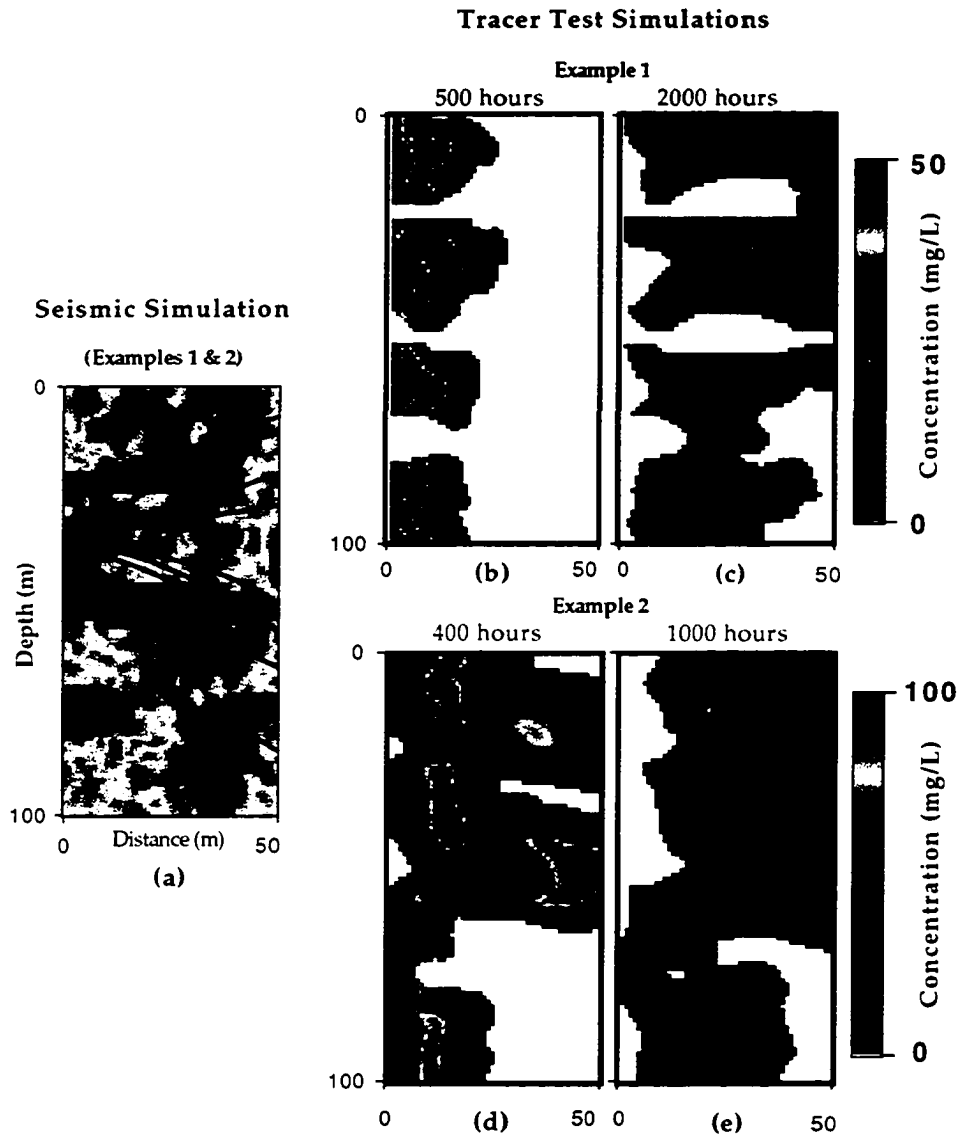


Fig. 2-4. Seismic and tracer simulations used to develop synthetic data sets. (a) Seismic rays are traced through the synthetic velocity image to obtain traveltimes "data". A few rays are illustrated. Advection and dispersion of a conservative tracer is simulated for a natural gradient test to obtain synthetic concentrations. In example 1 (b) & (c), the interbedded clay zones are barriers to flow and transport. In example 2 (d) & (e), all the zones permit tracer transport.

Seismic Travel time Generation

In field studies, the most commonly used data for seismic velocity inversions are the times for seismic waves to travel between source and receiver locations. For a cross-well test, a seismic source is activated by generating sound waves at specified depth intervals in one well, while hydrophones or geophones measure the propagated wave field at multiple depths in nearby wells. The received wave field is analyzed for key events, such as compressional wave arrival times at each receiver [Telford *et al.*, 1990]. Although not used here, other key wave field events include shear wave arrival times and reflection arrival times from lithologic interfaces.

Compressional wave travel times are simulated from source positions to receiver positions along discrete paths through the seismic velocity field. These discrete paths, or rays, bend in heterogeneous media because seismic energy is refracted as described by Snell's Law [Telford *et al.*, 1990].

The synthetic seismic travel times were generated to represent measured field data. To avoid using the same algorithm to generate the synthetic travel times as was used in the inversion, travel times were computed using two algorithms: one to simulate the times through constant velocity zones, and the other to simulate the effect of small scale variability on travel times. We used the accurate ray tracing algorithm of Cerveny [1985], modified for the cross-well geometry, to simulate travel times for large-scale constant velocity zones. These zones were separated by sharp boundaries and assigned the mean velocity values listed in Table 2-1. We then used the initial-value ray tracing algorithm of Harris [1992] to simulate travel times through these constant velocity zones, and through zones with added correlated variability (Figure 2-1c). The difference between these two sets of travel times simulated with the algorithm of Harris [1992], was added to the travel times simulated with the algorithm of Cerveny [1985] to make up our synthetic travel times. Figure 2-4a illustrates a subset of the simulated ray paths from one source through the seismic velocity field with correlated variability.

Synthetic Concentration Data

Along with seismic travel time data, our method requires solute concentration data. For our demonstration of the approach, we synthesized solute breakthrough data. These data were simulated for a natural hydraulic gradient (1%) tracer test from a slug input of solute into well on the left through the synthetic aquifers shown in Figures 1a and 1b. The simulated concentrations at the down-gradient well on the right were vertically flux averaged [*Parker and Van Genuchten, 1984*] assuming the well was fully screened and that multi-port sampling was not available. The flux averaged concentration was calculated as the sum of each well-grid-cell concentration times the specific discharge into each of these cells, divided by the total specific discharge into the well.

Measured concentration histories contain information about the nature of aquifer heterogeneity. The variability of hydraulic conductivity and the small-scale dispersivity are responsible for the solute spreading through time. Figures 2-4b and 2-4c illustrate advection and dispersion of the tracer plume through the hydraulic conductivity field of example 1 during its migration from the source well to the down-gradient well on the right. The low solute concentrations in the clay zones of example 1 verify that these zones represent effective barriers to flow. Figures 2-4d and 2-4e illustrate advection and dispersion of the tracer plume through the hydraulic conductivity field of example 2. Although these images illustrate the nature of solute transport in these types of aquifers, such spatial information between the wells was assumed to be unavailable and therefore was not used in the inversion.

INVERSION ALGORITHM AND RESULTS

The inversion algorithm we have developed (Figure 2-5) is implemented in four distinct stages. Given cross-well seismic travel time data and solute breakthrough data, these stages are:

- 1) Cross-well seismic tomography is used to estimate a two-dimensional image of seismic velocity between two wells, called a tomogram. This estimate is made up of a large number of rectangular pixels.
- 2) Our Split Inversion Method (SIM) is implemented with seismic travel times alone to extract an initial estimate of lithologic zonation from the tomogram in stage 1.
- 3) A tracer-test inversion is conducted to estimate the effective hydraulic conductivity of each zone found in stage 2 and the effective small-scale dispersivity.
- 4) The SIM is implemented with seismic and tracer data to update the estimate of lithologic zonation from stage 2. Updated hydraulic parameters are then estimated for this new zonation. This stage can be repeated until stable lithologic zones and hydraulic parameter estimates are obtained.

We now discuss each stage of the inversion algorithm and results for the two synthetic examples.

1) Cross-well Seismic Tomography

Cross-well seismic tomography is similar to the Computer Aided Tomography (CAT) scan developed for medical imaging [Dines and Lytle, 1979]. Compressional-wave travel times for each source-receiver pair are used in a tomographic seismic inversion to estimate the seismic velocity field between two wells. The seismic velocity in each pixel of a grid is obtained by iteratively tracing rays through a velocity field and projecting portions of the difference between simulated and observed (residual) travel times along these estimated ray paths [Harris, 1990]. This iterative nonlinear inversion has two sets of unknowns, the seismic slowness (inverse of seismic velocity) in every pixel and the ray paths connecting each source and receiver. The equation solved in this inversion involves integration of the seismic slowness along a ray path to determine a seismic travel time (2.2).

Parameter Estimation Algorithm

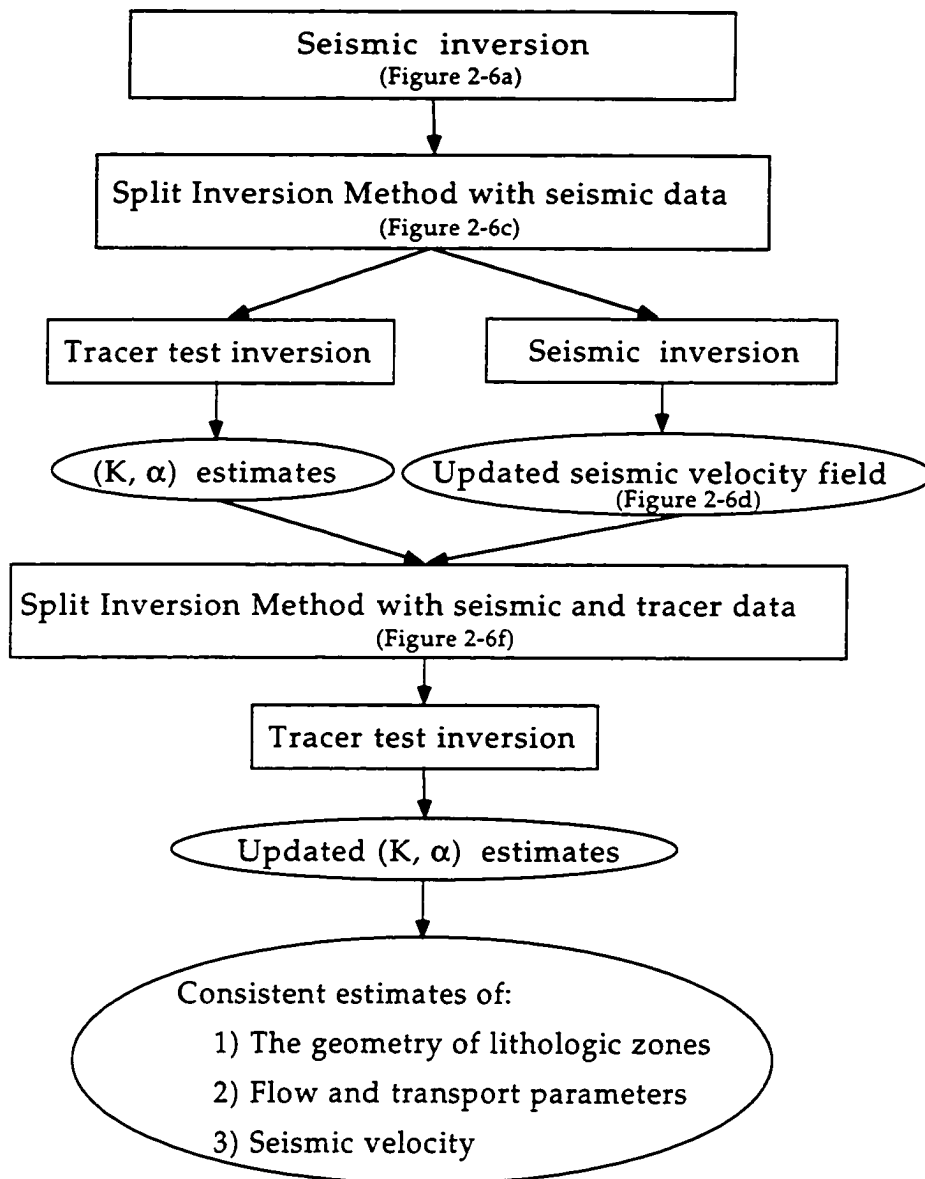


Fig. 2-5. Flow chart of the parameter estimation algorithm. If the estimated lithologic boundaries are not consistent, the routine iteratively updates the boundaries and the parameter estimates. The figure numbers correspond to tomograms at various stages of the algorithm.

$$t_i = \int_{\text{Ray Path}} S(x,z) d\ell \quad i = 1, \dots, N \text{ rays} \quad (2.2)$$

where

- t_i travel time between source and receiver for ray i , {T};
- $S(x,z) = 1./V(x,z)$, two-dimensional seismic slowness field, {T/L};
- $V(x,z)$ seismic velocity field, {L/T};
- $d\ell$ increment of path length along a ray, {L}.

To linearize (2.2), we write the slowness as the sum of a known background field (S_0) plus a small perturbation (δS) (i.e., $S = S_0 + \delta S$). We replace the unknown ray path in (2.2) with the ray path found for the background field (S_0). Thus, (2.2) reduces to a linear equation that relates the vector of travel time perturbations (δt) to the vector of slowness perturbations (δS):

$$\delta t = W \delta S \quad (2.3)$$

The elements of the projection matrix (W) are the ray path length in each pixel. We then invert (2.3) to find δS , which is then added to S_0 to form a new slowness field. This new slowness field is then used as a background and the inversion process is repeated until the slowness perturbations are small.

The projection matrix is sparse because each ray intersects only a small fraction of the grid cells. The system of equations (2.3) is large and cannot be easily inverted in closed form. The projection matrix is thus inverted using the Simultaneous Iterative Reconstruction Technique (SIRT) [McMechan *et al.*, 1987]. This technique determines the slowness residuals through the simultaneous superposition of the travel time perturbations from multiple rays. Other inversion algorithms, such as conjugate gradients, can also be used to invert the projection matrix.

Tomographic travel time inversion using SIRT is a robust seismic velocity estimation technique [Dines and Lytle, 1979; McMechan *et al.*, 1987; Harris, 1990]. Because SIRT is iterative, an initial estimate of the velocity field is needed to determine the initial ray paths. For our examples, the constant seismic velocity field that best fits the travel time data for straight ray paths was used. In a field test, seismic velocity logs taken in the source and receiver wells could be used to

provide a better estimate of this initial field. In the seismic inversion, rays are traced from each source, through this estimated velocity field, to each receiver. Only part of the residual between the simulated and measured travel time for each ray is then distributed along the estimated ray path in a process called back projection. Because the ray paths are unknown, back projection of the entire residual along these estimated paths would result in significant errors in the seismic velocity estimates. The small perturbation approximation is thus retained by damping the velocity changes from individual back projections. This procedure of tracing rays and back projecting residuals to form a new estimated velocity field continues until the travel time residuals are small. The result is convergence toward a relatively smooth velocity image, called a tomogram, which in our case (Figure 2-6a) exhibits the large-scale structure of the synthetic aquifer (Figure 2-6g).

2) Split Inversion Method (SIM) with Seismic Data

We have developed the Split Inversion Method (SIM) method to help determine large-scale lithologic geometry from tomographic images. The concept is to divide spatial parameter fields (i.e., seismic slowness) into a small number of lithologic zones and estimate parameters for these zones. The estimated zonal pattern is chosen to minimize a weighted sum of residuals between measured and simulated data sets, such as seismic travel times and tracer concentrations. Other available data, such as solute concentrations, seismic amplitudes, hydraulic potentials, and electrical resistance, could be used in this inversion framework as long as the underlying physical processes can be simulated and the data are sensitive to lithologic geometry.

Although this method can incorporate many different types of information, each data type needs to be weighted to provide approximately equal influence in the determination of lithologic zonation. Weighting allows for incorporation of data sets with greatly different magnitudes and units. We will discuss our determination of weights in Section 4 (Split Inversion Method (SIM) with Seismic and Tracer Data).

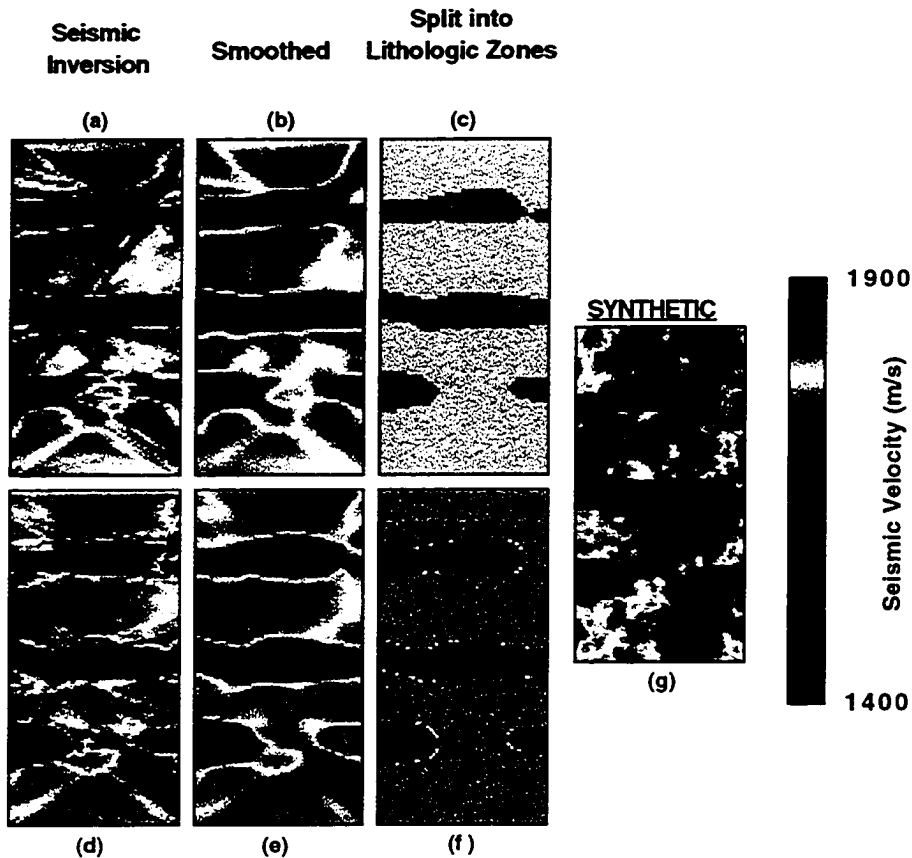


Fig. 2-6. Estimated seismic velocity fields (tomograms) for stages of the parameter estimation algorithm. These stages are: (a) Preliminary seismic inversion with constant velocity starting image, (b) Hanning smooth of (a), (c) Split Inversion Method (SIM) with seismic data alone, (d) Seismic inversion with (c) as starting estimate, (e) Hanning smooth of (d), (f) SIM with tracer and seismic data for Example 2. These tomograms can be compared with the synthetic seismic velocity field (g). The first 5 images (a – e) are the same for both examples because the tracer information does not effect the geometry until the final zonation (f). The final zonation for Example 1 is not shown because it is nearly identical to that presented for Example 2 (f), with the exception that the embedded zones are slightly smaller.

Our aim here is to demonstrate the combined use of cross-well seismic travel times and tracer-test concentrations to identify the geometry of the dominant large-scale lithologic zones and to estimate hydraulic and seismic parameters for these zones. This application of SIM is limited to the estimation of two populations of seismic velocity, although each spatial zone can have a different estimated value of hydraulic conductivity. As presented by *Marion et al.* [1992] there can be multiple hydraulic conductivities for different materials with equivalent seismic velocities. Marion's result motivated the second example in which silt and gravel have the same seismic velocity despite having very different hydraulic conductivities.

Using seismic travel times alone, SIM is designed to extract the lithologic geometry and effective zonal seismic velocities from the estimated seismic velocity field. For both examples, this method accurately identifies the general locations and shapes of zones with different lithologies.

The seismic velocity field estimated from traditional seismic tomography contains artifacts from the back projection of residuals into regions with few ray intersections and from errors in the travel times. These artifacts are seen as streaks through the tomogram in Figure 2-6a. To reduce the effect of these artifacts and retain the large-scale structure, we smooth the tomogram (Figure 2-6b) using a weighted averaging procedure called Hanning [*Tukey, 1977; Velleman and Hoaglin, 1981*]. We then generate a histogram of seismic velocity values (Figure 2-7b) from this smoothed tomogram. This statistical distribution of seismic velocity values gives a signature of lithologic properties, thus providing a basis for extracting large-scale features from the estimated seismic velocity field. In the example cases, this histogram shows a bimodal distribution. The dominant peak corresponds to high velocity sand, and the smaller peak indicates the presence of low velocity clay zones in example 1 and low velocity silt and gravel zones in example 2.

The SIM separates the tomogram into lithologic zones using statistical information from the histogram and spatial information from the tomogram. The lithologic zonation is adjusted by changing the estimated value of seismic velocity that separates low velocity zones from high velocity zones. We call this value the separation velocity. This method thus adjusts the separation velocity until it obtains the zonation that minimizes the mean square seismic travel time residual. The mean square travel time residual is used because it does not depend on the number of simulated rays, which can vary from one estimate of

lithologic zonation to another. An efficient bisection method called the golden search strategy [Press *et al.*, 1989] is used for this minimization. For each separation velocity that was evaluated, a constant seismic velocity value is assigned to each zone based on the histogram. For the high velocity zones, which represent sand in our case, we assign the mode of the estimated high velocity population because the mode is a good estimate of the central property of our bulk matrix material. For the low velocity zones, which represent clay, silt, and gravel in our examples, we assign the minimum seismic velocity from the estimated low velocity population.

The minimum smoothed velocity is chosen to represent these interbedded low-velocity zones, because extreme values within small zones are poorly estimated from seismic tomography. From our experience, other estimates of this seismic velocity, such as the median and mode of the low velocity population, consistently resulted in larger seismic residuals and overestimated the "true" mean value. Poor estimation of extremes, illustrated in the histograms of Figure 2-7, results from the damping imposed within the seismic travel time inversion and the subsequent smoothing of the estimates. The clay population centered at approximately 1520 m/s in Figure 2-7a is poorly represented in Figure 2-7b. Uniform back projection of residuals along entire ray paths leads to a relatively smooth estimated velocity field with few extreme values (Figure 2-6a). This field is then smoothed to remove artifacts of the seismic inversion, removing many of the remaining extreme values (Figure 2-6b), thus the minimum smoothed velocity is a reasonable estimate of the mean value for the low velocity zones.

The SIM with seismic data alone produces a tomogram (Figure 2-6c) with accurate estimates of the geometry of lithologic zones in the synthetic shown in Figure 2-6g, with the exception of a small extraneous zone near the upper portion of the well on the right. The mean values of seismic velocity estimated for these zones are similar to the synthetic mean values (Table 2-1). The lithologic zones determined from the SIM are used in a tracer-test inversion that provides preliminary estimates of zonal flow and transport parameters.

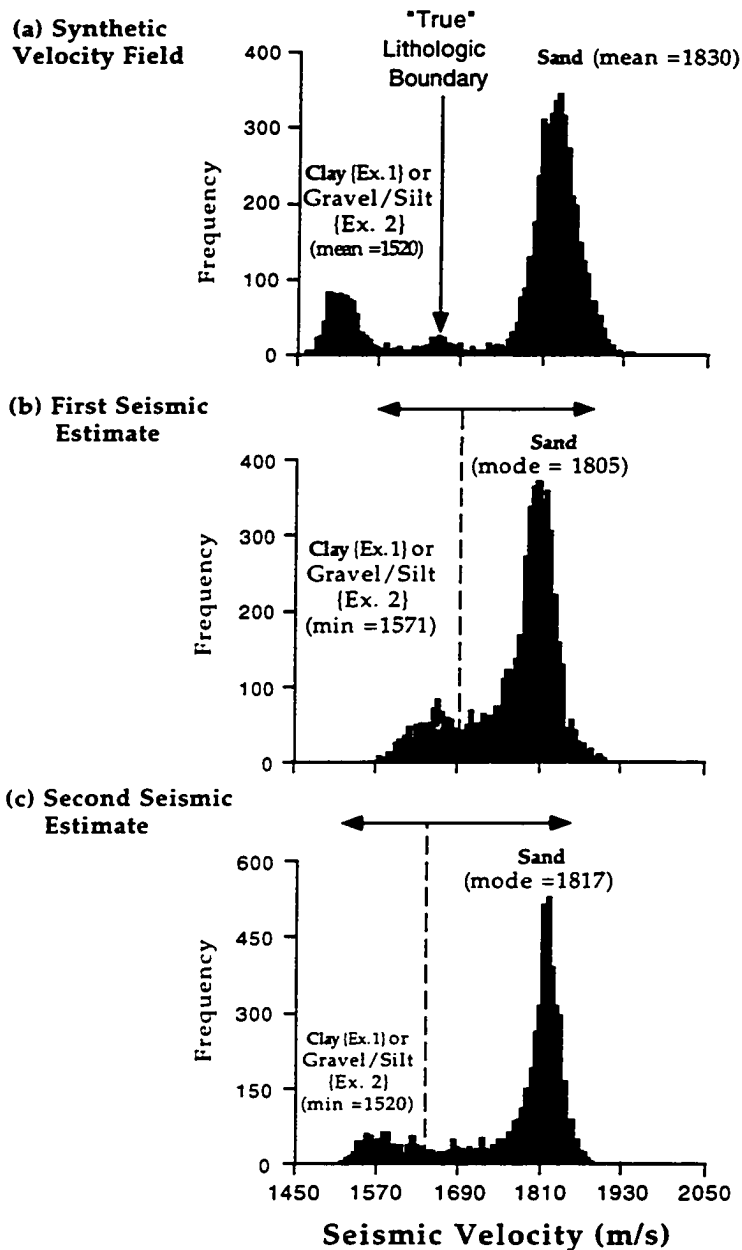


Fig. 2-7. Histograms of seismic velocity in: (a) The synthetic seismic velocity field (Figure 2-6g), (b) The smoothed seismic velocity field (Figure 2-6b) estimated using seismic tomography with a constant velocity starting model, (c) The smoothed seismic velocity field (Figure 2-6e) estimated using seismic tomography with the binary starting model of Figure 2-6c. The velocity that delineates the "true" lithologic boundaries is shown in (a). The vertical dashed lines in (b) and (c) distinguish the high velocity sand zones from the lower velocity clay or silt/gravel zones. The value that separates these two populations is determined using the Split Inversion Method. The value of the mode for the sand population is chosen to represent the high velocity zones. The value of the minimum smoothed seismic velocity is chosen to represent the interbedded low velocity zones.

3) Tracer-test Inversion

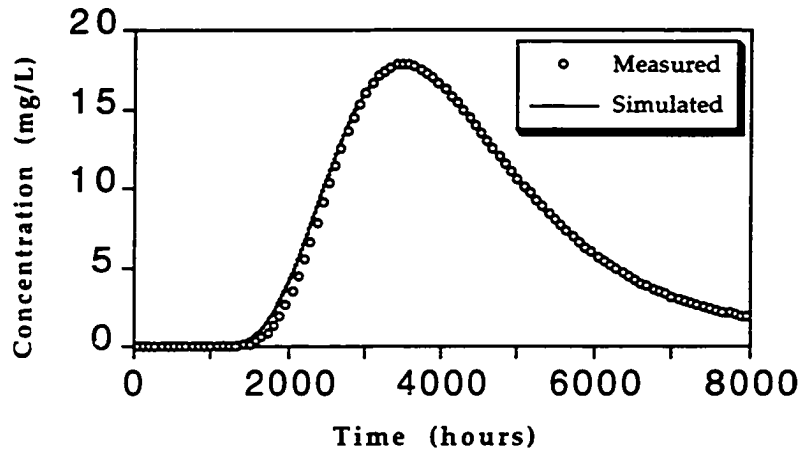
A simulation-regression procedure [Wagner and Gorelick, 1987; Gailey et al., 1991] is used to estimate hydraulic conductivity values for the zones delineated using the SIM with seismic data alone, and the value of effective small-scale longitudinal dispersivity. This methodology combines solute transport simulation (SUTRA, [Voss, 1984]) with weighted nonlinear least squares regression analysis (STARPAC, [Donaldson and Tryon, 1990]). Our formulation involves the minimization of the squared difference between simulated and observed concentrations, as well as the squared difference between simulated and observed peak concentration arrival time (2.4). Figures 2-8a and 2-8b illustrate least squares fits between the simulated and observed concentration histories for examples 1 and 2.

$$\text{Minimize } \mathbf{R}_C = \left(\sum_{T=0}^{T'} (C_{T,\text{meas}} - C_{T,\text{sim}})^2 + \chi (t_{p,\text{meas}} - t_{p,\text{sim}})^2 \right) \quad (2.4)$$

where

\mathbf{R}_C	concentration and peak arrival time residual $\{(mg/L)^2\}$;
$C_{T,\text{meas}}$	measured concentration at down-gradient well at time T, $\{mg/L\}$;
$C_{T,\text{sim}}$	simulated concentration at down-gradient well at time T, $\{mg/L\}$;
$t_{p,\text{meas}}$	measured time of peak concentration arrival, $\{\text{hours}\}$;
$t_{p,\text{sim}}$	simulated time of peak concentration arrival, $\{\text{hours}\}$;
T	time increment since tracer slug was input at well, $\{\text{hours}\}$;
T'	time that breakthrough is complete, $\{\text{hours}\}$;
χ	weighting factor, chosen to be one in this case, $\{[mg/(L\text{-hours})]^2\}$.

(a) Example 1



(b) Example 2

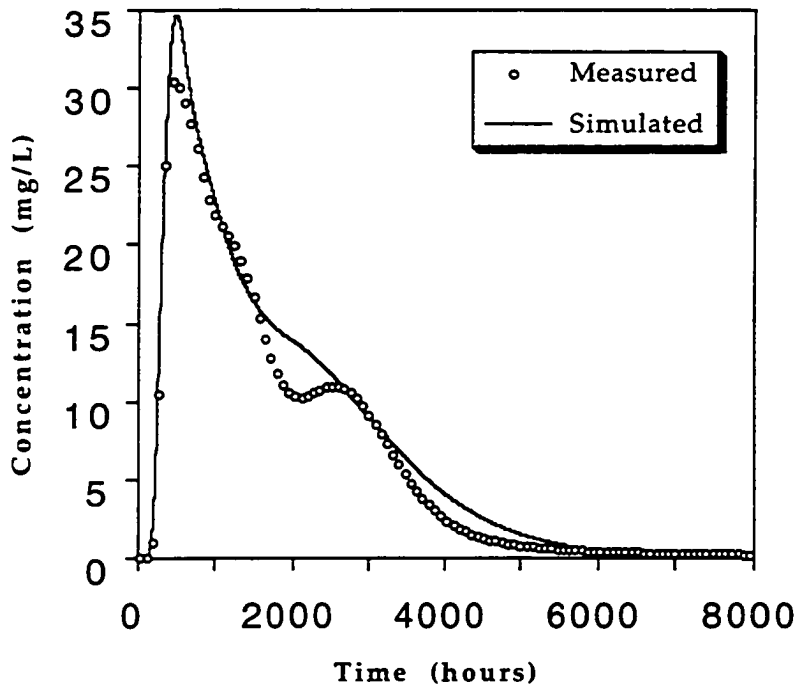


Fig. 2-8. Simulated and "measured" tracer concentration histories at the down gradient well for (a) Example 1 (Two Lithologies - Sand and Clay) and (b) Example 2 (Three Lithologies - Sand, Silt, and Gravel). Only one in every twenty measured data points are shown for clarity.

We simulate steady groundwater flow and nonreactive solute transport through a heterogeneous aquifer using:

The groundwater flow equation,

$$\nabla \cdot (\mathbf{K} \nabla h) = 0 \quad (2.5)$$

Darcy's Law,

$$\mathbf{v} = - \frac{\mathbf{K}}{\theta} \nabla h \quad (2.6)$$

and the advection-dispersion equation.

$$\frac{\partial c}{\partial t} + \mathbf{v} \cdot \nabla c - \nabla \cdot (\mathbf{D} \nabla c) = 0 \quad (2.7)$$

where

- ∇ gradient operator, $(\partial/\partial x, \partial/\partial z)$;
- x, z Cartesian coordinates, {m};
- \mathbf{K} hydraulic conductivity tensor, {m/s};
- h hydraulic head, {m};
- \mathbf{v} groundwater velocity, {m/s};
- θ effective porosity, {dimensionless};
- c concentration of a conservative tracer, {mg/L};
- t time, {s};
- $\mathbf{D} = \mathbf{D}(\alpha_\ell, \alpha_T, \mathbf{v})$, hydrodynamic dispersion tensor, {m²/s};
- α_ℓ, α_T longitudinal and transverse dispersivities, {m}.

The tracer inversion yielded reasonable estimates of the hydraulic conductivity and dispersivity values for both examples (Table 2-1). Despite small-scale variability in hydraulic conductivity, the conductivity estimates are similar to the mean synthetic values for both examples, with the exception of the low conductivity values. For example 1, the clay conductivities are estimated to be approximately two orders of magnitude less conductive than the sand zones. This provides enough resistance to flow that only small amounts of tracer are transmitted through these clay zones. Thus, the simulated concentrations are not sensitive to the extremely small values of clay conductivity. In example 2, the conductivity of the silt zones are also overestimated because of the poor sensitivity to these values. The transverse dispersivity was assumed to be one half the magnitude of the longitudinal dispersivity and was not estimated. The large-scale estimated longitudinal sand dispersivities, $\alpha_\ell = 2.65$ meters for

example 1 and 2.25 meters for example 2, are large compared to the synthetic small-scale value, $\alpha_l = 1.0$ meters. This difference is expected because these dispersivity estimates account for flow velocity variations at all scales smaller than the lithologic zones, which are treated as homogeneous bodies in the transport model. The dispersivity estimates thus represent effective parameters, and the general magnitude of these estimates is consistent with stochastic transport theory [Gelhar and Axness, 1983]. This theory predicts that the asymptotic longitudinal dispersivity (α_l) should be approximately:

$$\alpha_l = \sigma^2 \lambda / \gamma^2 \quad (2.8)$$

where

- σ^2 the variance of $\ln(K)$, {1.15 for example 1, and 0.25 example 2};
- λ the correlation length, {5.0 m for both example 1 and example 2};
- γ a flow factor, which was set to 1.0 in this case.

This asymptotic value would theoretically be reasonable after the solute has adequately sampled all scales of variability (after 40 to 50 correlation lengths according to Dagan [1982]). Other authors, such as Neuman *et al.* [1987], suggest that this flow factor should be neglected (i.e., set to 1.0), as was done for this comparison. This stochastic theory indicates that the asymptotic longitudinal dispersivity would be 5.75 meters for example 1. This theory indicates that the longitudinal dispersivity for example 2 would be 1.25 meters which is smaller than our estimate of 2.25 meters.

In our procedure, we place a lower bound on the estimated dispersivity value. Penalty weights were placed on dispersivity for values outside the range of numerical accuracy. Dispersivity is restricted to values greater than 0.25 meters to ensure concurrence with the Peclet criteria of $\frac{\Delta x}{\alpha} \leq 4$ [Voss, 1984], where the grid spacing (Δx) is one meter for these examples. This prevents numerical dispersion or oscillations that would create irregularities in the gradient of the objective function (4), which can cause significant problems in this type of estimation algorithm.

4) Split Inversion Method (SIM) with Tracer and Seismic Data

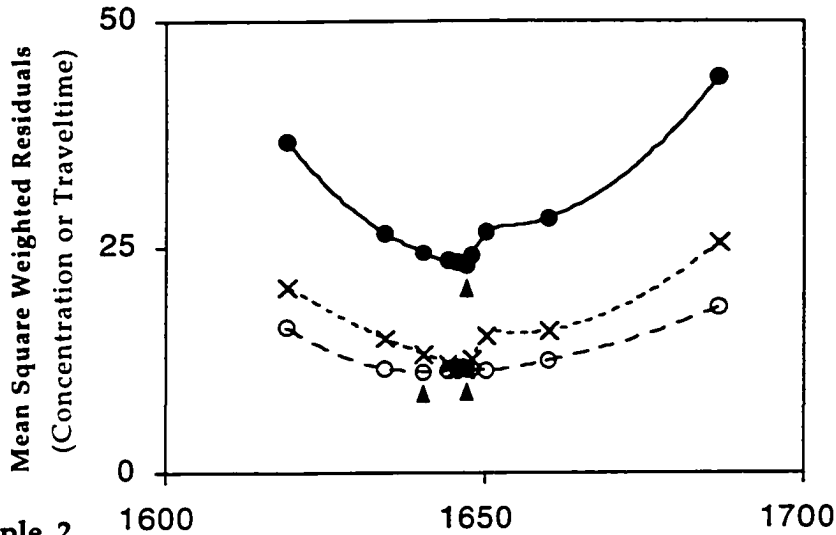
Independent inversions of the seismic and tracer data provide a reasonable first cut representation of both the lithologic zonation and the values of flow and transport parameters. As discussed earlier, the SIM with seismic data is used to estimate the shape of large-scale lithologic zones and the seismic

velocity within these zones. The tracer-test inversion then provides initial flow and transport parameter estimates for these zones (Table 2-1). The flowchart in Figure 2-5 shows where these initial estimates fit into the parameter estimation algorithm.

To implement SIM with seismic and tracer data, we first update our tomographic seismic field. This updated estimate of the seismic velocity field is obtained using seismic tomography with Figure 2-6c as the background velocity estimate. The resulting tomogram (Figure 2-6d) contains better estimates of the low velocity zones and fewer artifacts than the earlier tomogram (Figure 2-6a). The small-scale velocity structure was more accurately estimated in Figure 2-6d because the initial seismic velocity field for this inversion was much closer to the synthetic image. This tomogram was smoothed (Figure 2-6e) resulting in an image that retained the large-scale structure with significantly fewer artifacts than the tomogram in Figure 2-6b. The histogram of this estimated velocity field (Figure 2-7c) shows the two velocity populations of Figure 2-7a more clearly than the previous histogram (Figure 2-7b).

The SIM is then used to co-invert both seismic travel times and tracer concentrations for lithologic zonation. This was done by minimizing the weighted sum of residuals between simulated and observed seismic travel times, tracer concentrations, and peak concentration arrival times (Figure 2-9). To incorporate these different types of data, we weight the sets of residuals in the objective function (2.9). We chose the weights to provide equal mean square residuals for each data set. We set the weight on the seismic travel time residuals (β_T) to 1.0 and then determined the weight for the concentration residuals (β_C). This concentration weight is initially established by trial and error, and is then iteratively adjusted until the weighted mean square residual for each data set is approximately equal in the region of the estimated minimum. The final concentration weights (β_C) used in our examples were 88.0 for example 1 and 2.4 for example 2. The concentration weight (β_C) is significantly larger for example 1 because the fit of this concentration history is much better than the fit in example 2 (Figure 2-8).

(a) Example 1



(b) Example 2

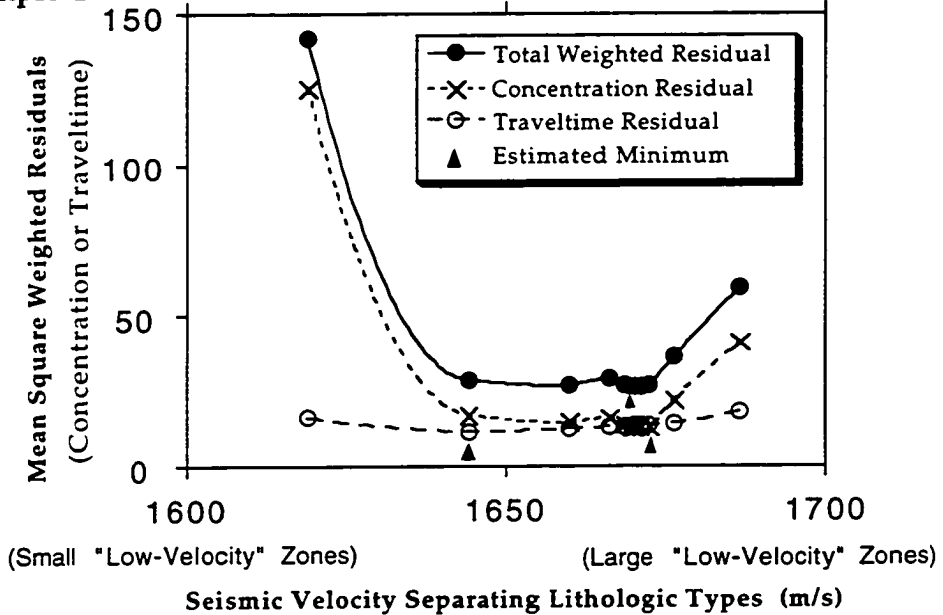


Fig. 2-9. Mean square weighted residuals for (a) Example 1 and (b) Example 2 versus values of seismic velocity which delineate the high and low velocity populations. The weighted sum of seismic traveltime and tracer concentration residuals is minimized. The seismic weight (β_T) is set equal to 1.0 and the concentration weight (β_C) is iteratively adjusted until the weighted mean square concentration residual approximately equals the traveltime residual. For Example 1, the concentration weight (β_C) equals 88.0, while for Example 2, the concentration weight equals 2.4.

$$\text{Minimize } (\beta_C R_C + \beta_T R_T) \quad (2.9)$$

where

- β_C concentration weight $\{(L/mg)^2\}$;
- R_C concentration and peak arrival time residual $\{(mg/L)^2\}$;
- β_T seismic travel time weight $\{(1./ms)^2\}$;
- R_T mean square seismic travel time residual $\{ms^2\}$.

In this stage of the algorithm, the SIM determines the zonation that best satisfies both the seismic and tracer data using the best tomogram (i.e., Figure 2-6e for examples 1 and 2). For examples 1 and 2, this stage of the algorithm improves the estimate of the large-scale lithologic zonation in the synthetic aquifer (Figure 2-6g). All the low seismic velocity zones are properly identified and the mean velocities within these zones are accurately estimated (Table 2-1). This stage of the algorithm also removes the extraneous zone from the upper right side of the earlier binary estimate (Figure 2-6c).

To quantify the effect of tracer data on lithologic zonation, we split the second smoothed tomogram (Figure 2-6e) into zones using seismic information alone and compared the results to the estimate made using seismic and tracer information (Figure 2-6f). We compared these estimates using the calculated percentage of cells that were misassigned to a lithology (i.e., a low-velocity cell assigned to a high-velocity zone, or a high-velocity cell assigned to a low-velocity zone). The tracer information reduced this percentage of misassigned cells from 5.3% to 4.9% for example 1, and from 5.3% to 3.0% for example 2. The change in zonation was more significant for example 2 because the tracer concentration history is more sensitive to the geometry of gravel and silt zones than to the geometry of clay zones.

For both examples, the minimum mean square seismic residual and the minimum mean square tracer concentration residual occur at similar values of separation velocity (Figure 2-9). This indicates that the zones are fairly consistent with both sets of information. The separation velocity for the minimum concentration residuals occurs at a slightly larger value than for the minimum seismic residuals. Thus for both examples, the best zonation for the tracer data contains slightly larger low-velocity zones than those predicted by the seismic data alone. This gives a more accurate estimate of the lithologic geometry than

obtained using seismic data alone. A final tracer inversion is performed using the new zonation to obtain flow and transport parameter estimates for the updated zones. The updated zonation changed very little for example 1; therefore, the tracer parameter estimates did not change significantly.

If the boundaries and parameter estimates are stable with minima at similar separation velocities, the inversion is complete. If there are still significant changes in the boundaries or the parameter estimates, this procedure iteratively updates the zonation and the parameter estimates. In example 2, the hydraulic conductivity estimates changed slightly for the updated zonation (Table 2-1). This prompted a second inversion for lithologic zonation using the updated conductivity estimates. This resulted in no significant change in the zonation, thus completing the inversion. In both examples, the co-inversion of two independent data sets resulted in refined zonation and parameter estimates that are consistent with the underlying physical processes of wave propagation and solute transport.

DISCUSSION

Assumptions and Limitations

The algorithm presented here is based on several assumptions. We used the common assumption of a two dimensional flow field. This implies that the two wells are in a plane parallel to the regional hydraulic gradient and that the lithology is horizontally continuous in a direction perpendicular to this gradient. Advection and dispersion in and out of this plane are neglected. Seismic wave propagation outside of this vertical plane is also neglected because seismic velocity is only weakly inhomogeneous in saturated sediments. Therefore, seismic waves tend to propagate on relatively straight paths in comparison with the more tortuous paths of solute particles.

The Split Inversion Method (SIM) is developed assuming that each data type contains information about large-scale lithologic zonation. We feel this is a reasonable assumption because both seismic and tracer measurements have sampled approximately the same physical environment. Example 2 demonstrates that the method does not rely on significant correlation between seismic and hydraulic parameters. We added a significant amount of variability to the parameter fields of both examples to simulate the effects of multiple scales of heterogeneity on both seismic and tracer measurements.

The present version of the SIM is designed to distinguish lithologic zones characterized by two seismic velocity populations. This should be adequate to describe many geological environments in which large scale zonal lithology is present. The histogram of the estimated seismic velocity values provides the information needed to determine the number of seismic velocity populations. If necessary the method may be extended to separate more than two seismic velocity populations to describe more complex geologic environments.

Conclusions

We have demonstrated an algorithm that couples geophysical and hydrogeologic data to estimate the location and shape of large-scale lithologic zones, the seismic velocity and hydraulic conductivity within these zones, as well as the small-scale dispersivity. Cross-well seismic tomography provides densely sampled information about heterogeneity in lithology, supplementing the spatially averaged information from the inversion of tracer-test data. The algorithm begins by estimating a seismic velocity field using traditional cross-well seismic tomography. The SIM then effectively extracts the large-scale lithologic structure from this estimated field by distinguishing between high velocity sand zones and the interbedded low velocity clay, silt and gravel zones. Flow and transport parameters are then estimated for these zones using a simulation-regression procedure which minimizes the difference between the simulated and measured concentration histories. The SIM then combines both seismic and tracer data to refine the lithologic zonation. This co-inversion is possible because both the tracer concentration data and the seismic travel time data are sensitive to the geometry of lithologic zones. Finally, the effective flow and transport parameters are estimated for the updated zones. This implementation of our algorithm provides estimates that are consistent with two independent data sets.

The algorithm we developed is directed toward future application to field data. Extensions of this work could utilize readily available seismic data. Using compressional wave travel times as our only seismic data, we have been able to identify lithologic patterns between wells. In field tests, the full seismic wave field is measured and the seismic velocity structure near the wells can be estimated using well logs. Modeling the full wave field or multiple wave attributes may offer significantly more information about aquifer lithology than provided by travel times alone. Lithologic estimates can also be improved by conditioning on local well log information.

The algorithm we developed can also be extended to three-dimensions if adequate data are available. In such a case, one possible tracer-test design consists of a recharge well which would inject water and tracer in the center of a group of pumping wells with multiple sampling zones at different depths. This type of test will provide three-dimensional information about the shape, location, and properties of lithologic zones. At contaminated sites, measured

contaminant concentrations at two or more locations through time can serve as the solute data set.

Other measured information could be used in our parameter estimation algorithm. This information could include pressure response at observation wells resulting from an applied stress at a pumping or recharge well. Hydraulic information could be especially useful if repetitive seismic tests are completed during a pump test. Different lithologic zones should have different pressure responses that might be monitored by analyzing the changes in seismic velocity through time. The time for a pressure pulse to dissipate is related to the hydraulic conductivity of the media, thus a pressure difference may be observed between high and low conductivity zones. If detected, this transient pressure response could be used to develop accurate estimates of hydraulic conductivity and the relationship between seismic velocity, hydraulic pressure, and hydraulic conductivity.

CHAPTER 3:

**TRAVEL TIME INVERSION FOR THE GEOMETRY OF
AQUIFER LITHOLOGIES**

ABSTRACT

Cross-well travel time tomography can provide detailed descriptions of the geometry of lithologic zones in aquifers and reservoirs. Traditional tomographic inversions focus on estimating a smooth field of seismic slowness values to best match the travel time data. We demonstrate a method, called the multiple population inversion (MPI), that co-inverts travel times between multiple well pairs to identify the spatial distribution of a small number of slowness populations. The lithologies and hydraulic parameters for these populations can then be determined from core data and hydraulic testing.

The MPI iteratively assigns pixels to a small number of slowness populations, based on the histogram of slowness residuals. By constraining the number of slowness values, this method is less susceptible to inversion artifacts and can resolve finer scale sedimentary structures than methods that smooth the slowness field. The MPI is demonstrated in two dimensions with a synthetic aquifer, and in three dimensions with the Kesterson aquifer in the central valley of California. In both of these cases, the MPI converges to an equal or smaller average travel time residual than obtained with an unconstrained tomographic inversion.

INTRODUCTION

Many geoscience and engineering disciplines would benefit from detailed descriptions of the geometry of lithologic zones. Cross-well seismic tomography, which was developed to bridge the gap between surface seismic and log measurements, has the potential to provide such descriptions. Cross-well methods may be used to characterize contaminated groundwater sites, but to date have been primarily used to characterize petroleum reservoirs.

The ultimate goal in both petroleum and environmental contamination applications is to estimate the spatial distribution of lithologies and their associated fluid flow properties. To achieve this goal, cross-well seismic inversions should constrain the number of slowness values rather than smoothing the estimated slowness field. The predominant lithologies in a region may be more accurately identified using imaging methods that find the best spatial distribution of a small number of slowness values. Although seismic slowness may be poorly correlated to hydraulic properties, significant contrasts in slowness should relate to changes in lithology. If the geometry of the predominant lithologies can be identified, hydraulic properties can be estimated from core samples, geophysical logs, or hydraulic tests.

Little work has been published on methods of estimating the zonation of lithologies. *Hyndman et al.* [1994] presented the split inversion method (SIM) to co-invert seismic travel times and tracer concentrations for a small number of lithologic zones and the seismic and hydraulic parameters for each zone. The first stage in this algorithm is an inversion of cross-well seismic travel times to obtain a slowness tomogram. This tomogram is then delineated into homogeneous slowness zones by minimizing the sum of squared travel time residuals relative to changes in the value of seismic slowness that separates high slowness zones from low slowness zones. Initial estimates of hydraulic conductivity for these zones and the regional aquifer dispersivity, used in solute transport modeling, are then developed. Finally, the SIM co-inverts seismic and tracer data to update the estimates of lithologic zonation, the hydraulic conductivity for each zone, and the dispersivity. Synthetic examples were used to demonstrate this method for a case in which the relation between seismic slowness and hydraulic conductivity was non-unique and unknown.

By combining seismic and tracer data *Hyndman et al.* [1994] were able to estimate both seismic slowness and hydraulic conductivity values without a

specified relation between these parameters. This is a critical element of any method that combines seismic and hydraulic data because there is an inherent non-uniqueness in the relation between parameters of wave propagation and parameters of fluid flow and solute transport [*Han et al.*, 1986; *Marion et al.*, 1992).

In this paper, we develop the multiple population inversion (MPI), which is a more direct and flexible approach than SIM, to estimate the geometry of dominant seismic slowness populations in a region using travel times alone. We then implement the MPI with both synthetic and field *P*-wave travel times; however, the method could be modified to use other types of data that provide detailed spatial sensitivity to lithologic contrasts.

The objective of the MPI is to minimize the average absolute travel time for rays simulated through pixels constrained to a small number of seismic slowness values. By limiting the number of possible slowness values, the MPI efficiently and effectively estimates the geometry of the predominant lithologies between two wells. In regions with multiple cross-sections or multiple wells, the MPI can co-invert all available travel times to generate consistent regional slowness estimates. These regional estimates can then be interpolated into three-dimensions and used in inversions for flow properties.

THE MPI METHOD

Our multiple population inversion (MPI) method is designed to co-invert seismic travel times taken between several well pairs for the regional zonation of seismic slowness. These seismic slowness zones can then be interpreted as lithologies assuming that connected regions of similar slowness adequately represent lithologic zones. While the relationship between slowness and lithology may not be one-to-one and certainly not unique, subsequent interpretation of the MPI estimate may be useful in delineating zones with similar properties, such as clay content, porosity, or even permeability.

The MPI was developed using cross-well seismic travel times because path integral inversions (i.e., ray theory) provide high resolution information about slowness contrasts between wells. This information allows the MPI to iteratively update the slowness tomogram to minimize travel time residuals. The foundation for this implementation of the MPI is a small perturbation expansion of the travel time equation (3.1), which we derive below.

For each iteration of the MPI, we simulate ray paths through the latest slowness estimate using a fourth order Runge-Kutta approach [Harris *et al.*, 1992]. We approximate the travel time (t_i) for the i^{th} source-receiver pair as the integral of slowness (S) along the simulated ray path (C_i):

$$t_i = \int_{C_i} S(x, z) d\ell \quad i = 1, \dots, m \quad (3.1)$$

where ($d\ell$) is the increment of path length along a ray.

We use rectangular pixels as orthogonal basis functions (φ_j) to provide a discrete representation of the slowness:

$$S(x, z) = \sum_{j=1}^N S_j \varphi_j \quad (3.2)$$

where the basis functions $\varphi_j = \begin{cases} 1 & \text{inside } j^{\text{th}} \text{ rectangular pixel} \\ 0 & \text{outside } j^{\text{th}} \text{ rectangular pixel} \end{cases}$

$$t_i = \sum_{j=1}^N S_j \ell_{ij} \quad i = 1, \dots, M \quad (3.3a)$$

$$\text{where} \quad \ell_{ij} = \int_C \varphi_j d\ell \quad (3.3b)$$

Both the ray path and the slowness are unknown in (3.3), thus we can not directly invert this equation for the unknown slowness field. Instead, we linearize (3.3) using a small perturbation approach. We write the slowness field (S_j) as the sum of a known background field plus a field of unknown slowness perturbations (ΔS_j).

$$S_j = S_{0j} + \Delta S_j \quad j = 1, \dots, N \quad (3.4)$$

We calculate the slowness perturbations by replacing the unknown ray path in (3.1) with the ray path simulated through the known background field (S_{0j}), which is the slowness estimate from the previous iteration. Thus, (3.3) reduces to a linear set of equations that relate travel time residuals (Δt_i) to slowness perturbations (ΔS_j) using a projection matrix (ℓ_{ij}), which has elements of ray path length in each pixel.

$$\Delta t_i = \sum_{j=1}^N \Delta S_j \ell_{ij} \quad i = 1, \dots, M \quad (3.5a)$$

$$\text{where} \quad \ell_{ij} = \int_{C_{0i}} \varphi_j d\ell \quad (3.5b)$$

We then calculate the slowness perturbations (ΔS_j) by inverting (3.5a) using a simultaneous iterative reconstruction technique (SIRT) [Dines and Lytle, 1979; Harris et al., 1990; McMechan et al., 1987]. Other inversion schemes, such as conjugate gradients, could be used instead of SIRT.

Rather than adding the spatial field of slowness perturbations to the background slowness field, as would be done in most tomographic inversions, the MPI separates the slowness field into a small number of populations based on the histogram of the estimated slowness perturbations (ΔS_j).

The following steps are used for each iteration of the MPI (Figure 3-1):

- 1) Simulate ray paths through the known background slowness field and calculate travel time residuals.
- 2) Invert (3.5a) for a spatial field of slowness perturbations using SIRT.
- 3) Assign pixels to a small number of slowness populations based on the histogram of values in this spatial field of slowness perturbations.
- 4) Calculate a representative slowness value for each population, as the previous estimate plus the median of the slowness perturbations for pixels assigned to a population.
- 5) Check that each pixel's population change does not result in an unreasonable change in slowness. Place all pixel's that experience unreasonable slowness changes, such as change greater than ten times the estimated slowness perturbation, back to their previous population. This allows for smooth convergence of the travel time residuals.

We describe the details of the MPI method below.

The MPI is an iterative estimation method, thus an initial guess of the seismic slowness field is needed. A homogeneous background slowness field will generally be the best choice, although prior geologic information could be used to construct the initial multiple population slowness model. The Householder transform [Golub, 1989] was used to invert the overdetermined system of travel time equations for a regional value of slowness (S_0), although other methods such as least squares inversion could also be used.

The number of allowed slowness populations can be set equal to the number of predominant lithologies in the region, based on core samples and geologic inference. A specified proportion of pixels with the largest absolute slowness perturbations are then assigned to the determined number of populations based on the histogram of slowness perturbations (Figure 3-1) for all pixels of the region. This proportion, which we determine using sensitivity analysis, does not include pixels which belong to the extreme population in the direction of the calculated slowness perturbation. This allows pixels to change populations for all MPI iterations, even after most of the pixels are constrained to a population. The population assignment is done by ranking the absolute slowness perturbations for all pixels in the region, and picking the minimum absolute perturbation value as a cutoff for allowed population change. Pixels are only allowed to change if the absolute perturbation is greater than this cutoff value, and pixels can only change one population per iteration.

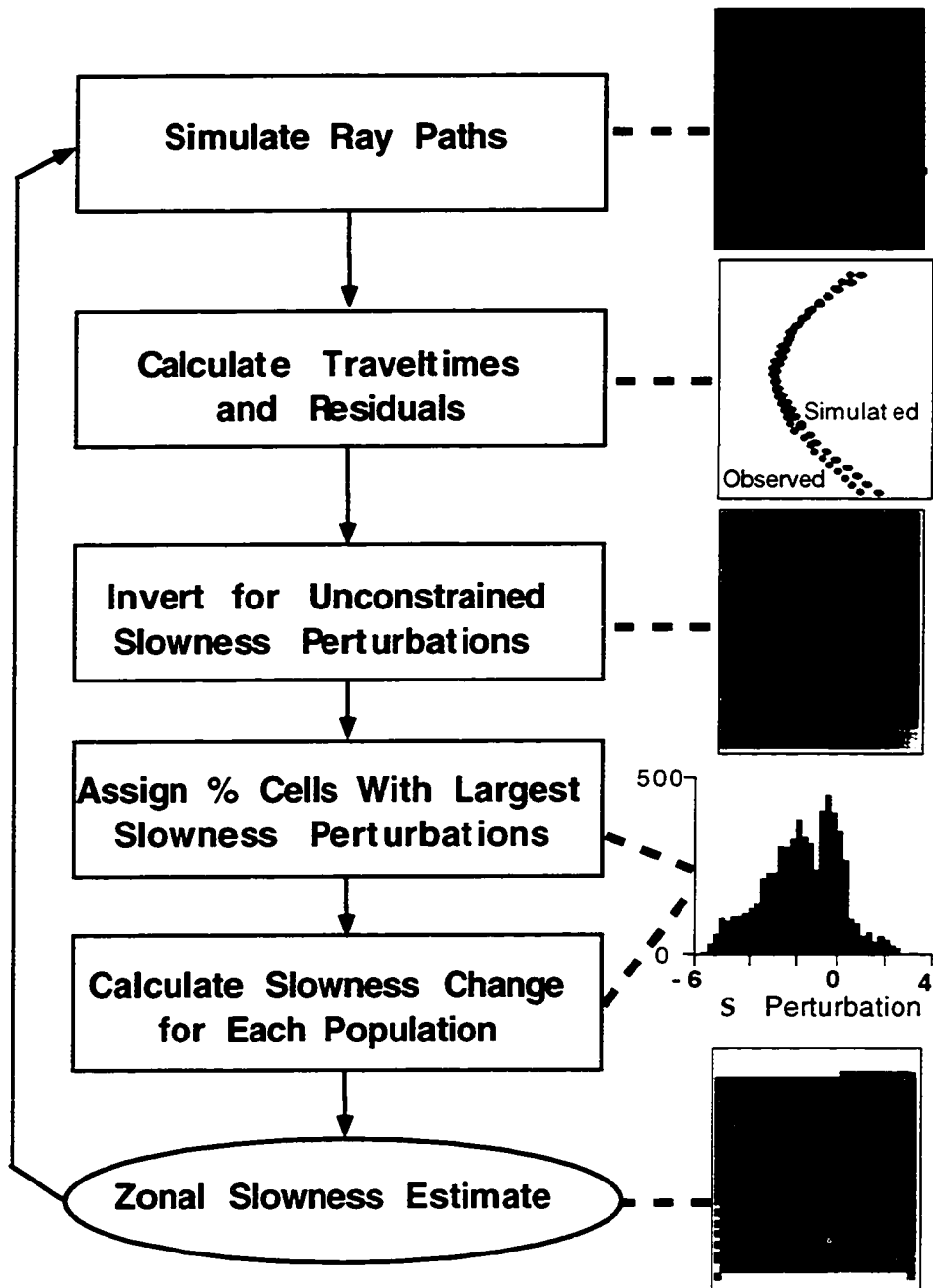


Fig. 3-1. Flow chart of the multiple population inversion (MPI) algorithm. The images to the right side of the figure illustrate the stages of the algorithm for a single cross-section. The final slowness estimate in the lower right was developed using several iterations of the MPI.

Our experience demonstrates that populations should be progressively added to obtain the expected number of populations, rather than starting the inversion with multiple populations. Each population is added in the direction of the skew of the slowness perturbation histogram. Thus, if this histogram is skewed toward large negative slowness perturbations, a low slowness population would be added. If no prior information exists, the number of populations can be increased until the average travel time residual is no longer reduced by repeated iterations and the slowness perturbation histogram has little skew.

Each population (p) is then assigned a representative slowness value (S^p), which is the population's previous slowness estimate (S_0^p) plus a perturbation (ΔS^p). Thus (3.4) has been modified to constrain the slowness values to (K) slowness populations.

$$S^p = S_0^p + \Delta S^p \quad p = 1, \dots, K \quad (3.6a)$$

$$\text{where } \Delta S^p = \text{median}\{\Delta S_j^p\} \quad j = 1, \dots, N \quad (3.6b)$$

In this implementation of the MPI, each perturbation is calculated as the median of the slowness perturbations for pixels assigned to a population. Each slowness population is thus parameterized by a single slowness value, which is the median of the slowness distribution. The median of the perturbations is used because it is insensitive to the largest perturbations, allowing for smooth convergence.

The objective is to minimize the average absolute travel time residuals.

$$\text{Minimize } \left\{ \left(\sum_{i=1}^m |\Delta t_i| \right) / m \right\} \quad (3.7)$$

For each MPI iteration, rays are traced through the perturbed slowness field and the changes are accepted as long as this objective is reduced, or at worst slightly increased. This inversion is similar in philosophy to simulated or threshold annealing.

Annealing algorithms allow large numbers of changes to an estimated field early in the inversion when the estimate is far from the optimal value. Fewer changes occur with later iterations as the estimate converges toward a stable solution. Each perturbation is accepted if the objective value is improved (reduced) or slightly degraded (increased). An increase in the objective value may be accepted early in the inversion, because this allows the algorithm to escape a local minimum in the objective value [Dueck, 1990; Deutsch and Journal, 1992]. For the MPI, we allow a large proportion of pixels to change populations for early iterations and reduce this proportion for later iterations.

The process of updating the spatial distribution of populations and adding

perturbations to each population is iteratively repeated until the travel time residuals increase for several consecutive iterations. When this occurs, the proportion of pixels allowed to change populations is reduced and the inversion is restarted using the slowness model with the minimum travel time residual. If the objective value is not improved by this change, the estimate with the minimum travel time residual is taken to be the optimal slowness field for the specified number of populations.

If multiple cross-sections are available in a region, the MPI can co-invert all the cross-sections to obtain a consistent estimate of the multi-two-dimensional structure of the region. To determine if populations are likely to be the same in each of the cross-sections, the MPI can be applied to each cross-section individually to see if the populations are reasonably consistent for the region. If the region appears to have a small number of populations, co-inversion of the travel times with the MPI should improve consistency between multiple tomograms.

The final multi-population estimates can be used as starting models for an unconstrained-value tomographic inversion. This confirms the MPI estimates and allows smaller perturbations to be added to the estimated slowness populations. Iterative tomographic inversions work best when the perturbation from the starting model is small because the predicted ray paths are closer to the true paths. Therefore, the updated MPI estimate should be better than estimates obtained from unconstrained-value tomography alone because the zonal slowness estimate from the MPI is a better starting model than a homogeneous model.

In cases where the ultimate goal is to estimate fluid flow properties or determine the lithologic structure of a subsurface reservoir or aquifer, the MPI offers significant advantages over many commonly used inversions. Tomographic inversions generally place few constraints on the slowness values, resulting in relatively smooth slowness models with inversion artifacts. The MPI improves structural interpretations and reduces inversion artifacts, especially in environments with a small number of slowness populations.

After a brief comparison of the MPI to the split inversion method (SIM), which is another zonal estimation method, we demonstrate the MPI with both synthetic and field cross-well *P*-wave travel times. The synthetic travel times were simulated through a slowness field with two dominant populations and added correlated variability [Hyndman *et al.*, 1994]. The field data were collected by researchers at the Lawrence Berkeley Laboratories, using multiple well pairs from the central valley of California [Ernie Majer, personal communication, 1994].

The Split Inversion Method (SIM): Comparison to MPI

The SIM and the MPI were both developed to determine the geometry of dominant lithologic zones and parameter values for these zones. Both methods are capable of estimating the structure of dominant slowness populations from seismic travel times, and then estimating lithologies and hydraulic properties that correspond to the slowness zonation using information such as well logs. The assumption, hence the philosophy, behind these inversions is that information about the zonation of lithologies is contained in cross-well seismic travel times. Although the general philosophy of SIM and MPI is the same, the methods are significantly different.

The SIM assumes that an unconstrained seismic tomogram contains accurate information about the slowness structure, and thus splits this tomogram into zones using a post-inversion step [Hyndman *et al.*, 1994]. The objective of the SIM using seismic data alone is to find the seismic slowness zonation that minimizes the mean square seismic travel time residual. For a two population case, the zonation is adjusted by changing the estimated value of seismic slowness that separates low slowness zones from high slowness zones. For each evaluated zonation, a seismic slowness value is assigned to each zone based on the histogram of slowness values in the unconstrained tomogram. In other words, the SIM assumes that information about the representative slowness value for each population can be derived from the histogram of slowness estimates. This assumption could be relaxed by directly inverting the matrix of travel time equations for the zonal slowness values using the path lengths through each zone. This would provide the best estimates of zonal slowness for each potential zonation. Hyndman *et al.* [1994] also demonstrated the SIM for co-inversion of seismic and tracer data for the best lithologic zonation and hydraulic and seismic parameters for each zone. In this manner, lithologic information can be derived from multiple complementary data sets. The SIM is thus a flexible inversion method that can be formulated to best combine multiple data types.

The MPI more directly inverts for the seismic slowness structure by estimating the spatial distribution of a small number of slowness populations. Thus the MPI parameterizes the inversion to determine zones rather than extracting the zonal information from an estimated tomogram. The MPI also iteratively updates each population slowness value based on the slowness

perturbations propagated to the population, rather than using values from the histogram of slowness estimates. The MPI is implemented in a similar manner to unconstrained-value tomography, but residual artifacts are greatly reduced in the MPI by constraining the number of slowness values acceptable in a region. The MPI thus provides a method to estimate the lithologic structure without the potential biasing effect of smoothing, which is the most common method of reducing residual artifacts for tomographic inversions.

RESULTS FOR A SYNTHETIC AQUIFER

We compare the multiple population inversion (MPI) to the split inversion method (SIM) with a previously published synthetic data set [Hyndman *et al.*, 1994]. This data set, composed of cross-well seismic travel times, was created by simulating the propagation of *P*-waves through a synthetic seismic slowness field (Figure 3-2a) as discussed by [Hyndman *et al.*, 1994].

One advantage of the MPI, relative to the SIM, is improved computational efficiency. For each iteration of the SIM, rays are first traced to estimate the continuous tomogram, then rays are traced through many potential zonations of this continuous tomogram to find the zonation that minimizes travel time residuals. An average of 13 additional ray tracing steps were used to assess the optimal zonation for each iteration of the SIM. In contrast, each iteration of the MPI involves tracing rays only once.

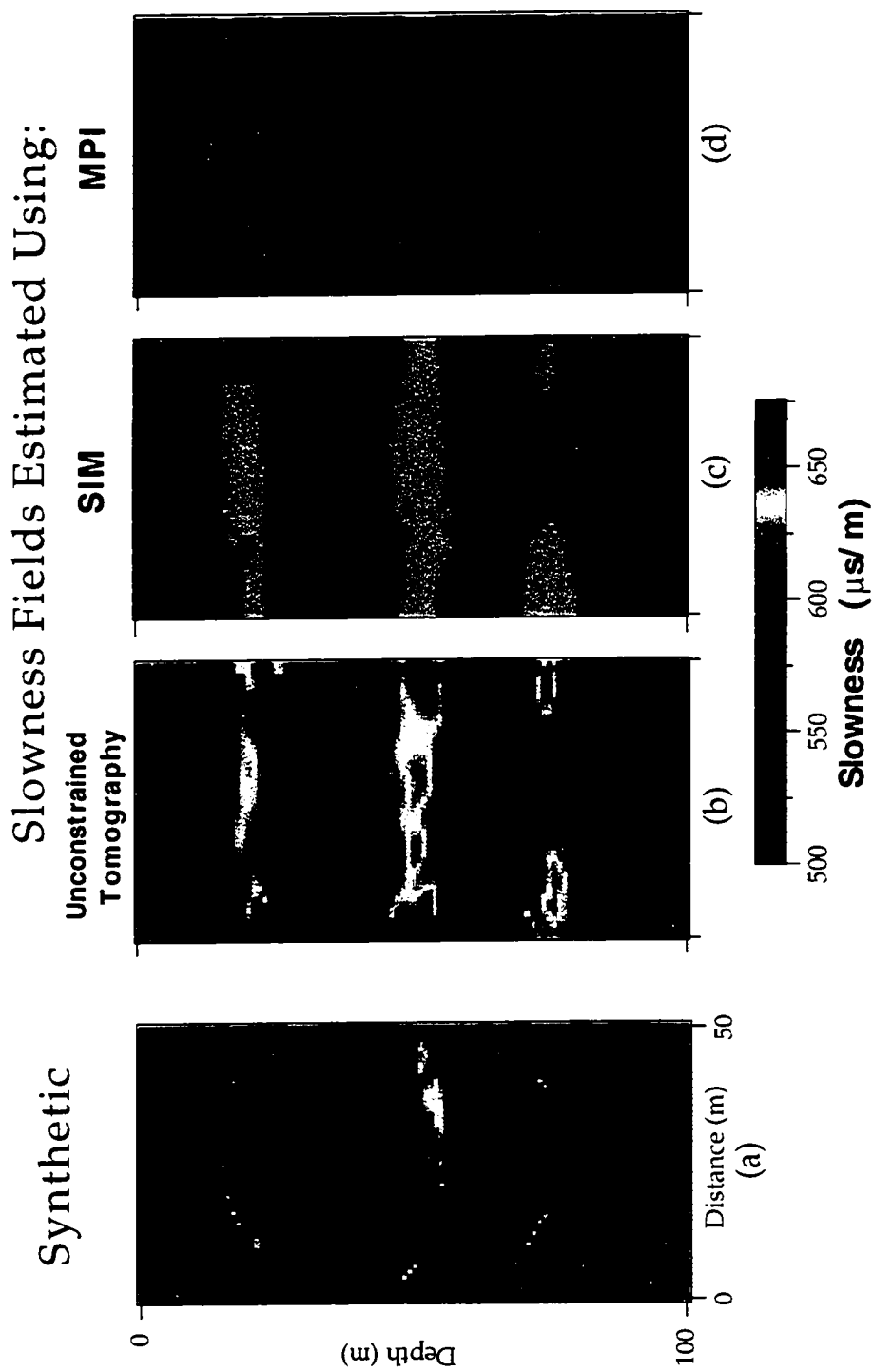


Fig. 3-2. Comparison of (a) the synthetic slowness field to models estimated using: (b) unconstrained value tomography, (c) the split inversion method (SIM), and (d) the multiple population inversion (MPI).

Figure 3-3 illustrates the convergence of the MPI (with 25 percent of the pixels allowed to change populations) and the SIM relative to the convergence of unconstrained-value tomography. The minimum travel time residuals were obtained using 16 iterations of the MPI with one ray tracing and back projection step for each iteration and six iterations of the SIM. Recall that each SIM iteration involves an average of 14 ray tracing steps compared to only one for MPI, thus the MPI is approximately 5.25 times more computationally efficient than the SIM for this example. After the 16th iteration, the MPI began to diverge slightly (Figure 3-3), and lowering the percentage of pixels allowed to change populations did not improve the objective value. This slight divergence only occurred after the optimal value for two populations had been reached.

The convergence of the MPI is faster than unconstrained-value tomography for all but the first iteration, and the MPI converges to a solution with a lower travel time residual (Figure 3-3). The convergence of the MPI can be sped up by increasing the proportion of pixels allowed to change populations or multiplying the median perturbation by a value greater than one, but this may result in a degraded objective value (i.e., larger average travel time residual). The value for the proportion of pixels allowed to change populations (25%) was determined by sensitivity analysis for this synthetic aquifer. Although the MPI is not very sensitive to this parameter, several inversions were completed with different proportions to determine the best value within five percent. Figure 3-3 also illustrates the convergence of the SIM to approximately the same average travel time residual as obtained using unconstrained-value tomography. The dramatic divergence of the SIM in the seventh iteration was caused by overestimating the slowness of the embedded zones and as a result, greatly misestimating the zonation.

To compare the results from MPI and SIM, we used the same starting slowness field and ray tracing parameters for both inversion methods. Table 3-1 compares the results using the SIM and the MPI in this synthetic aquifer. Although the SIM results in a slightly smaller percentage of pixels assigned to the wrong population, the MPI estimate has a lower travel time residual and a more accurate low slowness value. The difference between the number of pixels estimated correctly is minimal and both estimation methods generate satisfactory results for this synthetic aquifer. The estimates from both SIM and MPI have fewer artifacts than the estimate from unconstrained-value tomography, leading to better estimates of the dominant scale of heterogeneity (Figure 3-2).

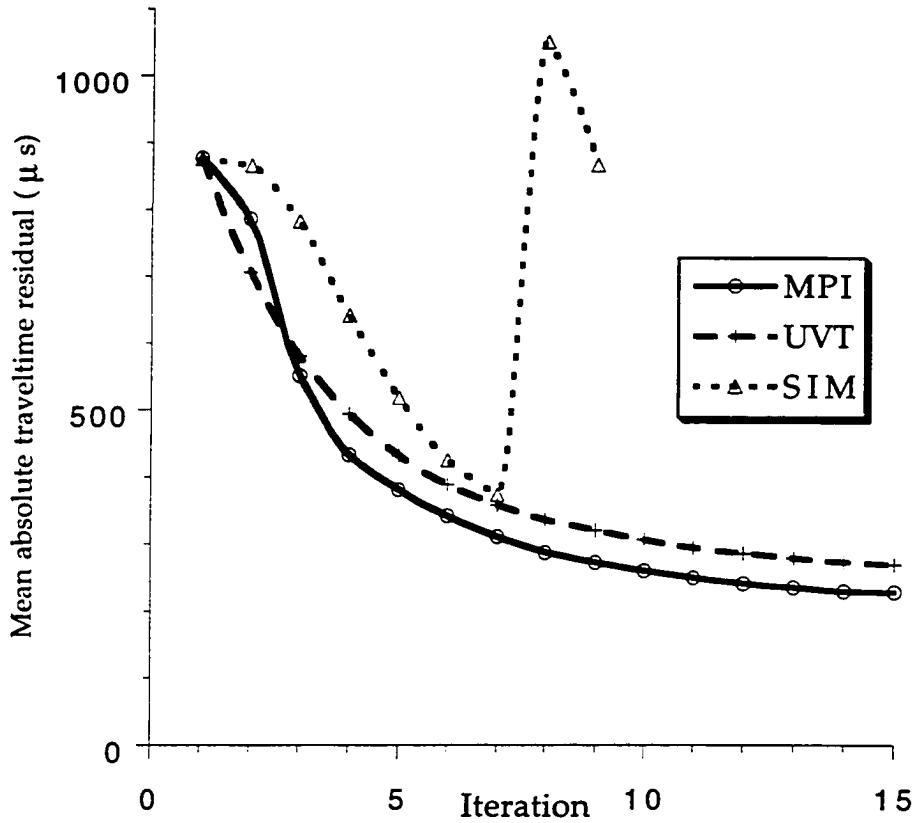


Fig. 3-3 Comparison of mean travel time residuals using the multiple population inversion (MPI), the split inversion method (SIM) and unconstrained-value tomography (UVT) for the synthetic presented by Hyndman et al. [1994]

Table 3-1. Comparison of the split inversion method (SIM) with the multiple population inversion (MPI) for a synthetic data set.

	SIM	MPI	True Arithmetic Mean Values	True Harmonic Mean Values
Average travel time				
residual per ray (μs)	373.22	224.30	---	---
% miss assigned pixels	2.93	4.04	---	---
High slowness value ($\mu\text{s}/\text{m}$)	646.39	645.39	646.76	645.71
Low slowness value ($\mu\text{s}/\text{m}$)	552.55	546.16	547.28	547.12

RESULTS FOR THE KESTERSON FIELD SITE

We also used the multi-population inversion (MPI) to co-invert travel times from seven cross-well seismic surveys collected through a near surface aquifer in California's Central Valley. This unconsolidated shallow aquifer, near the Kesterson Reservoir, was deposited by the San Joaquin River as sequences of sand, silt, and clay [Benson, 1988].

An extensive network of approximately 100 wells was set up to estimate the seepage from Kesterson reservoir and study the distribution of selenium in the region's groundwater [Benson, 1988]. The area used for this study (Figure 3-4), which has wells spaced from 1.5 to 14 meters apart, is a subsection of this much larger well network. To predict the transport of selenium in groundwater, the subsurface lithologies need to be identified, and groundwater flow and solute transport properties need to be estimated for these lithologies. The MPI is applied to this field site to estimate the seismic slowness structure of the aquifer along the available planes of seismic data. We will examine other aspects of this estimation problem, such as: 1) generating three-dimensional seismic slowness realizations from multi-two-dimensional estimates using geostatistics; and 2) combining seismic and tracer information to estimate the lithologies and the three-dimensional permeability field at the site, in future papers.

To determine the number of dominant slowness populations at the Kesterson site, we first independently inverted each cross-section with the MPI. We then used the same homogeneous starting model with the regional average seismic slowness for each inversion. This average slowness of 577.7 microseconds per meter was determined using the Householder transform to invert the system of travel time equations describing straight ray paths through all seven cross-sections. The single cross-section inversions indicated that the Kesterson travel times could be co-inverted for three regional slowness populations.

The initial convergence of the MPI is slower than unconstrained-value tomography, but both inversion methods converge to approximately the same average absolute travel time residual on the tenth iteration (Figure 3-5). By constraining the slowness to just three populations with the MPI we have parsimony. With no other available information, the constrained slowness model from the MPI is a better choice than the unconstrained slowness model.

Kesterson Well Field

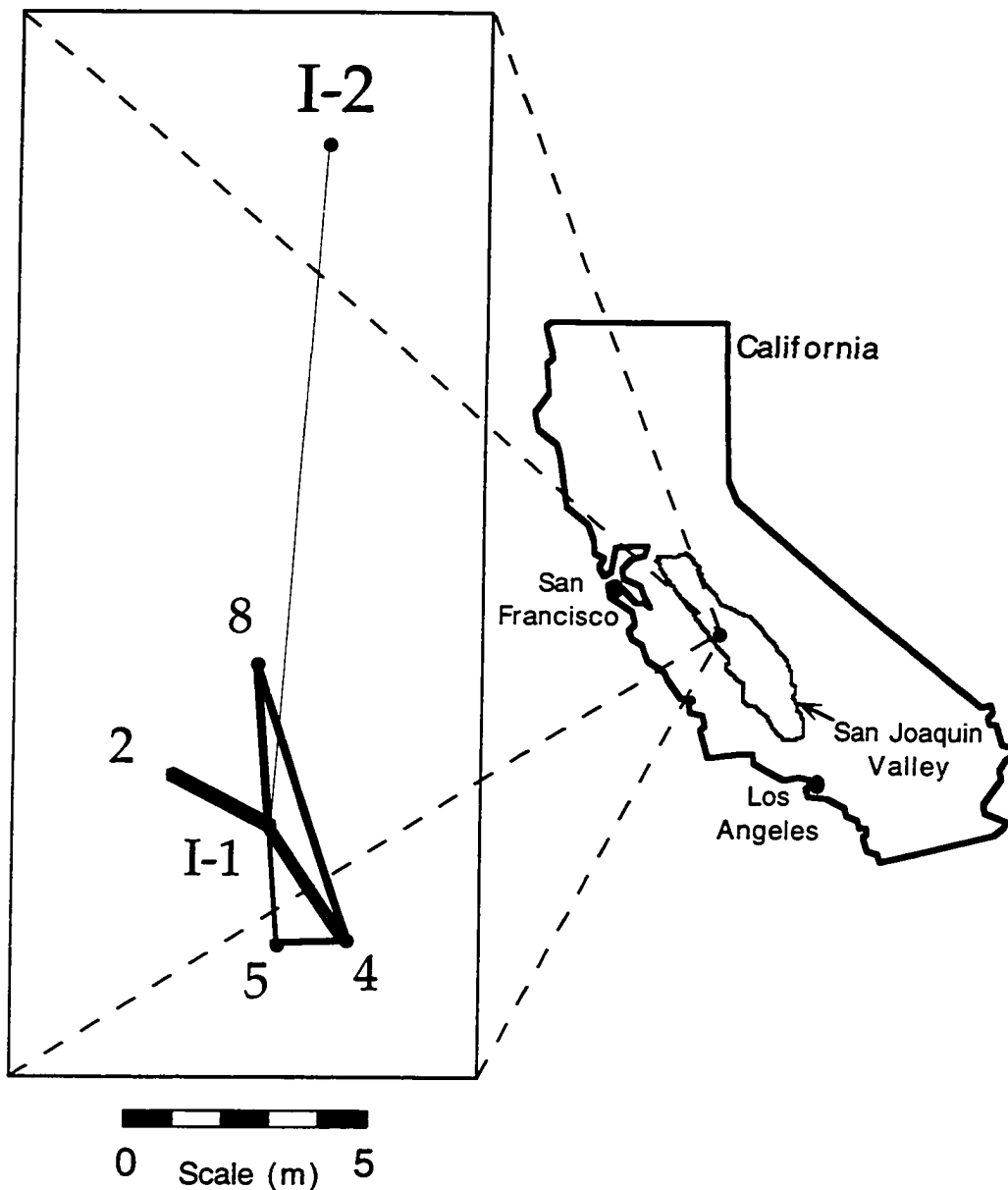


Fig. 3-4. Well field at the Kesterson Reservoir field site located in central California. Cross-well seismic travel times were collected along the cross-sections between the numbered wells. Figure 3-6 illustrates the slowness estimates in two dimensions by unfolding the sections from thin to thick lines.

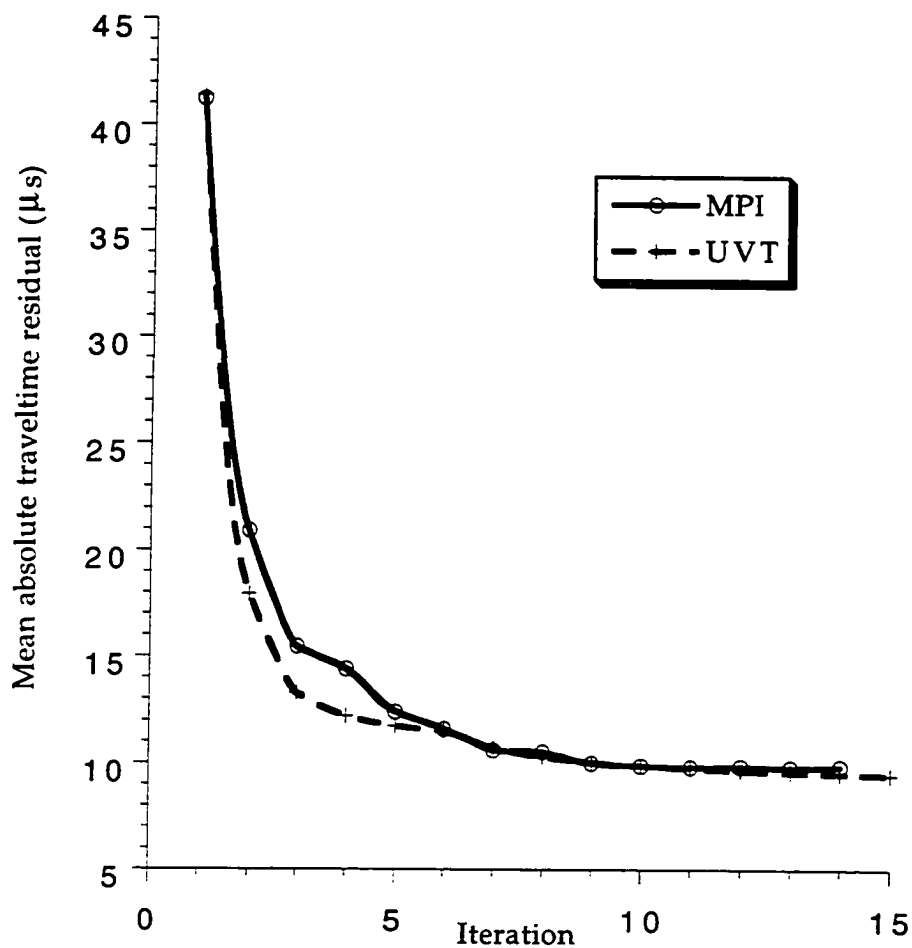


Fig. 3-5 Comparison of mean travel time residuals for iterations of the multiple population inversion (MPI), and unconstrained-value tomography (UVT) for the Kesterson field data.

The MPI's convergence rate increased after the fourth iteration because a third population was introduced (Figure 3-5). For the first four iterations, 30 percent of values were allowed to change to two populations, then 10 percent of the values were allowed to change to three populations for the remainder of the iterations. These percentages were determined using sensitivity analysis, and we found that the inversion was not very sensitive to these parameters. The significant decrease in residuals resulting from the addition of a third population indicates that this is a reasonable addition to the slowness model. The convergence of the travel time residuals to approximately the same value as the unconstrained tomography indicates that three populations are probably sufficient to describe the heterogeneity at this site.

Figure 3-6 illustrates the nature of heterogeneity in the Kesterson aquifer by unfolding the tomograms into a plane as described in Figure 3-4. The tomograms obtained from unconstrained-value tomography and MPI show that the aquifer has much higher continuity of structure in the horizontal dimension relative to the vertical dimension, but the aquifer is not perfectly stratified. The three population tomograms, derived from MPI, describe the main heterogeneity seen in the unconstrained-value tomograms. The tomograms from both methods show good correlation at the wells and provide consistent regional slowness estimates. Since the MPI slowness values are constrained, we can estimate the slowness tomograms without smoothing, which is often used to reduce inversion artifacts. The MPI can thus locate and describe smaller scale variability than tomographic methods that rely on smoothing for stability.

The histogram of slowness perturbations is dramatically narrowed using the MPI. Figure 3-7a illustrates this histogram of slowness perturbations for all pixels of the homogeneous starting model, and Figure 3-7b illustrates the histogram for all pixels of the three population model. This final relatively symmetric distribution of perturbations contains only small values clustered around zero, again indicating that the three estimated seismic slowness populations adequately describe this region of the Kesterson aquifer.

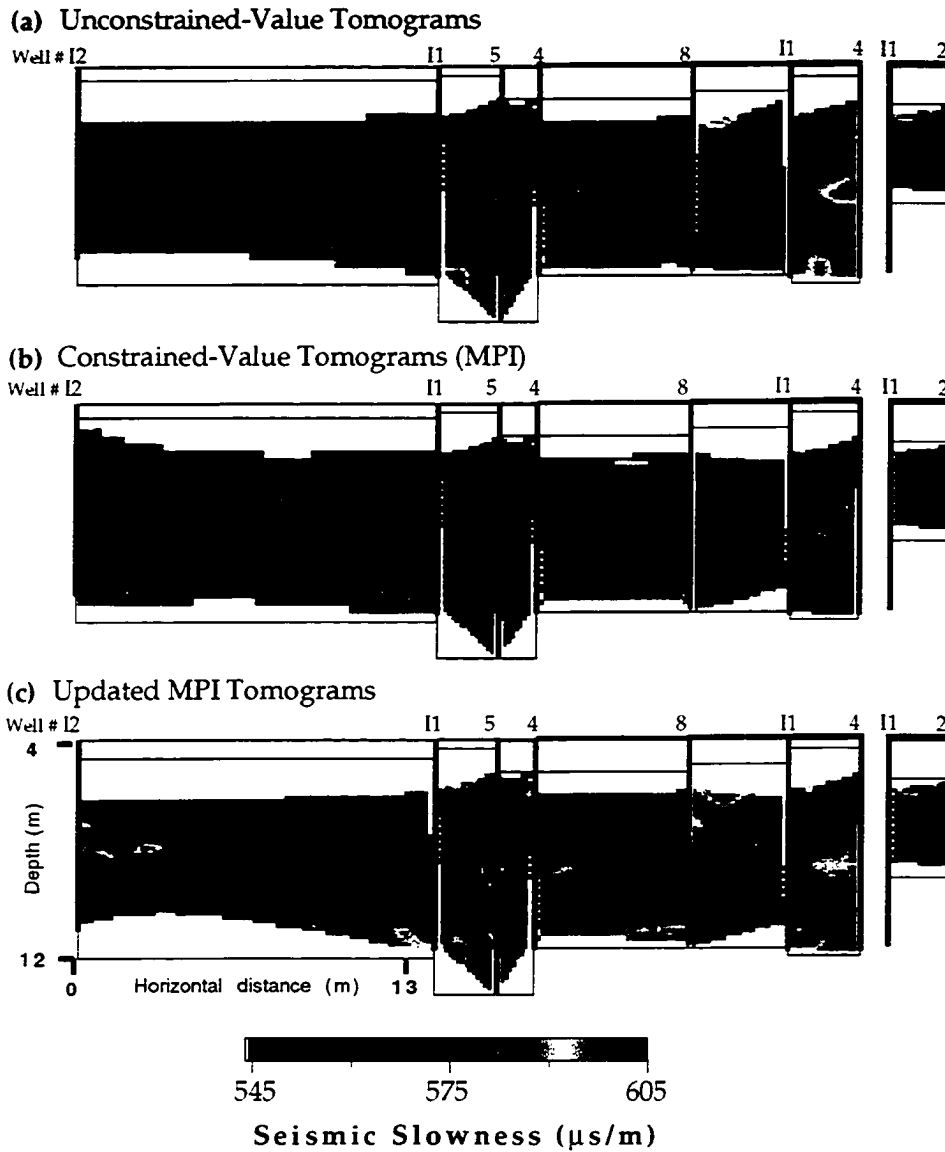


Fig. 3-6. Comparison of slowness tomograms for the Kesterson aquifer estimated using: (a) unconstrained-value tomography, (b) the multiple population inversion (MPI), and (c) updated MPI estimates using unconstrained-value tomography. The updated MPI tomograms are shown in three dimensions in Figure 3-8.

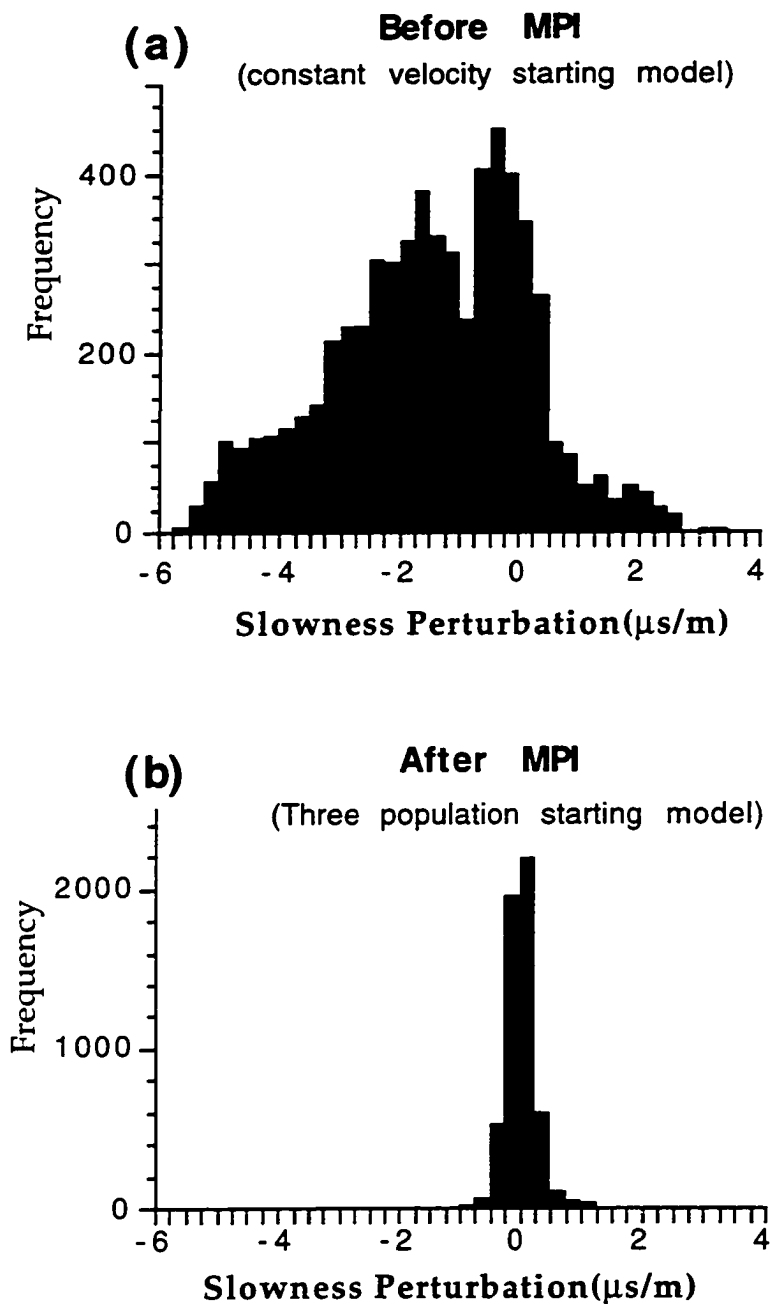


Fig. 3-7. Histograms of spatially distributed slowness perturbations (a) before and (b) after the multiple population inversion.

The three population slowness model was then used as a starting model for unconstrained-valued inversions. The resulting estimates preserve the general large-scale structure and add some smaller perturbations to the estimates (Figure 3-6c). Since the general structure of the estimates did not change when the slowness constraints were relaxed, the assumption of three slowness populations appears to be reasonable. The most notable changes were in the cross-section from I1 to I2, which is expected since this cross-section has the least ray path coverage, thus the greatest uncertainty. The updated three population estimates, which are also illustrated in three dimensions (Figure 3-8), appear geologically reasonable for alluvial deposition.

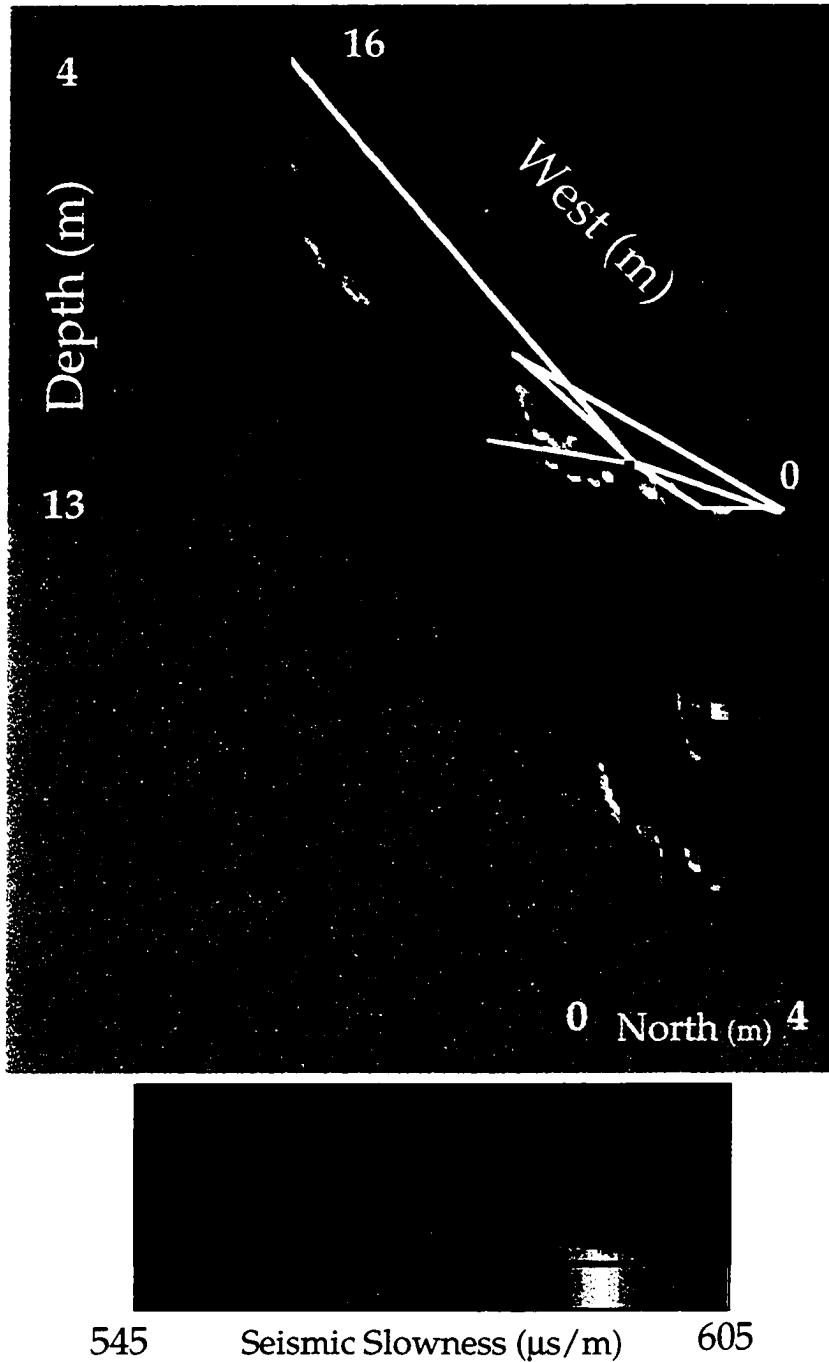


Fig. 3-8. Seismic slowness fields estimated using the multiple population inversion (MPI) then updated using unconstrained-value tomography. The histogram illustrates the distribution of slowness values.

DISCUSSION

In this paper, we develop the multiple population inversion (MPI) to estimate the spatial distribution of a small number of seismic slowness populations and determine mean slowness values for each population. We present the application of the MPI to cross-well seismic *P-wave* arrival times for both synthetic and field data. We have shown that the MPI is a useful method to extract the structure of dominant seismic slowness populations from travel time data.

For the synthetic aquifer, the MPI accurately characterized the structure of two slowness populations, resulting in a smaller average travel time residual than obtained from unconstrained-value tomography. Since reasonable constraints on the slowness model actually improve the objective value, the MPI method is a better approach for this case. The split inversion method (SIM) was also used for comparison. For the synthetic data set, the SIM also generates accurate results, however it is less efficient and relies on more assumptions than the MPI. The primary advantage of the SIM is its flexible objective function that can easily combine multiple data types to estimate the aquifer zonation.

For the shallow Kesterson aquifer, the MPI co-inverted travel times between seven well pairs to provide a regional three-population slowness estimate. For comparison, unconstrained-value tomograms were independently estimated for each cross-section. Both methods converged in ten iterations to approximately the same travel time residual. The tomograms from both methods are fairly consistent where they intersect at wells. Given that no significant improvement is gained by allowing the values of slowness to be unconstrained, the MPI appears to be a better method for inverting the data from this field site. The MPI also appears to resolve detailed structures, which could be fine layers that control fluid flow, better than methods which rely on smoothing the slowness model.

The application of cross-well seismic techniques to shallow aquifers appears promising, although extreme care must be taken to accurately survey the well field. Unlike petroleum applications which involve distant wells, we are dealing with wells from 1.5 to 14 meters apart and minor errors in the measurement of offset between wells can have significant effects on the estimated slowness values. At the Kesterson site, the distance between wells was measured with a tape measure and the wells were assumed to be deviated but straight, thus the deviation was measured as an angle from vertical and a horizontal azimuth angle. This provided reasonable results although the offset between several well pairs had to be adjusted slightly. We determined that very minor adjustments to the well offsets improved the coherency between cross-sections and reduced the travel time residuals in the co-inversion. The largest adjustment was just over one percent of the well offset, which is within the range of surveying error.

The next stage of this research will be to combine tracer data with seismic travel times to estimate the three-dimensional structure of the Kesterson aquifer. If no tracer data were available at this site, estimates of the hydraulic properties would be derived from either core data or local pump test data. If the lithologies could be identified from the original well logs or core data, lithologic information could be assigned to the seismic slowness zones and initial estimates of the hydraulic properties could be made. Well log data would also be useful to verify the estimates at the well, however this information is not available in this region of the Kesterson aquifer. In Chapters 4 and 5, we estimate the hydraulic properties in three dimensions at the Kesterson site using seismic and tracer data.

CHAPTER 4:

MAPPING LITHOLOGIC AND TRANSPORT PROPERTIES IN THREE DIMENSIONS USING SEISMIC AND TRACER DATA: THE KESTERSON AQUIFER

ABSTRACT

The identification of aquifer heterogeneities, particularly flow paths and barriers, has become a critical research topic in hydrology. Cross-well seismic tomography may provide the needed resolution when used in conjunction with either pump test or tracer data. We demonstrate a field application and sensitivity analysis of the split inversion method (SIM), which combines seismic and tracer data to estimate the three-dimensional zonation of aquifer properties along with the hydraulic properties for these zones. For the Kesterson aquifer in the central valley of California, we first invert seismic travel times between six well pairs to obtain seismic slowness ($1/Seismic\ Velocity$) cross-sections or tomograms. We then use conditional simulation to provide three-dimensional seismic slowness realizations. Next, the SIM is used to split several realizations into three lithologic zones and assign hydraulic properties to the zones to best match six concentration histories for a multiple-well tracer test with an injection/withdrawal well pair.

INTRODUCTION

Spatial variability of hydraulic conductivity provides a predominant control on groundwater flow and solute transport. Hydraulic conductivity varies over several orders of magnitude for different lithologies, and aquifers generally exhibit complex lithologic patterns. Thus, accurate conductivity estimates are needed to predict the fate of contaminants in aquifers and to efficiently design remedial schemes for contaminated sites.

Hydraulic conductivity values are typically derived from a small number of estimates at wells and from well pump tests [Yeh, 1986]. At highly heterogeneous sites, these data are inadequate to fully describe the conductivity variations. A common approach is to parameterize the domain into homogenous zones and assign a hydraulic parameter to each zone [Cooley, 1977; Cooley, 1979], however, there are rarely enough data to uniquely parameterize a region into meaningful zones and determine the conductivity value for each zone [Yeh, 1986].

A potential solution to this problem is to use densely sampled geophysical information to help determine parameter zones and values. Geophysical methods, such as cross-well seismic tomography, can be used to infer the pattern of lithologies between wells. Cross-well seismic tomography is the process of inverting seismic travel times for a seismic slowness ($1/Seismic\ Velocity$) image between wells. It is similar to the computer aided tomography (CAT) scan used in medical imaging [Dines and Lytle, 1979], however one uses sound waves to image subsurface geology rather than using X-rays to image the human body. Seismic tomography has been used to successfully characterize petroleum reservoirs, but it has rarely been used to characterize shallow aquifers.

Several authors have indicated that seismic information can be used to determine the hydrogeologic properties of aquifers and reservoirs. *Araktingi and Bashore* [1992] explored the effect of adding three-dimensional surface seismic data to well-log data for petroleum reservoir characterization. *Coptly* [1994] presented a stochastic method that combines surface seismic data and lithologic logs to identify subsurface lithologies. *Doyen et al.* [1991] estimated lithologies from seismic data and lithologic observations in wells using a Monte-Carlo approach. *Rubin et al.* [1992] developed an approach to invert pore pressure data for a permeability field, given perfect knowledge of the seismic velocity field and

a known relation between seismic velocity and permeability. This method was then extended by *Coptly et al.* [1993] to estimate the spatial distribution of permeability given a seismic velocity field with spatially uncorrelated errors. A significant limitation of these methods is their reliance on knowledge of the relation between seismic velocity and the hydrogeologic properties (lithology or permeability), which is generally unknown at the field scale.

To address this limitation, *Hyndman et al.* [1994] introduced the theoretical concept of the split inversion method (SIM) that does not rely on knowledge of the relationship between seismic velocity and hydraulic conductivity. The SIM co-inverts seismic travel times and tracer concentration histories for the zonation of lithologies, hydraulic conductivity values for each zone, and the value of dispersivity for the region. The motivation for the SIM is that seismic energy and tracer concentrations have each independently sampled regions of the same physical environment. Their combined analysis can improve the description of this environment relative to estimates made with either data set alone. Cross-well seismic travel times provide densely sampled spatial information along planes between wells, which complements the spatially-averaged three-dimensional information from pump tests and tracer tests. *Hyndman et al.* [1994] demonstrated the SIM for two synthetic sandy aquifers, one with embedded clay zones and the other with embedded silt and gravel zones. These examples illustrated the ability of the SIM to estimate the hydraulic conductivity field despite an unknown and non-unique relation between seismic velocity and conductivity. The SIM accurately estimated the lithologic zonation and hydraulic parameters for both examples.

In this paper, we demonstrate a field application and sensitivity analysis of the SIM. Cross-well seismic travel times and tracer concentration arrival histories from the Kesterson aquifer in California's central valley are jointly analyzed to identify the lithologic zonation and hydraulic conductivity values. We will show that seismic and tracer information can be combined to estimate the three-dimensional structure of aquifer lithologies and the zonal hydraulic conductivities and a single dispersivity value for this site. This work extends the concept of *Hyndman et al.* [1994] to the case of three dimensions with three unique zonal lithologic classes.

HYDROGEOLOGIC SETTING

Several regional groundwater studies have been completed in the San Joaquin Valley, California, due to the importance of the region's agriculture [National Research Council, 1993]. The U. S. Geological Survey conducted a regional study in the San Joaquin Valley to evaluate the aquifer system, identify changes due to development, and simulate past and present conditions [Williamson *et al.*, 1989]. Belitz *et al.* [1992] then developed a three-dimensional groundwater flow model of the central part of the Western San Joaquin Valley to assess alternatives to agricultural drains. These studies offer some insight into the characteristics of the aquifer.

The shallow aquifer below Kesterson reservoir, which is located in the San Joaquin Valley, was contaminated with agricultural return water during the six year operation of the reservoir ending in 1986. Regional collector drains were installed in the western part of the valley in the early 1980s to prevent reduced agricultural production due to shallow saline water. This saline water was pumped from the collector drains to Kesterson reservoir where approximately 50 percent of the water seeped into the ground [Benson *et al.*, 1991].

The Kesterson site received public attention when a high rate of deformities was found in the embryo of waterfowl that nest in the Kesterson region. These deformities were linked to high selenium concentrations in the water discharged to Kesterson reservoir. The naturally occurring selenium leached from the irrigated farmlands of the San Joaquin Valley [Ohlendorf *et al.*, 1986].

The sediments of the shallow semi-confined Kesterson aquifer were deposited by the San Joaquin River, which meandered through the valley depositing sand and silt from the Sierra Nevada. These sediments are stratigraphically above and thus younger than the Corcoran clay, which is approximately 620,000 years old [Dalrymple, 1980]. The Corcoran clay, which is the major confining layer for the deeper aquifers, is approximately 75 meters deep in the San Joaquin Valley trough [Hotchkiss and Balding, 1971]. Widespread lacustrine clay deposits such as the Corcoran are present at several depths throughout the valley. One of these clays, at approximately 20 meters depth, separates the aquifer that is the focus of our study from the deeper semi-confined aquifer [Benson, 1988]. The saturated thickness of the shallow aquifer is

approximately 19 meters since the water table at the Kesterson site was approximately one meter deep in 1985 [Benson, 1988].

We use two data sets to map the heterogeneous hydraulic properties of the shallow Kesterson aquifer, tracer concentration histories and seismic travel times. A multiple well fluorescein tracer test was conducted in the shallow Kesterson aquifer by [Benson, 1988] to predict the movement of the selenium plume and determine the nature of heterogeneities at the site. In addition, seismic travel times were collected between six well pairs that cover the central portion of the tracer test [Ernie Majer, personal communication, 1994]. Figure 4-1 is a map of the Kesterson aquifer with lines connecting the well pairs used in the seismic test and gray dots at the locations of the tracer measurement wells. The well screens were located at different depths (Table 4-1) to provide sensitivity to hydraulic conductivity with depth.

In the remainder of this paper, we demonstrate how these seismic and tracer data are combined to deduce the lithologic zonation and flow and transport properties of the shallow Kesterson aquifer. First, the seismic travel times for all available well pairs are co-inverted for two-dimensional slowness tomograms through the aquifer. Geostatistical methods are then used to generate equally likely three-dimensional conditional slowness realizations. Finally, randomly chosen realizations, which are conditioned to the six two-dimensional tomograms, are split into three lithologic populations and each population is assigned a hydraulic conductivity value to best match the tracer data. In this manner, seismic travel times provide an estimate of the lithologic structure, then tracer concentrations are used to split the seismic estimate into lithologic zones and assign conductivity values to each zone.

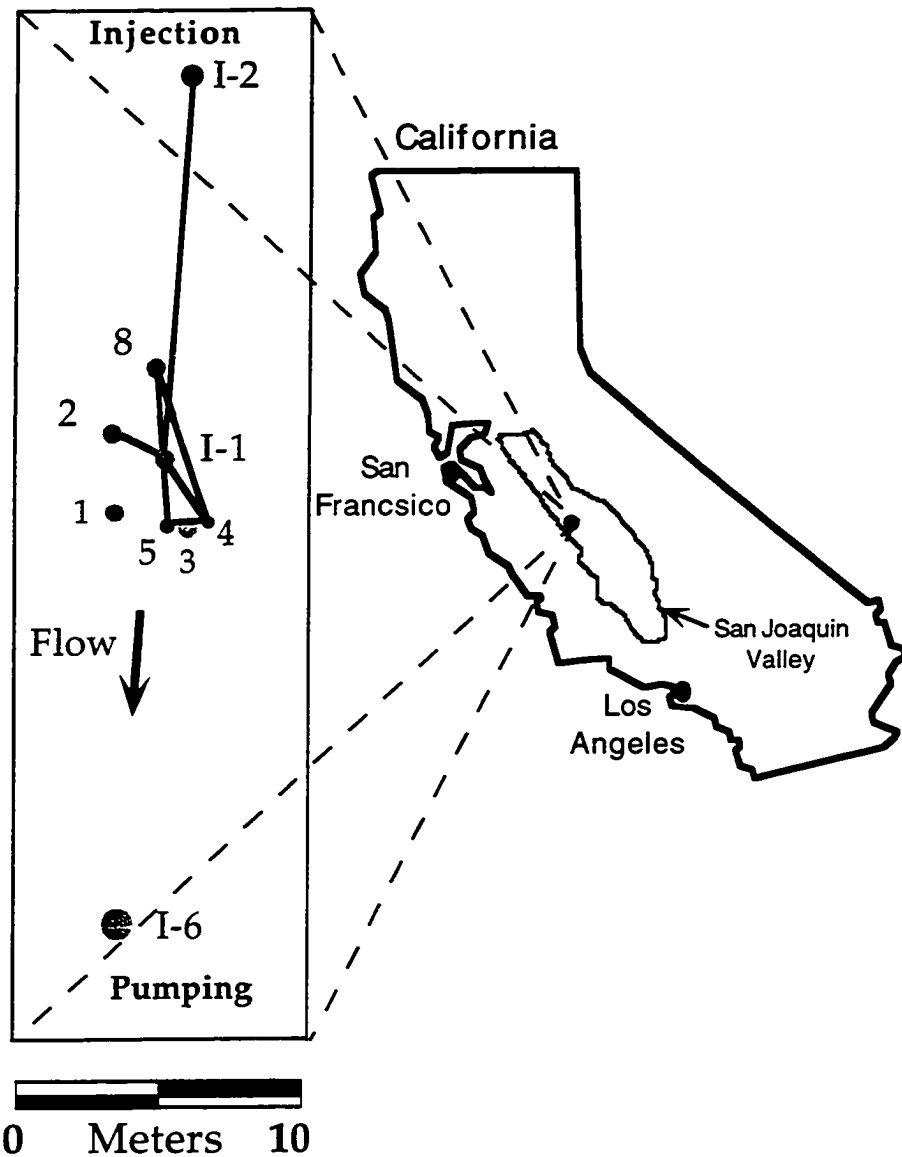


Fig. 4-1 Site map for the Kesterson Aquifer located in California's San Joaquin Valley. At this site, seismic traveltimes were collected between the six well pairs connected with black lines. Water was pumped at well I6 and reinjected at well I2. A pulse of fluoroscein dye was injected into well I2 and the resulting concentrations were measured at the six gray wells throughout the 10 day tracer test.

Table 4-1. Kesterson Tracer Well Locations and Conductivities
(after *Benson* [1988])

Well	X coordinate (m)	Y coordinate (m)	Screened Interval (m)	Diameter (m)	Hydraulic Conductivity (m/s)
I2	-0.5734	16.1150	6.1 - 12.2	0.10	2.1×10^{-4}
ST1	-3.3822	0.9600	6.1 - 7.6	0.05	6.0×10^{-4}
ST2	-3.4336	3.3700	7.6 - 9.1	0.05	5.9×10^{-4}
ST3	-0.6498	-0.0500	9.1 - 10.7	0.05	1.6×10^{-4}
ST4	0.0900	0.0000	10.7 - 12.2	0.05	2.4×10^{-4}
ST5	-1.3557	-0.0300	12.2 - 13.7	0.05	–
ST8	-1.8284	5.6300	10.7 - 12.2	0.05	–
I1	-1.5034	2.3430	6.1 - 12.2	0.10	3.4×10^{-4}
I6	-3.3988	-13.8738	6.1 - 12.2	0.10	1.4×10^{-4}

SEISMIC INVERSION

The first stage in estimating the hydraulic properties of the shallow Kesterson aquifer involved collection of seismic travel times (data provided by Ernie Majer, Lawrence Berkeley Laboratory), which were inverted for seismic slowness ($\frac{1}{\text{Seismic Velocity}}$) cross-sections at the site. Seismic energy (sound waves) of a predetermined frequency was generated at equal depth intervals in the source well (0.3 meters for the Kesterson site). There were between 13 and 23 source locations per well. The resulting signal from each source was measured at 12 to 29 receivers (0.3 m interval) in nearby wells. For this experiment, the seismic source was a piezo-electric bender bar and the receivers were hydrophones. Sound waves of specified frequency (1 - 10 kilohertz) were generated at the source by controlling an electric current through the piezo-electric material, which expands and contracts in response to this current. The measured signal is an amplitude plot that can be compressed into a few key measures such as travel times and amplitudes, which can then be inverted for geophysical properties. The compressional-wave travel times between each source and receiver serve as our data for cross-well seismic tomography, although as discussed in our conclusions seismic amplitudes could be inverted for attenuation coefficients that may also be correlated to hydraulic properties.

We used an algorithm, called the multiple population inversion (MPI), to invert all the measured Kesterson travel times for the geometry of three slowness populations [Hyndman and Harris, 1995]. The objective of the MPI is to minimize the average absolute travel time residual for all source-receiver pairs with measured travel times. The MPI constrains the slowness field to a specified number of values, which reduces artifacts commonly seen in unconstrained tomographic inversions without smoothing the estimated image. Smoothing is the most common method of reducing artifacts from ray-based tomographic inversions, but smoothing reduces the ability of the inversion to resolve small scale heterogeneities.

The MPI converged to approximately the same objective value as obtained from an unconstrained form of this tomographic inversion, despite the constraint that only three slowness values were allowed for the region [Hyndman and Harris, 1995]. This indicates that a model with only three discrete slowness values is a reasonable description of the subsurface. The zonal estimate was then used as a

starting model for an unconstrained tomographic inversion, which preserved the large-scale structure and added some finer scale heterogeneities. This was done because unconstrained iterative inversions work well when the starting model is close to the true slowness field, and the unconstrained estimates can be used to infer the correlation structure of the Kesterson lithologies. These updated slowness tomograms are shown in Figure 4-2 with a corresponding histogram of the estimated values. The estimated slowness cells are 15 cm on a side, providing very dense information about the seismic slowness structure of the aquifer. The size of these cells is controlled by the vertical spacing of sources and receivers (30 cm), and by the wavelength of the seismic signal. The finest resolution possible from a seismic signal is approximately a quarter wavelength (λ), which is calculated using $\{\lambda/4. = 0.25 / (f * S)\}$ to be approximately 4 cm for the mean Kesterson slowness (S) of 574. $\mu\text{s}/\text{m}$ and a frequency (f) of 1000. Hz.

These slowness tomograms (Figure 4-2) illustrate an irregularly shaped low slowness region dipping slightly to the south through the aquifer, and several less continuous high slowness regions. These slowness regions appear as different populations in the histogram (Figure 4-2) with high slowness corresponding to high conductivity and low slowness corresponding to low conductivity. Although these slowness regions may represent different lithologies, other data, such as tracer concentrations, are needed to determine the zonation and aquifer properties.

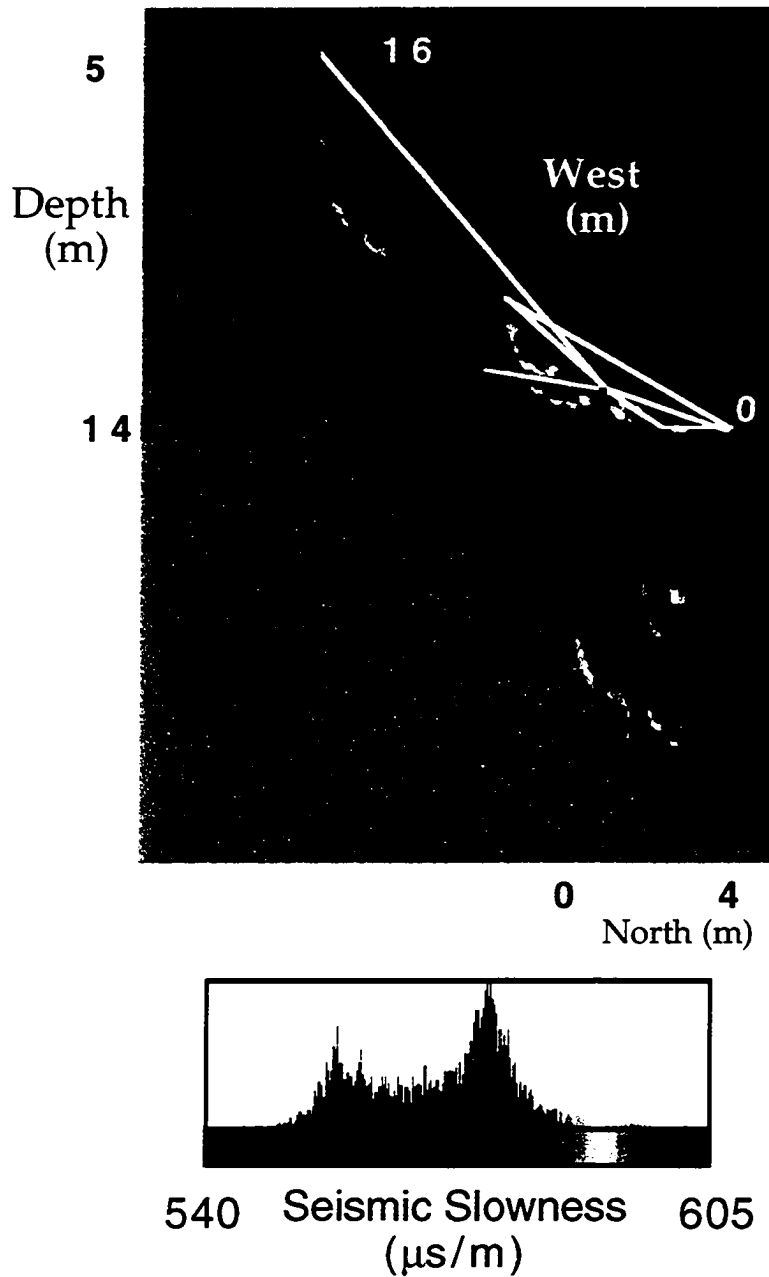


Fig. 4-2. Three-dimensional layout of seismic slowness estimates at the Kesterson site, in which the red lines represent well locations. Wells ST5 and ST4 are on the close side of the image and well I2 is at the top (See Figure 4-1 for location map). The histogram illustrates the bimodal nature of the slowness estimates at the site.

EXTENSION FROM MULTIPLE 2D IMAGES TO 3D USING CONDITIONAL GEOSTATISTICS

Although the two-dimensional slowness tomograms provide useful information about the nature of heterogeneity at the site, we would like estimates of the aquifer properties in three dimensions. Full three-dimensional slowness estimates can be extrapolated from the tomograms using geostatistical methods, such as kriging and conditional simulation.

The range of likely correlation parameters for these conditional simulations can be inferred from the tomograms in Figure 4-2. Figure 4-3 illustrates the calculated sample variograms from both a single tomogram (between wells 4 and 8) and a joint analysis of all the tomograms. We first estimated the correlation lengths by fitting exponential variograms ($\lambda_h = 5 - 9$ m, $\lambda_v = 0.9$ m, $\sigma^2 = 104$.) to these sample variograms (Figure 4-3). These values are for seismic slowness. We then explored a range of correlation lengths and found that realizations generated with a horizontal correlation length of 9 meters and a vertical correlation length of 0.9 meters best fit the tracer data, as discussed in the sensitivity analysis section. If long tomograms had been available in multiple directions, we also could have estimated the direction and magnitude of the horizontal anisotropy. The estimated sample variance appeared to be isotropic, thus only the correlation lengths changed with direction.

For this study, we used sequential gaussian simulation to generate equally-likely slowness realizations that are conditioned on the six slowness tomograms with different orientations. We refer to these slowness tomograms as "data". The steps of this conditional simulation approach are [Deutsch and Journel, 1992]:

- 1) Transform the slowness estimates (mean = 574. $\mu\text{s}/\text{m}$, variance = 104.) to have a standard normal probability distribution (mean = 0., variance = 1.0) using a normal scores transform;
- 2) Generate a random path that visits each node of the three-dimensional grid once;
- 3) For each node, determine the mean and variance of the conditional distribution function using simple kriging of the normally distributed slowness "data", using an anisotropic search radius (vertical = 0.1 \times horizontal) and a variance of 1.0. Then draw a simulated value from this conditional distribution and add this simulated value to the data set. Continue along the random path until all locations are estimated;

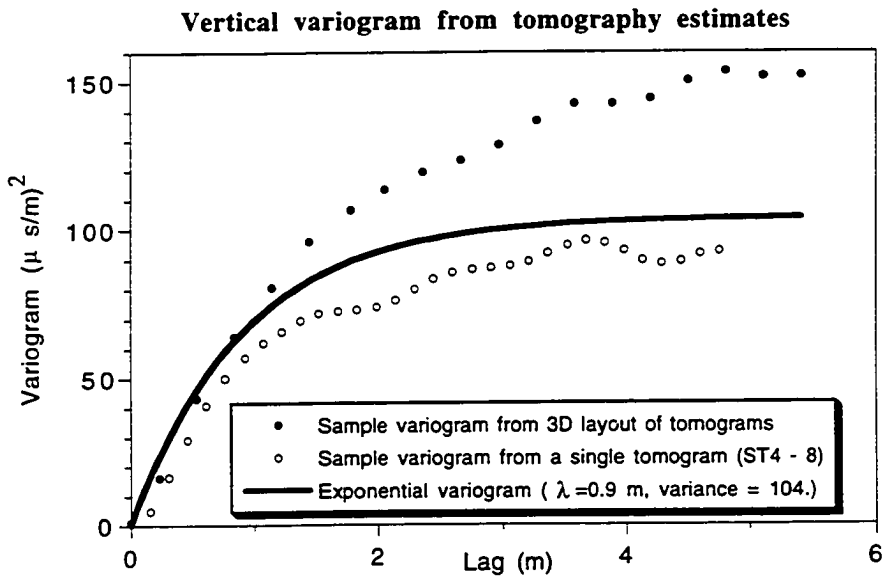
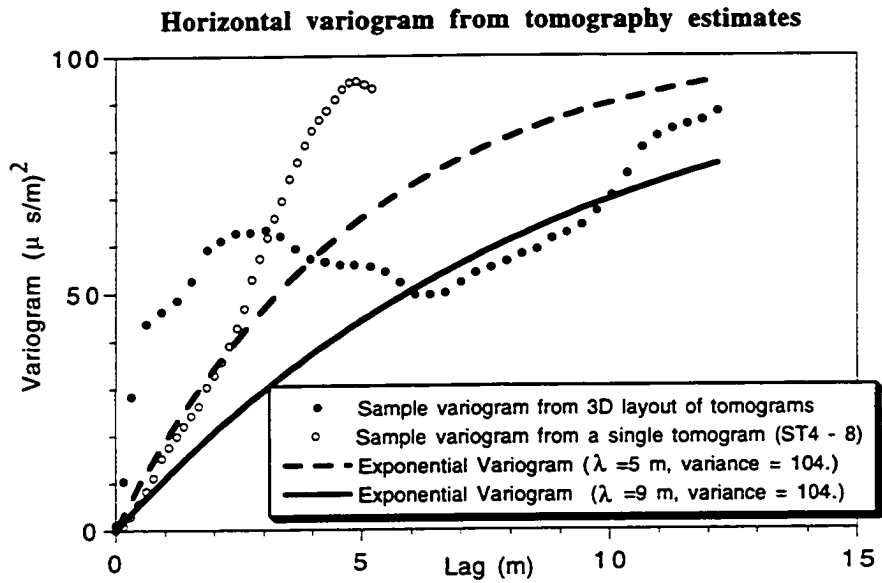


Fig. 4-3. Horizontal and vertical variograms derived from the tomographic slowness estimates in Figure 4-2. Exponential fits to these sample variograms are also illustrated.

- 4) Back transform the normally-distributed three-dimensional estimates to have the original distribution of values (mean = 574. $\mu\text{s}/\text{m}$, variance = 104.), using the reverse of the transform used in step 1.

Each estimated value is thus a weighted average of the "data" and previously simulated points, with the weights specified by the estimated horizontal and vertical variograms (Figure 4-3). Each realization from this method preserves the seismic slowness values along the six tomographic planes (Figure 4-3), the slowness histogram, and the horizontal and vertical correlation structure from the specified variograms. This approach also preserves the probability distribution of the two-dimensional slowness estimates, as illustrated by the nearly perfect agreement between histograms in Figures 4-2 and 4-3.

Figure 4-4 illustrates a randomly chosen slowness realization generated with an exponential variogram ($\lambda_h = 9. \text{ m}$, $\lambda_v = 0.9 \text{ m}$, $\sigma^2 = 104.$) for the Kesterson aquifer. The cell size for these realizations is 1.5 meters on a side and 0.4 meters vertically, which preserves most of the structure from the tomograms but is a reasonable grid size for solute transport simulation. Figure 4-3 is illustrated with additional interpolated cells for visual clarity (four times the horizontal cells and two times the vertical cells with linear interpolation).

Each realization preserves the slowness values at locations where we have conditioning data from the tomograms, but away from the conditioning data the realizations can differ significantly from one realization to the next. Thus, the uncertainty in our three-dimensional slowness estimates is low near the tomograms and high near the edge of each estimated slowness realization.

The next stage of our approach is to include the analysis of the tracer data. The slowness realizations are split into zones using the split inversion method (SIM) and these zones are assigned flow and transport parameters to match the tracer data. In this paper, the results are shown for just one slowness realization, although the SIM was repeated for several realizations. The results were similar for five realizations with the same variance and correlation lengths because of the large quantity of conditioning "data" in the region of the tracer test.

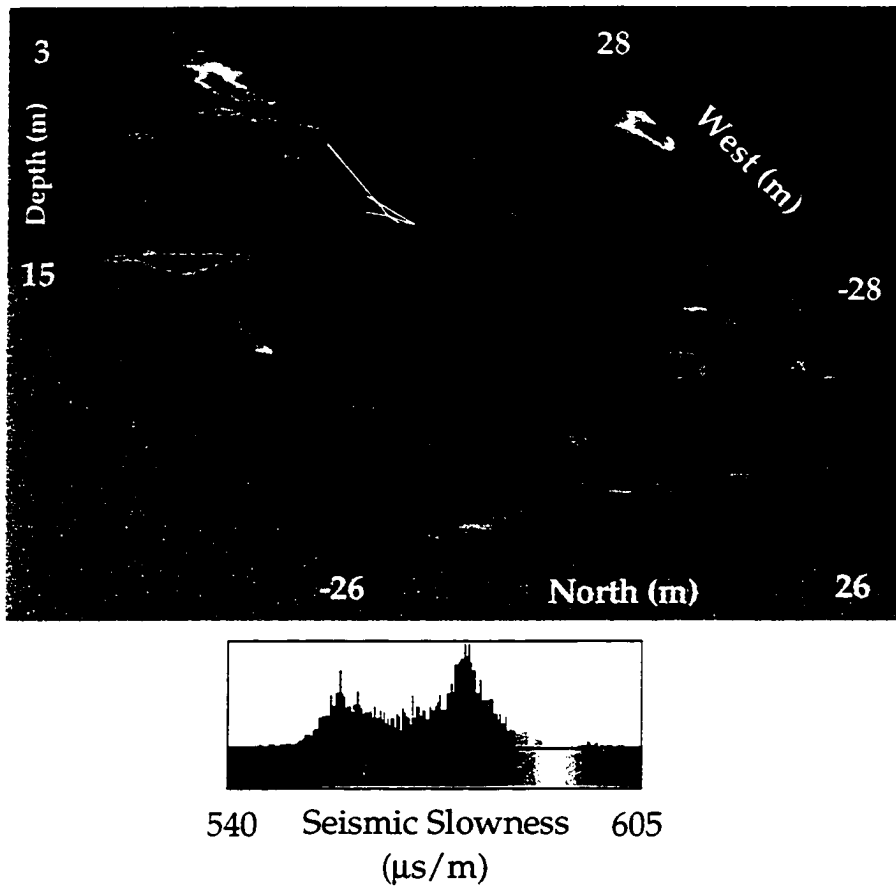


Fig. 4-4. Three-dimensional realization of seismic slowness generated using sequential Gaussian simulation. This approach preserves the specified horizontal and vertical correlation lengths and the slowness probability distribution from the seismic tomograms (compare to histogram in Figure 4-2). The resulting image provides a geologically reasonable estimate for the Kesterson site.

TRACER INVERSION

In July, 1986, *Benson* [1988] completed a multiple-well tracer test with an injection/withdrawal well pair to infer the flow and transport properties of the shallow Kesterson aquifer. The pumping and injection rates were maintained at $4.73 \times 10^{-3} \text{ m}^3/\text{s}$ (75 gallons/minute) for 24 hours. A 3180 second (53 minute) pulse of fluorescein dye was then put into the injection well providing an inflow concentration of approximately 320 ppm [*Benson*, 1988]. Fluorescein is a weakly sorbing tracer as determined by *Smart and Laidlaw* [1977] using batch experiments with different sediments. Thus, for this study we assume that fluorescein is a conservative tracer. The resulting concentrations were then measured throughout the following ten days at six down gradient wells (see Figure 4-1 and Table 4-1 for well locations and depths). These six concentration histories serve as the data to determine the lithologic zonation and hydraulic properties for each zone.

The split inversion method (SIM) was used to split the three-dimensional slowness realizations into three populations, estimate the hydraulic conductivity for each population, and infer a regional dispersivity value. In other words, the SIM splits the slowness realizations into zones that represent different lithologies. The lithologies can be inferred from the hydraulic property estimates, knowledge of the regional geology, and correlation of the estimates with lithologic logs.

Tracer tests provide information that can be used to infer the flow and transport properties of porous media. The SIM is implemented as a simulation-regression algorithm [*Gailey et al.*, 1991; *Wagner and Gorelick*, 1987] to best match the measured concentration histories for six physically-based parameters. These parameters are: two seismic slowness values that split the slowness realizations into zones, three hydraulic conductivity values (one for each slowness zone), and a single longitudinal dispersivity value (assuming $\alpha_t = 0.2 \alpha_\ell$) for the region (Table 4-2). Using these parameters, we simulate steady-state groundwater flow and nonreactive solute transport through the Kesterson aquifer using numerical approximations to the three-dimensional groundwater flow equation (4.1), Darcy's Law (4.2), and the three-dimensional advection-dispersion equation (4.3).

Table 4-2. Kesterson Aquifer Parameter Estimates

Parameter	Value
Low Slowness Split ($\mu\text{s}/\text{m}$)	569.4
High Slowness Split ($\mu\text{s}/\text{m}$)	587.8
Hydraulic Conductivity (m/s)	
(Low Slowness zone)	1.4×10^{-4}
(Mid Slowness zone)	3.6×10^{-4}
(High Slowness zone)	5.0×10^{-4}
Dispersivity (m) - Longitudinal[*]	9.1×10^{-2}
Transverse [‡]	1.8×10^{-2}

* Determined using sensitivity analysis

‡ Fixed at $0.2 \times$ longitudinal dispersivity

$$\nabla \cdot (\mathbf{K} \nabla h) = W \quad (4.1)$$

$$\mathbf{v} = - \frac{\mathbf{K} \nabla h}{\theta_e} \quad (4.2)$$

$$\frac{\partial c}{\partial t} + \nabla \cdot (\mathbf{v} c) - \nabla \cdot (\mathbf{D} \nabla c) = \frac{c' W}{\theta_e} \quad (4.3)$$

where

- ∇ gradient operator, $(\partial/\partial x, \partial/\partial y, \partial/\partial z)$;
- x, y, z Cartesian coordinates, {m};
- \mathbf{K} hydraulic conductivity, {m/s};
- h hydraulic head, {m};
- W fluid source sink term (positive for source), {1/s};
- \mathbf{v} vector groundwater velocity components, {m/s};
- θ_e effective porosity, {-};
- c tracer concentration in pore fluid, {ppm};
- c' tracer concentration in source or sink, {ppm};
- t time, {s};
- \mathbf{D} $\mathbf{D} = \mathbf{D}(\alpha_l, \alpha_T, \mathbf{v})$, hydrodynamic dispersion coefficient, {m²/s};
- α_l, α_T longitudinal and transverse dispersivities, {m}.

The effective porosity is assumed to be homogeneous at 30 percent [LBL, 1986; Liu and Narasimhan, 1994], which is reasonable since porosity is known to vary over a much smaller range than hydraulic conductivity. The tracer velocity scales proportionally to hydraulic conductivity divided by effective porosity according to Darcy's law (4.2), thus the quantity conductivity over effective porosity is the parameter we are estimating using tracer data. If the assumed effective porosity is incorrect, the hydraulic conductivity estimates should be scaled by the ratio of true to assumed porosity. If adequate head data were available, both the conductivities and effective porosities could perhaps be simultaneously estimated.

The objective of the SIM was to minimize the sum of squared residuals between measured and simulated tracer concentration arrival time quantiles at the six measurement wells (4.4). The zonation of the slowness image and the hydraulic conductivity values are adjusted to minimize this objective value. Each tracer concentration history was represented using nine quantiles. Each quantile represents the time at which a specified percent (e.g., 10%, 20%, ... 90%) of the tracer mass passes the measurement well.

$$\text{Minimize} \left(\left(\sum_{i=1}^9 (\tau_{i,\text{meas}}^w - \tau_{i,\text{sim}}^w)^2 \right) + \beta \left((\Delta h_{\text{meas}} - \Delta h_{\text{sim}})^2 \right) \right) \quad w = 1, 2, 3, 8, 12, 16 \quad (4.4)$$

where:

- R** sum of squared residuals, {days²};
- $\tau_{i,\text{meas}}^w$ *i*th measured concentration arrival time quantile for well *w*, {days};
- $\tau_{i,\text{sim}}^w$ *i*th simulated concentration arrival time quantile for well *w*, {days};
- i* quantile index, {-};
- w* well identification index, (see Figure 4-1 for locations), {-};
- β weight to provide sensitivity to both the tracer and drawdown data, {(days/m)²}.
- Δh_{meas} measured drawdown at well HO60 (See Figure 4-1 for location), {m};
- Δh_{sim} simulated drawdown at well HO60, {m}.

The weighting factor (β) can be adjusted to equalize the contribution of different data sets. In all cases there is an implicit weight because of the specified units for the two data sets. For example, if the drawdown were measured in cm, the squared drawdown residuals would have an implicit weight 10,000 times larger than if drawdown were measured in meters, without changing the units on concentration arrival time quantiles. In this case, 1076 provided sufficient sensitivity to both the hydraulic and tracer data.

MODFLOW, which is the U. S. Geological Survey's quasi-three-dimensional groundwater flow algorithm [McDonald and Harbaugh, 1988], is used to solve (4.1) for the hydraulic head field given appropriate boundary conditions (no flow through bottom and constant head of 14.6 m on all sides, based on head measurements by Benson [1988]; ground surface is at 15.25 m) and a zonal estimate of the hydraulic conductivity field. We modified this algorithm to automatically calculate the vertical hydraulic conductivity based on the specified horizontal conductivity field, assuming no anisotropy. We believe that flow and transport through this aquifer can be adequately described using isotropic hydraulic conductivity at the scale of a grid cell. We also adapted MODFLOW to automatically distribute the total well flow rates in proportion to the hydraulic conductivity of each screened grid cell.

MT3D [Zheng, 1992] was then used for the tracer simulations because the Method-Of-Characteristics approach employed in this model is an efficient and effective method to calculate concentrations through time for advectively dominated systems [Zheng, 1993] such as the Kesterson aquifer. Finite difference

or finite element solutions to the advection-dispersion equation have several disadvantages for this type of problem. First, there are no widely accepted three-dimensional finite difference or finite element solute transport algorithms. Second, even if one were available, the computational time would be unmanageable because both the time steps and the grid cells would have to be extremely small to maintain a non-oscillating solution with no numerical dispersion. Computational efficiency is especially important for simulation-regression algorithms, because large numbers of forward simulations are needed to obtain accurate parameter estimates.

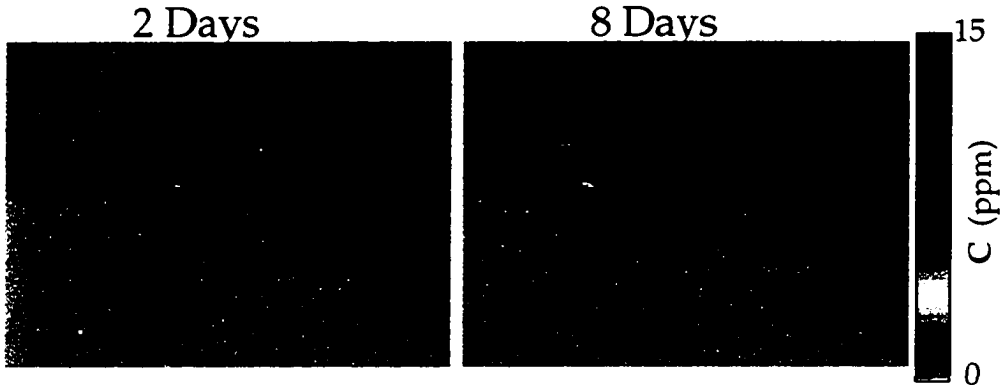
MT3D first calculates the groundwater velocities using Darcy's law (4.2) and the hydraulic head field from MODFLOW. Then it tracks particles of varying concentrations as they move through the predicted velocity field. At the end of each time step, the dispersion term is calculated using a finite difference approach. Thus, MT3D uses a mixed Eulerian-Lagrangian approach to calculate the tracer concentrations through the three-dimensional grid for each time step. For each measurement well, the concentrations were vertically flux averaged (weighted proportional to the estimated hydraulic conductivity at each depth) through the screened interval [*Parker and Van Genuchten, 1984*]. The regression model then compares the simulated and observed tracer quantiles at the six measurement wells and the drawdown at well HO60, and minimizes the objective value (4.4)

RESULTS

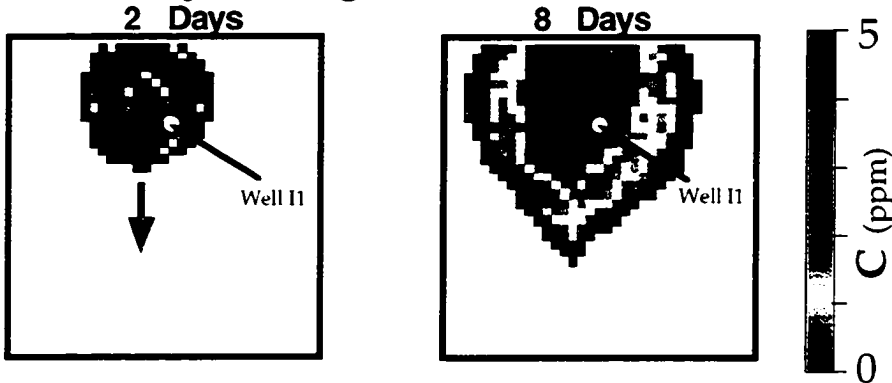
Figure 4-5 illustrates tracer simulations and the resulting concentration histories for the parameters listed in Table 4-2 and the slowness realization illustrated in Figure 4-4. The specified slowness splits result in the zonation of hydraulic conductivity illustrated in Figure 4-6. The region is modeled using the same rectangular cells from the slowness realizations, with specified head boundaries on all four sides of the region pictured in Figure 4-4. The bottom of the region was considered to be a no flow boundary since a clay is present at a depth of approximately 20 meters in wells throughout the Kesterson region [Benson, 1988]. The 4 meters of the aquifer below the ground surface were described as a fine grained surficial layer by Benson *et al.* [1991], and was thus modeled as a low conductivity zone (3.5×10^{-6} m/s as measured by Luthin [1966]). All the inflow boundaries were specified as zero concentration cells. The effect of these boundary conditions was reduced by placing the boundaries far from the injection and withdrawal locations.

Simulated concentration profiles for the parameter estimates in Table 4-2 are illustrated in Figure 4-5a. The injection well is located approximately in the center of the tracer plume in Figure 4-5a and the pumping well is approximately at the center of the green arrow. Groundwater is flowing in the direction of the green arrow, from the injection well to the pumping well. Two days after the tracer injection, the simulated concentration front of 1. ppm (red isocontour in Figure 4-5a) appears to be fairly spherical around the injection location. At eight days, the effects of the heterogeneous hydraulic conductivity field are apparent as the tracer has moved more rapidly toward the withdrawal well in the yellow near-surface high-conductivity zone than in the blue low-conductivity zone at depth (Figure 4-4). The hydraulic conductivity values were determined by inverting the tracer data, rather than inferring these properties directly from the seismic estimates, because the relationship between slowness and conductivity is unknown. The heterogeneity in the conductivity field results in significant variability in the simulated concentration histories at the measurement wells.

a) 3D Tracer Simulation



b) Vertically Averaged Concentrations



c) Match Concentration History

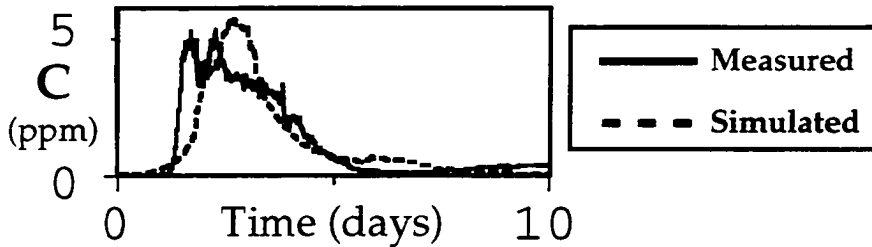


Fig. 4-5. Three-dimensional solute transport simulations (a) are used to match the tracer concentration histories at each measurement well. The vertically averaged concentrations are shown for well I1 (shown as a white dot) that has a long screened interval and thus measures approximately the vertically averaged concentration. The values of slowness splits and hydraulic conductivity are adjusted to minimize the difference between the measured and simulated concentration histories (c).

Vertically-averaged concentrations are illustrated in Figure 4-5b with the noted location of well I1, which is screened through most of the simulated aquifer depth. These vertically-averaged concentrations do not indicate the degree of heterogeneity at the site because most of the conductivity variability is in the vertical direction. Figure 4-5c shows the match between measured and simulated tracer concentration arrival histories at well I1 for the parameters in Table 4-2. This illustrates that the vertically averaged concentrations are fairly representative of the measured concentrations for a well with a long screen, but we either need wells at multiple depths or multilevel samplers to fully infer the vertical heterogeneity at this site.

The estimated parameters in Table 4-2 and zonation illustrated in Figure 4-6 result in a reasonable match of all the concentration histories as illustrated in Figure 4-7. The central tendency and main peaks of the concentration histories are matched at all measurement wells with the possible exception of well 8. These results illustrate that seismic and tracer data can be combined to generate estimates of subsurface lithologic zonation and determine the flow and transport properties for each zone that are consistent with all of the data.

The tracer inversion begins with an initial guess of the parameters and adjusts the parameters to minimize the objective value (4) using a gradient search. We employed multiple line searches in the direction of each parameter because of the highly nonlinear nature of this inversion. For each parameter, a line search is used to find the minimum objective value to a predetermined convergence criteria [Press *et al.*, 1989]. Each parameter's line search first brackets the minimum, then uses parabolic interpolation to converge toward the optimal parameter value. After a line search is completed on each parameter, all the parameters are updated based on the calculated gradient of the objective function. This approach does not find a local minima if the step size for parameter adjustment is large. As the inversion proceeds the step size can be reduced to obtain a slightly improved objective value. Although this nonlinear estimation approach worked well for this field case, different techniques can be used depending on the nature of the objective function. For this case, the need to escape from local minima was critical to the success of the inversion, thus the step size determination was important.

Starting at different initial parameter values is useful to determine if the estimates are at a local minima. Since this is a highly nonlinear inversion, multiple starting points were used to determine if the parameter estimates

provide a global optimum, or if the problem is non-unique. If the starting values are far from optimal, convergence may be slow, or the method may converge to one of the local minima. Thus, the first stage of the inversion is to bracket the parameter values to put the concentration peaks in roughly the correct places using forward simulations. Then the inversion is used to adjust the values to obtain the best fit to the measurements.

The range of hydraulic conductivity values that we found was from 1.4×10^{-4} m/s to 5.0×10^{-4} m/s (Table 4-2), which compares favorably to previous estimates from this area. Conductivities in the range of 1.4×10^{-4} to 6.4×10^{-4} m/sec (Table 4-2) were reported for pump tests at the HO site where the multiple well tracer test was completed [Benson, 1988; Benson et al., 1991]. Benson [1988] also reported conductivities in the range of 8.8×10^{-5} m/s to 1.1×10^{-3} m/s for 20 single well pump tests from the shallow 12 meters of the Kesterson aquifer.

Benson [1988] interpreted the tracer concentration histories using the superposition of many one-dimensional advection dispersion solutions. With this approach, Benson [1988] estimated the thickness, flow velocity, and dispersivity for multiple one-dimensional paths to each tracer measurement well. The number of paths was increased until all the peaks were matched. Although providing a good starting point, that analysis has limited physical significance because no simultaneous analysis of the paths was attempted. The tracer data alone were not sufficient for Benson to determine the three-dimensional structure of conductivity at this site. Our method indicates that the full three dimensional flow and transport system can be described using the cross-well seismic data to help parameterize the hydrogeologic inversion. Benson [1988] estimated the longitudinal dispersivities to be on the order of 3 cm for this site which somewhat below our estimate of 9 cm, which we determined from sensitivity analysis.

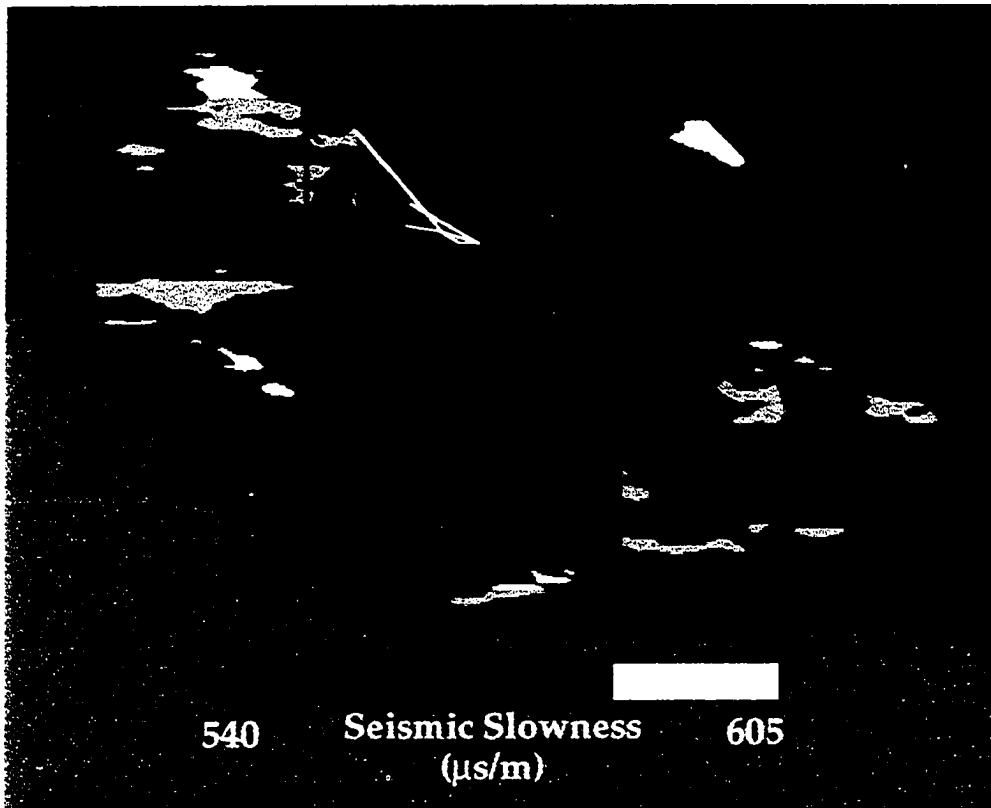


Fig. 4-6 Estimate of subsurface geology obtained with the split inversion method. This zonation was found to be the best split for this realization with splits at 569.4 and 587.8 $\mu\text{s/m}$. The estimated hydraulic conductivity values are: 1.4×10^{-4} m/s for the blue regions; 3.6×10^{-4} m/s for the green regions; and 5.0×10^{-4} m/s for the yellow regions. For reference, the seismic cross-sections are below the white lines and the red line is well ST4.

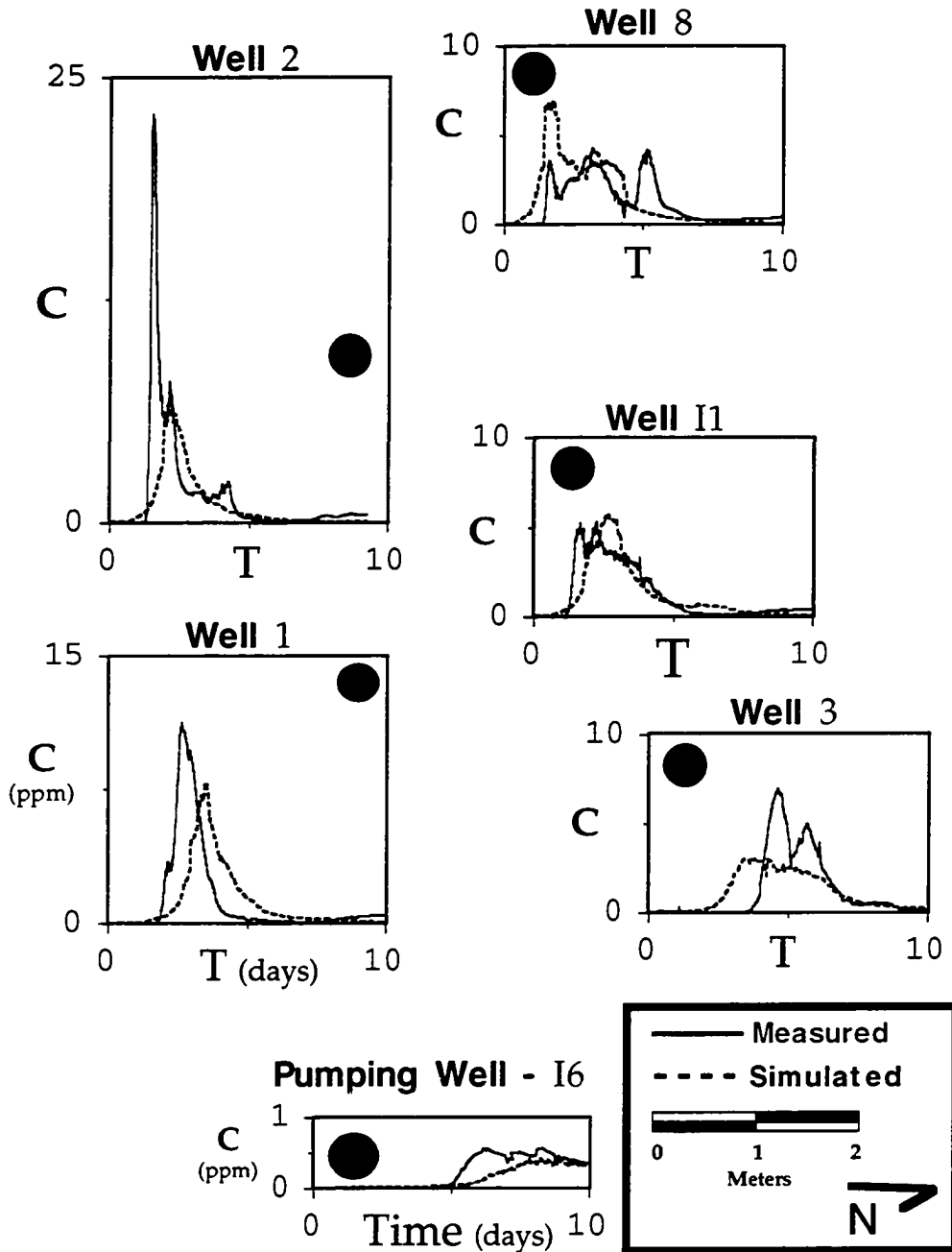


Fig. 4-7 Match of simulated and observed tracer concentration histories for the lithologic zonation shown in Figure 4-6. The concentration histories are illustrated at the well locations indicated by red dots. Well I6 is approximately 15 meters East of well 3 (shifted West for figure). The values of hydraulic conductivity and dispersivity for this match are shown in Table 4-2. The main features of the measured concentration histories are preserved in the simulated histories.

SENSITIVITY ANALYSIS

We estimated the longitudinal dispersivity using sensitivity analysis, rather than including this as a parameter in the inversion, to substantially reduce the computation. For a particular dispersivity value, the objective (4.4) was minimized by adjusting the slowness values that determine the zonation of the aquifer, called seismic slowness splits, and the zonal conductivity values. With this approach, we used dispersivity values in the range of 0.5 cm to 30 cm and found that a value near 9 cm best matched the observed data. If the peaks are too broad and the peak magnitudes are lower than observed, the dispersivity estimate is too large and thus should be reduced. The transverse dispersivity was adjusted from 0.1 to 0.2 times the longitudinal values, and the best fits were obtained using 0.2 times the longitudinal value.

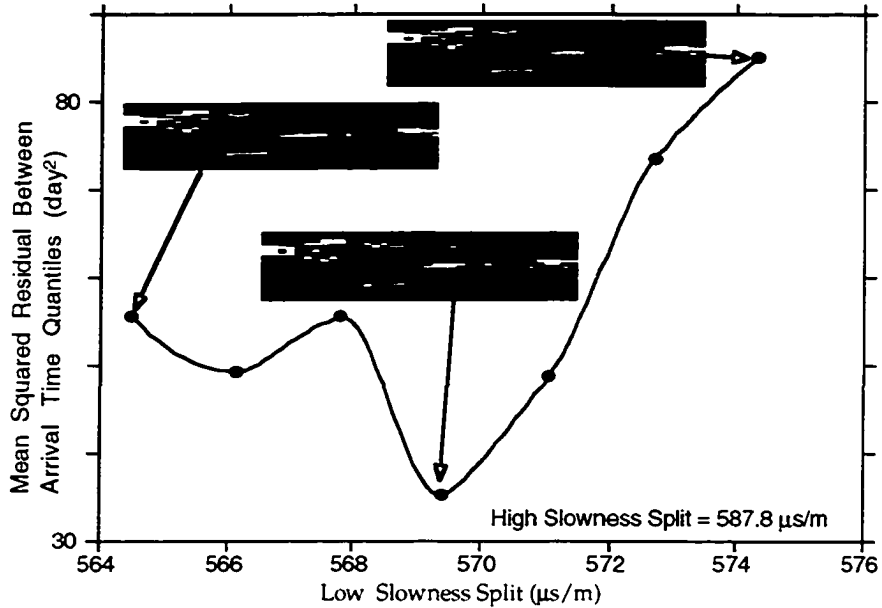
To illustrate the sensitivity of the objective value to the zonation of aquifer properties, the two slowness splits are adjusted with all other parameters held constant. Figure 4-8 demonstrates how tracer concentration residuals change nonlinearly due to changes in the slowness splits, which determine the zonation for hydraulic conductivity. Although several local minima are apparent in these sensitivity plots, the SIM appears to have converged to a global minimum with respect to these parameters.

The optimum parameter set for the Kesterson inversion (Table 4-2) appears to provide a global minimum of the specified objective function (4.4) with respect to the relative zonal conductivity values. The tracer data provide sensitivity to the differences of conductivity between zones and the geometry of these zones, while the drawdown data provided sensitivity to the average value of hydraulic conductivity at the site.

This emphasizes the need to collect hydraulic head data during tracer tests, such as the measured drawdown of 0.15 meters at well HO60 during the 1986 tracer test. In cases with no constraint on the hydraulic gradients, reducing the average conductivity while using constant head boundaries proportionally increases the hydraulic gradient to achieve the same total flow rate. This results in approximately the same average fluid and tracer velocities. At the Kesterson site, the measured drawdown constrained the hydraulic gradients at the site, which allowed us to determine the average conductivity as well as the differences between zones.

We also examined the sensitivity of the tracer concentrations to the horizontal and vertical correlation lengths as well as the type of variogram used (exponential and gaussian). We tried horizontal correlation lengths of 1., 5., 9., and 18. meters, with vertical correlation lengths of either 0.1, 0.5, or 0.9 meters. None of these sets of geostatistical parameters reproduced the tracer concentration histories as well as the realizations generated with an exponential variogram with $\lambda_h = 9. \text{ m}$, $\lambda_v = 0.9 \text{ m}$, $\sigma^2 = 104$. The vertical correlation length estimated from the seismic tomograms thus provided a reasonable description of the correlation of hydraulic properties. The seismic estimates also provided a reasonable initial estimate of the horizontal correlation length.

(a) Sensitivity to low slowness split



(b) Sensitivity to high slowness split

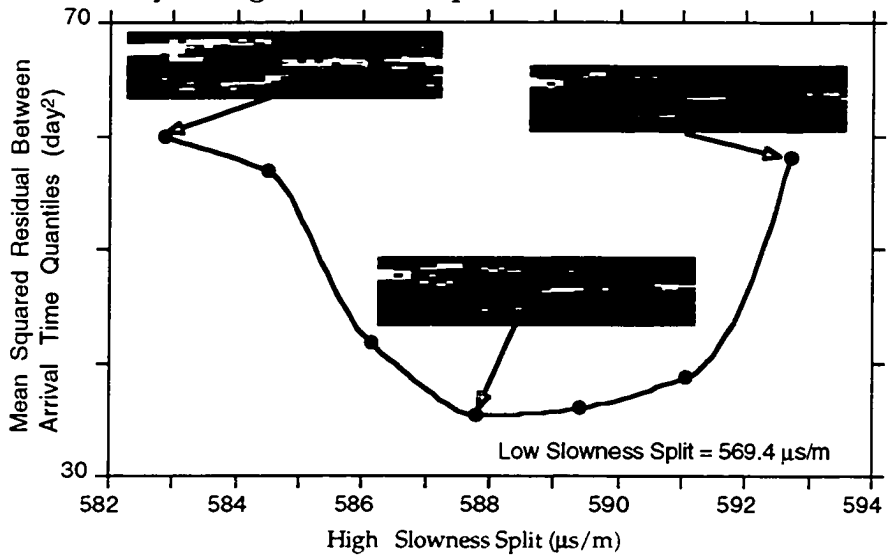


Fig. 4-8. Sensitivity of the objective value (squared concentration residuals) to the two values of seismic slowness split that determine the hydraulic conductivity zonation. The estimated conductivity values listed in Table 4-2 were used for each simulation. (a) Shows the sensitivity to the low slowness split (between green and blue on Figure 4-6). (b) Shows the sensitivity to the high slowness split (between green and yellow on Figure 4-6).

SUMMARY AND CONCLUSIONS

We have demonstrated the split inversion method (SIM) to combine seismic and tracer data to map the lithologic zonation of the Kesterson aquifer, estimate the hydraulic conductivity for each zone, and estimate the dispersivity for the region. This is the first paper that we know of that combines seismic and tracer data to map the three-dimensional hydraulic conductivity structure of an aquifer. The SIM adjusts five parameters to obtain the best fit to tracer concentration histories. These parameters are: two values that split seismic slowness realizations into three populations; and three hydraulic conductivity values, one for each population. Other parameters are determined using sensitivity analysis, such as the regional value of dispersivity and the horizontal and vertical correlation lengths at the site.

The results demonstrate that seismic and tracer data can be combined to provide reasonable estimates of aquifer zonation and hydraulic properties. The seismic data provided three-dimensional estimates of the aquifer structure even though the relationship between seismic slowness and the hydraulic parameters of interest is unknown and potentially non-unique. The tracer data allow us to split the slowness estimates into geologically reasonable zones in three dimensions, and assign flow and transport properties to the zones. By combining seismic and tracer data, we were able to obtain more information about subsurface properties than if we had used either data set alone.

Several objective functions were attempted for this Kesterson inversion to provide rapid convergence. The one that worked best was minimizing the squared difference between arrival time quantiles from the concentration histories. This objective converges even if the starting estimates are far from optimal. An objective of minimum absolute concentration residual was originally attempted, but this objective did not converge. We then minimized the squared concentration residuals, which converged if the starting estimates were fairly close to the optimal values. This least squares approach had problems with local minima because the objective heavily penalized simulated peaks of the proper magnitude, even if they were just slightly offset from the measured peaks. The highest peaks also dominated the solution, thus the parameter estimates from this objective may not provide an optimal solution for all the measured concentration histories. It is important to examine the fit to the data for a variety of parameter sets to help develop the best objective function. Some objective functions will not

converge toward accurate fits to the data, and overly complicated objectives may have competing factors that hamper convergence. The objective could include many other indices of the concentration arrival histories, such as peak concentration arrival times as presented by *Hyndman et al.* [1994], peak magnitudes, and temporal moments of the concentration histories.

As discussed in the results section, tracer concentration histories between an injection/withdrawal well pair provide information that can be used to determine the relative hydraulic conductivities for a site. However, these data are fairly insensitive to the magnitude of the mean hydraulic conductivity if the boundary conditions are also unknown. There are several ways around this problem including: 1) collect multiple sources of data, such as tracer concentrations and hydraulic head measurements, 2) determine values of specified flux boundaries for the site, 3) use pump test data to constrain the mean conductivity values. Detailed hydraulic head measurements, which are easy to collect and do not require expensive analyses, constrain the average hydraulic conductivity. Hydraulic head data could also be used to constrain the potential range of hydraulic conductivity values before using the much more numerically expensive tracer simulations.

Although the SIM was presented for seismic travel times, tracer concentrations, and drawdown, many other applications are possible. Other hydrologic data, such as transient hydraulic head measurements, could be used instead of (or in addition to) tracer concentrations. Other seismic attributes can also be inverted to obtain more information about hydraulic properties. For example, seismic amplitudes can be inverted for attenuation coefficients. These coefficients are likely correlated to hydraulic conductivity because the ease of fluid movement affects the attenuation of seismic energy. Geophysical methods, such as ground penetrating radar and cross-well resistivity, should also provide valuable data sets to help delineate aquifer structure and properties for different geological regimes. Ground penetrating radar works best when both the clay content and the electrical conductivity of the soil are low, but cross-well radar methods may allow us to image the structure of sand zones between clay lenses with very high resolution.

CHAPTER 5:

**INFERRING THE RELATION BETWEEN SEISMIC SLOWNESS
AND HYDRAULIC CONDUCTIVITY IN HETEROGENEOUS
AQUIFERS**

ABSTRACT

Cross-well seismic tomography can be used to determine the slowness structure of aquifers. For groundwater flow and solute transport simulations, one would like to know the relation between seismic slowness ($1./$ seismic velocity) and hydraulic conductivity to provide more detailed estimates of the conductivity field. Unfortunately, this relation is poorly understood, resulting in poor characterization of hydraulic properties from seismic estimates. This relation is generally derived from laboratory measurements, but slowness values measured with very high frequencies in the lab are often poorly correlated to lower frequency cross-well and surface seismic slowness values. To address this problem, we developed an approach to infer the relation between slowness and hydraulic conductivity using field scale geophysical and hydrogeologic measurements.

We demonstrate this approach for the Kesterson aquifer, California, using cross-well seismic tomography in conjunction with hydraulic property estimates from cores and pump tests, and a multiple-well tracer test. We first develop an a priori relation between the conductivity measurements and the cross-well slowness estimates at the same locations. Multiple three-dimensional slowness realizations, conditioned on the cross-well estimates, are then generated. The slope and intercept of the slowness to log conductivity relation are then adjusted, and for each adjusted relation we map a slowness realization into a conductivity field. We simulate groundwater flow and tracer transport through the potential three-dimensional conductivity fields and calculate the residuals between measured and simulated drawdown and concentration arrival time quantiles. The sum of squared tracer concentration arrival time quantile residuals is minimized to find the optimal relation between slowness and log hydraulic conductivity as well as the dispersivity for the aquifer.

For the Kesterson site, seismic slowness estimates provided valuable information about aquifer properties. The groundwater flow and tracer transport simulations, through the estimated conductivity realizations, match the tracer concentration histories for two multiple well tracer tests and the drawdown measured only during the first tracer test. The concentration histories from the second tracer test were used to check the conductivity estimates since these data were not used in the inversion. In addition to estimates of seismic slowness and hydraulic conductivity, this approach provides information about the relation between slowness and log conductivity, and could be used to infer additional relations between geophysical and hydraulic properties.

INTRODUCTION

The identification of aquifer heterogeneities has become a critical research topic in hydrogeology. Groundwater flows preferentially along paths of high hydraulic conductivity within the three-dimensional structure of an aquifer. Accurate estimation of heterogeneous flow properties is critical for accurate prediction of solute transport along such paths.

Estimating values of subsurface hydraulic properties is difficult because the environment is largely inaccessible and common measurements used to deduce these properties are sparse. Geophysical measurements could provide the needed high resolution estimates of aquifer properties, but the relations between the estimated geophysical properties and the desired hydraulic properties are unknown at the field scale. An improved understanding of these relations would allow more quantitative use of geophysical measurements to estimate hydraulic properties.

Many researchers have tried to explain the relations between geophysical and hydraulic properties at the lab scale. In this paper, we focus on relations between seismic slowness ($1./\text{seismic velocity}$) and hydraulic conductivity at the field scale where we have high-resolution slowness images, called tomograms, between wells. Relations may also exist between hydraulic conductivity and both the seismic attenuation coefficient [*Prasad and Meissner, 1992*] and the dielectric constant (estimated using ground penetrating radar measurements) [*Beres and Haeni, 1991; Knoll et al., 1991*]. The velocity of seismic energy is a function of the elastic properties (density, bulk modulus and shear modulus) of the media [*Telford et al., 1990*], which depend on both lithologic and fluid properties. Several empirical averaging equations and transforms were developed between seismic velocity and porosity [*Raymer et al., 1980; Wyllie et al., 1956*]. *Han et al.* [1986] showed that much of the scatter in these empirical relations could be reduced by adding clay content as an additional parameter. *Marion et al.* [1992] developed a conceptual model to describe the relationship between seismic velocity and porosity of sand-clay mixtures. *Rubin et al.* [1992] then used Marion's model as a seismic velocity to permeability relation.

Although these lab derived empirical relations can provide some insight into the field scale relations, they may have limited predictive power. Several complicating factors, such as seismic velocity dispersion and sample alteration,

limit the use of lab derived relations for field prediction. Velocity dispersion causes different wavelengths of energy to arrive at different times [Bourbie *et al.*, 1987]. In other words, the core sample is not representative of the larger volume. Cores taken from the field are always disturbed and field conditions are not reproduced in the laboratory, resulting in different properties at lab and field scales. Well bores are disturbed during drilling, causing similar uncertainty in the estimated seismic velocities from well logs.

Instead of estimating the relation at the lab scale for prediction at the field scale, we combine field scale seismic and hydrologic data to estimate the relation for a particular site. This estimated field relation could then be used for nearby sites with a similar depositional environment, assuming the relation is the same across the region. This approach does not rely on the assumption of scale independence that is required to use lab derived relations at the field scale. The nature of the estimated relation will depend on the types of available field data.

In this paper we demonstrate a new approach for estimating aquifer parameters that infers a linear relation between slowness and hydraulic conductivity. This approach involves only three parameters for each slowness realization: the slope and intercept of the relation, and the dispersivity. We combine cross-well seismic tomography with core measurements, pump tests, and a multiple-well tracer test to infer this relation and the dispersivity for the Kesterson aquifer. The slope and intercept of the linear relation between slowness and conductivity are adjusted along with the dispersivity for three-dimensional slowness realizations to find conductivity realizations that best match the measured tracer and drawdown data. A second forced gradient tracer test in a perpendicular direction to the first is used to check the estimated conductivity and dispersivity estimates.

The philosophy of this inversion is that such a relation may exist, but this relation is most useful if it has been developed at the field scale for which it will be used. Estimating such a relation at the field scale provides a valuable tool for in-situ aquifer property estimation. Once such a relation is estimated for a particular depositional environment, this relation could be used as a starting estimate to map nearby seismic data into hydraulic property estimates. This would allow for more accurate solute transport predictions in regions with little available hydraulic data, but extensive seismic data.

OVERVIEW OF THE KESTERSON SITE

The Kesterson aquifer, which is located in California's San Joaquin valley (Figure 5-1), has been characterized in detail during the last decade because of selenium contamination of both surface water and groundwater. Agricultural return waters containing high concentrations of selenium and other contaminants were discharged to the Kesterson Reservoir in the early 1980's. Approximately fifty percent of this return water infiltrated, creating a large groundwater contaminant plume. The predominant lithology at the site is clean sand that was deposited by the meandering San Joaquin river. Several data sets were collected to characterize the shallow Kesterson aquifer, including seismic travel times between six well pairs and tracer concentration arrival histories at six wells during a tracer test with an injection/withdrawal pair.

Benson [1988] conducted two tracer tests using an injection/withdrawal well pair and multiple observation wells at different depths. The first tracer test was conducted in 1986 by pumping 4.7 L/s from well LBL-6 and injecting this same water back into well LBL-12, which is approximately 30 meters to the west. The injection/withdrawal well pair was pumped for 24 hours prior to the tracer test in order to approach a steady state flow field. A concentrated fluorescein solution was then pumped into the injection stream for 3180 seconds (0.883 hours) to achieve a total injection concentration of approximately 320 ppm. Concentrations were then monitored at six wells throughout the ten day tracer test (Wells 1, 2, 3, 8, I1, and I6 – See Figure 5-1 for locations). Fluorescein is a weakly sorbing tracer as determined by *Smart and Laidlaw* [1977] using batch experiments with different sediments. Thus, for this study we assume that fluorescein is a conservative tracer.

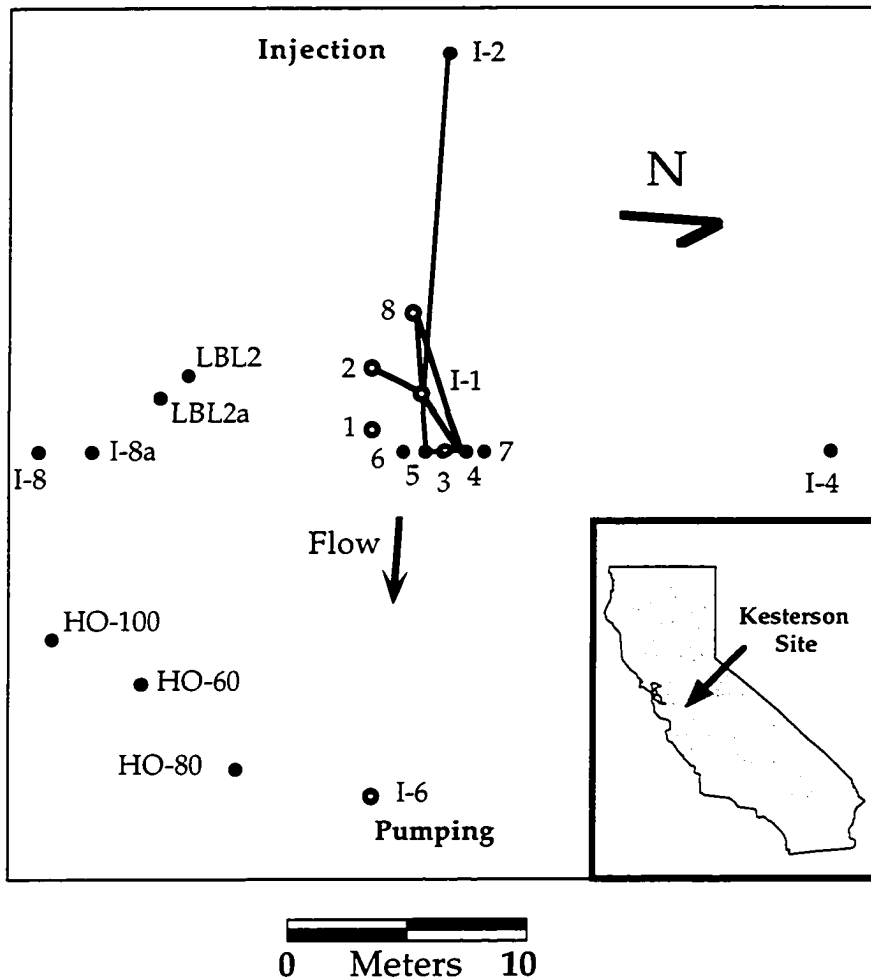


Fig. 5-1. Site map for the Kesterson Aquifer located in California's San Joaquin Valley. At this site, seismic travel times were collected between the six well pairs connected with black lines. Water was pumped at well I6 and reinjected at well I2 for the 1986 tracer test. A pulse of fluorescein dye was injected into well I2 and the resulting concentrations were measured at the six wells noted with open circles throughout the 10 day tracer test. Drawdown was measured at HO60 during the 1986 test.

Our earlier work on the Kesterson site led to the estimation of the relation between slowness and conductivity that we present in this paper. *Hyndman and Harris* [1995] co-inverted the six cross-sections of seismic travel times for three seismic slowness populations that likely represent different lithologies. We then generated multiple three-dimensional conditional realizations of seismic slowness and estimated the zonation of lithologies, hydraulic conductivity values for each zone, and a regional value of dispersivity for five realizations based on the tracer data. *Hyndman and Gorelick* [1995] then split each slowness realization into zones and estimated the conductivity values for these zones to minimize the squared residuals between simulated and observed tracer concentration histories. This approach accurately matched the tracer concentration histories using reasonable estimates of the hydraulic parameters and geologically reasonable lithologic zonations for the site, but involved a great deal of computation to resolve five parameters for each slowness realization. We show that a linear relation can be fit between the slowness estimates and the zonal log hydraulic conductivity estimates for the Kesterson site (Figure 5-2), providing the incentive to estimate this relation.

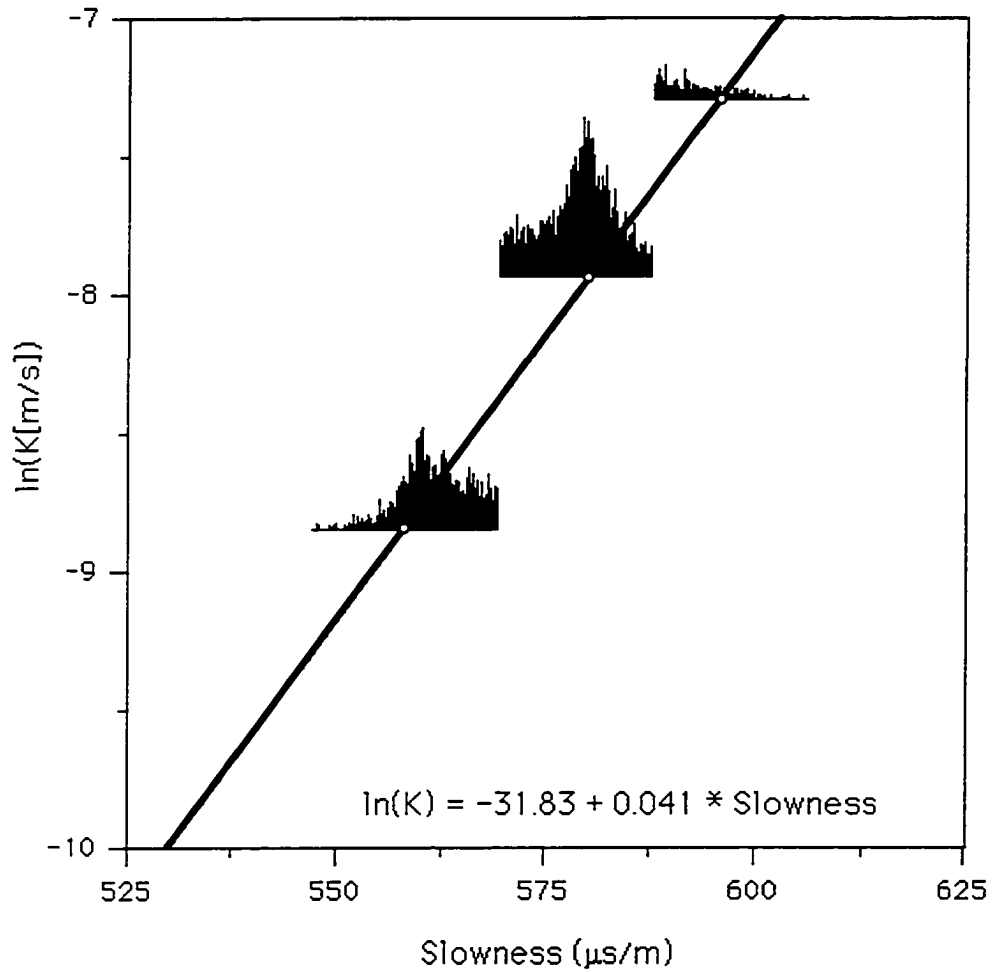


Fig. 5-2. Linear fit between slowness and natural log conductivity estimates from the Split Inversion Method [Hyndman and Gorelick, 1995]. The 41440 values represent slowness estimates from a 3D realization versus the hydraulic conductivity values assigned by SIM for the corresponding points. The slowness values prior to the split are illustrated by the histograms.

INVERSION METHOD

The main steps of our approach are:

- 1) Invert seismic travel times measured between well pairs for seismic slowness fields (tomograms) using the multiple population inversion approach of *Hyndman and Harris*, [1995], and update these estimates using a traditional tomographic inversion.
- 2) Generate equally likely conditional slowness simulations using sequential gaussian simulation as described by *Hyndman and Gorelick* [1995].
- 3) Estimate an a priori relation between seismic slowness and log hydraulic conductivity using available field data.
- 4) Use the estimated relation to map slowness realizations into log conductivity fields for groundwater flow and solute transport simulations, and calculate the residual between measured and simulated concentration arrival histories.
- 5) Systematically perturb the estimated relation, using a line search algorithm, to minimize the difference between arrival time quantiles from the simulated and measured concentration histories, and the difference between measured and simulated drawdown at well HO60 (see Figure 5-1 for location).

We describe these steps in more detail below.

The multiple population inversion approach of *Hyndman and Harris* [1995] was used to invert seismic travel times between six well pairs for seismic slowness tomograms (estimated vertical cross-sections). This method iteratively co-inverts the travel times from all six well pairs for the best spatial distribution of three slowness populations. In other words, the geometry of these three slowness zones is iteratively adjusted, along with the slowness value for each population, to minimize the residuals between measured and simulated travel times. This approach provided high resolution estimates of the lithologic structure of the Kesterson aquifer along these cross-sections. These tomograms are then updated using a traditional unconstrained tomographic inversion to provide more continuous slowness estimates (Figure 5-3).

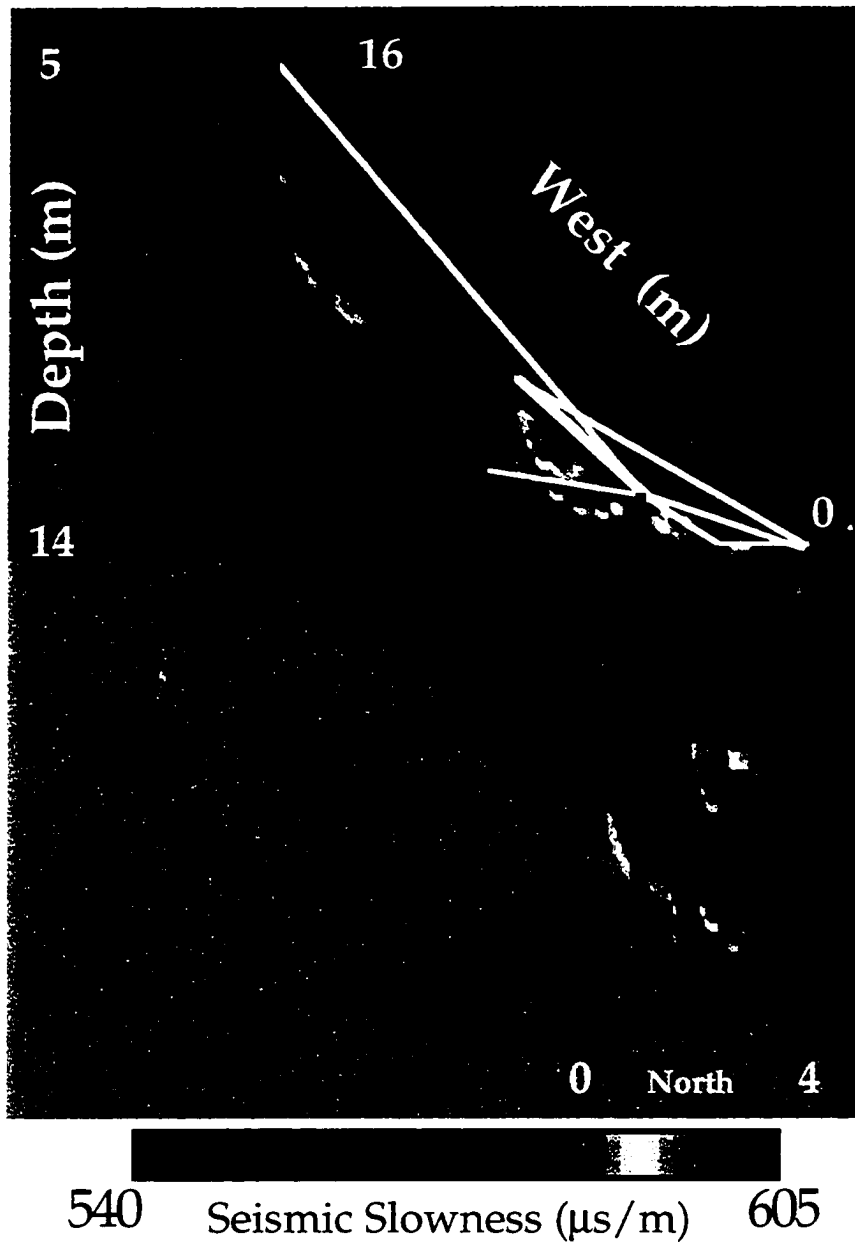


Fig. 5-3 Three-dimensional layout of seismic slowness estimates at the Kesterson site from *Hyndman and Harris* [1995], in which white lines designate the map view locations of the cross-sections, and red lines represent wells. Wells ST5 and ST4 are on the close side of the image and well I2 is at the top (See Figure 5-1 for location map).

Equally likely three-dimensional slowness estimates were then generated using a geostatistical method called sequential gaussian simulation [*Deutsch and Journal*, 1992]. This approach honors the values at all the estimate locations, as well as the correlation length, variance, and sample probability distribution of the tomographic slowness estimates. We calculated sample variograms for the slowness tomograms in Figure 5-3 and fit exponential variograms ($\lambda_h = 5. - 9. \text{ m}$, $\lambda_v = 0.9 \text{ m}$, $\sigma^2 = 104.$) to these sample variograms to explore the likely range of correlation lengths. Realizations with a horizontal correlation length of 9 meters and a vertical correlation length of 0.9 meters best fit the tracer data. There were not enough long seismic tomograms in multiple directions to detect any horizontal anisotropy at the site.

We then determined an a priori relation between seismic and hydraulic parameters, which we later update using a simulation-regression approach to obtain the best match to the available field data. One method to infer the a priori relation between slowness and conductivity is to analyze the slowness and conductivity of core samples in the lab. However, *Copty* [1994] found very little correlation between lab derived seismic velocity (or slowness) and log hydraulic conductivity values (Table 5-1; data collected by Jill Geller at Lawrence Berkeley Laboratory) for a core at the Kesterson site (Figure 5-4).

At the Kesterson site, we developed an a priori relation between the estimated zonal slowness tomograms from *Hyndman and Harris* [1995] and the hydraulic conductivity estimates from both core samples and pump tests in the region of these seismic tomograms. These data are summarized in Figure 5-5, which illustrates that a linear relation between seismic slowness and log hydraulic conductivity from both pump tests and core data may be adequate for this site. The lab derived conductivity values are better correlated to the slowness values estimated at the field scale than to the lab derived slowness values from the cores.

Table 5-1. Slowness and conductivity measurements in a core near well ST5*.

Depth (m)	Tomogram [†] Slowness ($\mu\text{s}/\text{m}$)	ln K (m/s)	Lab Slowness ($\mu\text{s}/\text{m}$)	Effective Pressure* (KPa)	
				Axial	Lateral
3.78	–	-9.1475	561.80	68.95	27.58
3.84	–	-8.9688	549.45	68.95	27.58
5.15	578.92	-8.0972	571.43	82.74	34.48
5.18	558.91	-7.7161	568.18	75.85	27.58
5.28	558.91	-8.6195	529.10	55.16	55.16
6.47	558.91	-9.0844	540.54	62.06	27.58
6.54	595.65	-6.9822	549.45	62.06	27.58
6.60	578.92	-7.8492	571.43	68.95	27.58
6.66	578.92	-7.4831	537.63	75.85	27.58

* Core is approximately 0.9 meters from well ST5 in the plane of the seismic tomogram toward well I1 (laboratory data collected by Jill Geller, LBL; N. Coptly, personal correspondence 1994).

† The estimated tomographic slowness values were derived using the multiple population inversion approach of *Hyndman and Harris* [1995].

* Data presented for the lowest available effective pressures, although each sample was analyzed for two to three effective pressures as presented in *Coptly* [1994].

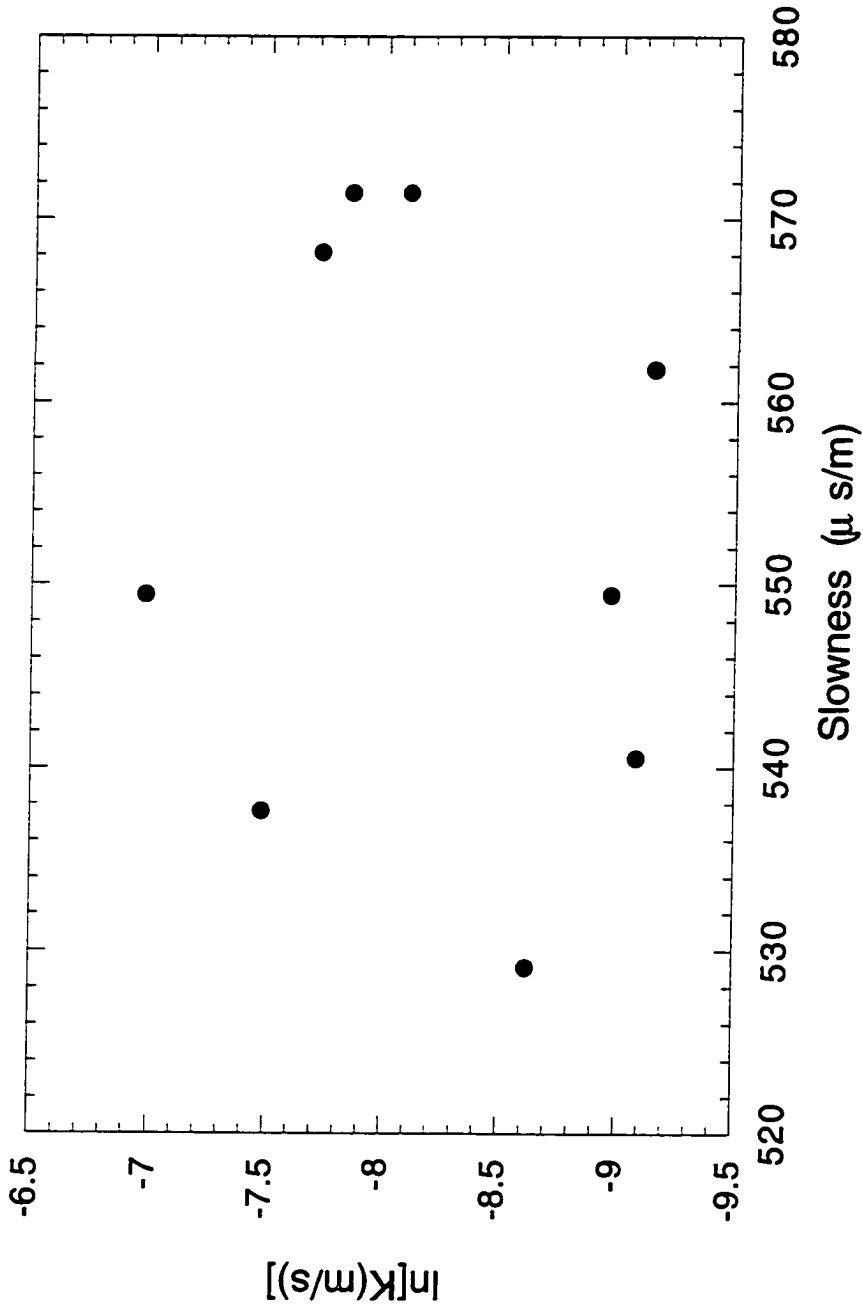


Fig. 5-4. Scatterplot of lab derived seismic slowness versus natural log hydraulic conductivity values. There is no meaningful correlation between these data sets.

Relation between S and ln(K) for the Kesterson Aquifer

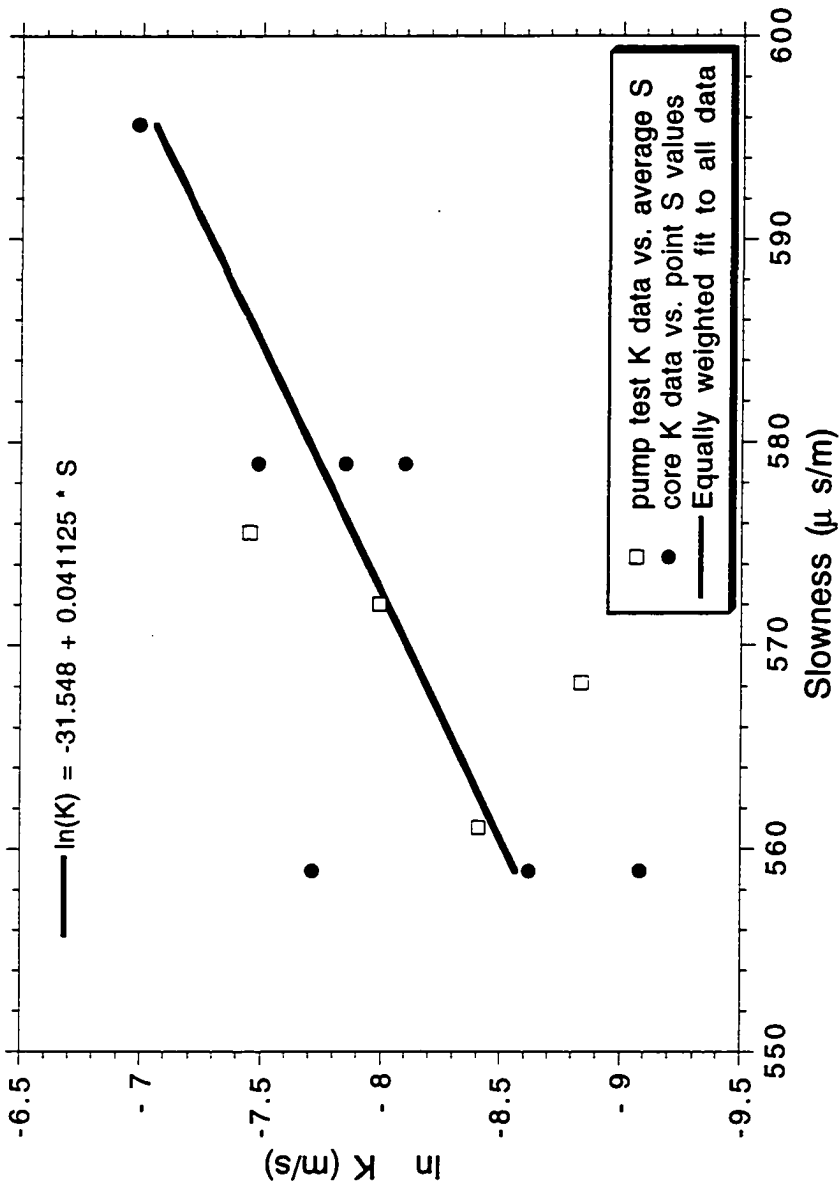


Fig. 5-5. A-priori relation between seismic slowness and natural log hydraulic conductivity. The slowness estimates are derived from tomography, while the conductivity estimates are from cores and pump tests. The correlation coefficient is 0.74732 for this data.

The pump test conductivity estimates from *Benson et al.* [1991] are plotted with respect to the average of the zonal slowness estimates for cells adjoining the well screen. A nonlinear relation could also be fit between the slowness and log conductivity estimates, but a linear relation appears to be adequate given the limited available information and uncertainty in slowness and conductivity estimates. The cores were sampled approximately 0.9 meters from well I1 along the cross-section toward well 5 (Figure 5-1). At this site, log conductivities from the cores are plotted with respect to the three-population tomographic grid cell slowness estimates from *Hyndman and Harris* [1995]. The best linear fit between the tomographic slowness values ($\mu\text{s}/\text{m}$) and the log conductivities (m/s) from both core and pump tests (Figure 5-5) is given by (5.1) below.

The relation in (5.1) is used to map each slowness realization into an initial estimate of the log conductivity field.

$$\ln(K) = a + b S \quad (5.1)$$

where	a	Intercept = 31.55
	b	Slope = 0.0411
	K	Hydraulic conductivity, {m/s}
	S	Seismic slowness, { $\mu\text{s}/\text{m}$ }

Each log conductivity field is then used as input to a three-dimensional groundwater flow and solute transport model for the region. MT3D [*Zheng, 1992*] was used for these simulations because of the dominance of advection at the site.

For each realization, the slope and intercept of the slowness to log conductivity relation were then adjusted to best match the tracer and drawdown measurements. Each time the slope or intercept is adjusted, the slowness realization is mapped into a zonal log hydraulic conductivity field (Figure 5-6) and groundwater flow and tracer transport are simulated. The simulated concentration histories and drawdown are compared to available measurements (Figure 5-6) for each adjustment. The slope and intercept of the linear relation between conductivity and slowness was adjusted to minimize the weighted sum of squared residuals between nine quantiles of the measured and simulated concentration arrival times and a single value of drawdown at well HO60. The nine quantiles represent the times at which ten to ninety percent of the tracer concentration pass the measurement well. The slowness splits and hydraulic conductivity values are adjusted to minimize this objective value.

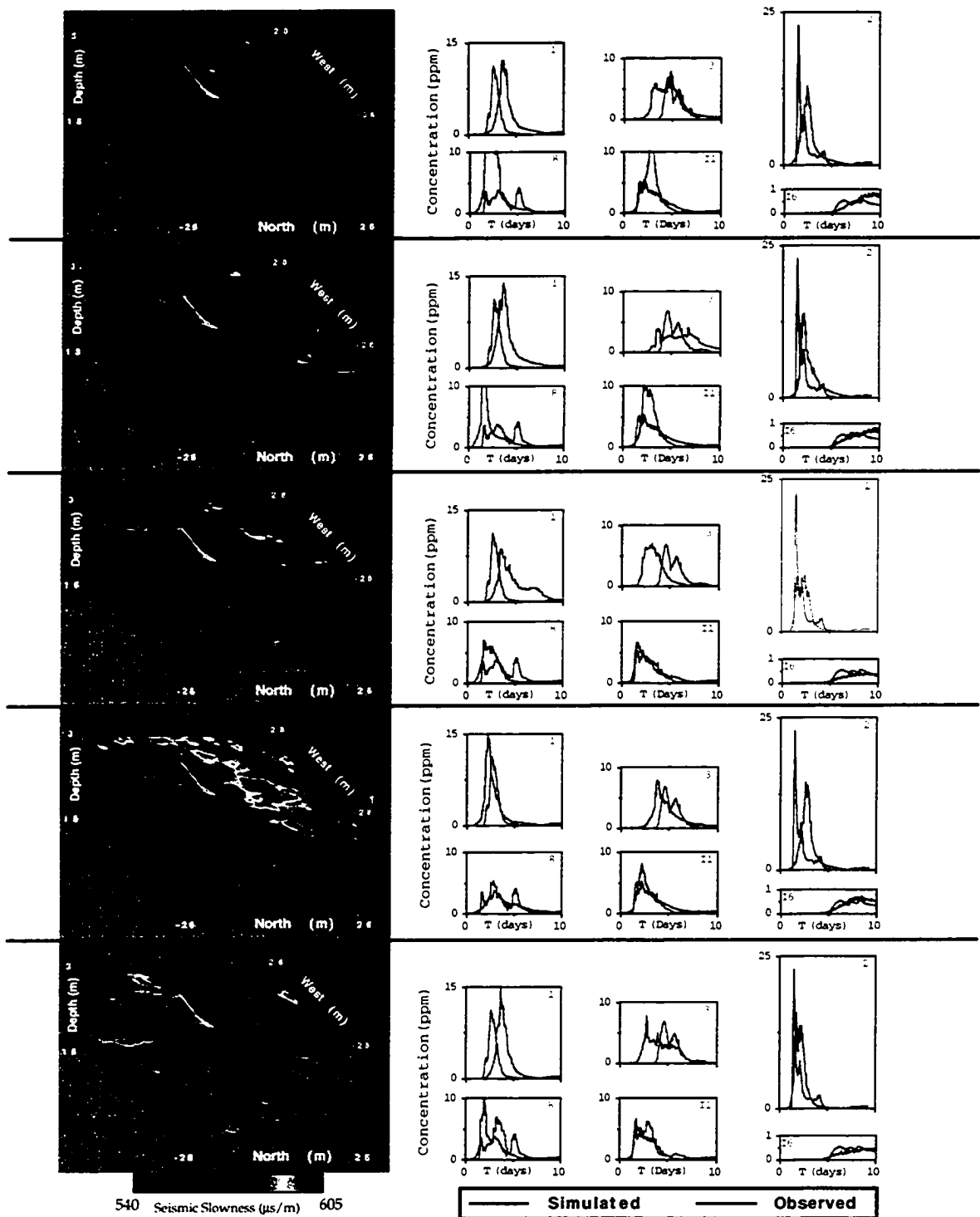


Fig. 5-6. Slowness realizations with corresponding simulated and observed concentration histories.

$$\text{Minimize} \left(\left(\sum_{i=1}^9 (\tau_{i,\text{meas}}^w - \tau_{i,\text{sim}}^w)^2 \right) + \beta \left((\Delta h_{\text{meas}} - \Delta h_{\text{sim}})^2 \right) \right) \quad w = 1, 2, 3, 8, 12, 16 \quad (5.2)$$

where:

$\tau_{i,\text{meas}}^w$ i^{th} measured concentration arrival time quantile for well w , {days};

$\tau_{i,\text{sim}}^w$ i^{th} simulated concentration arrival time quantile for well w , {days};

i quantile index, {-};

w well identification index, (see Figure 5-1 for locations), {-};

β weight to provide sensitivity to both the tracer and drawdown data, {(days/m)²}.

Δh_{meas} measured drawdown at well HO60 (See Figure 5-1 for location), {m};

Δh_{sim} simulated drawdown at well HO60, {m}.

The weighting factor (β) can be adjusted to equalize the contribution of different data sets. In this case, 10764 provided sufficient sensitivity to both the hydraulic and tracer data. The weighting factor is most important when the two data sets have different minima, and thus the weighting factor places the parameter estimates somewhere in between the two individual minima depending on the assigned weight. In all cases there is an implicit weight because of the specified units for the two data sets. For example, if the drawdown were measured in cm, the squared drawdown residuals would have an implicit weight 10,000 times larger than if drawdown were measured in meters, given no change in the units of concentration arrival time quantiles. For this Kesterson inversion, the weighting factor had little effect on the estimated parameters, although the convergence rate differed. This is because the head data are most sensitive to the intercept (of the slowness to log conductivity relation), while the tracer concentration arrival time quantiles are most sensitive to the slope and the dispersivity.

Concentration arrival time quantiles were used in the objective because of the complex nature of the concentration arrival time histories. Originally we used the squared difference between measured and simulated concentrations through time at all locations. However, if the parameters were far from their optimal values and the simulated and measured concentrations histories did not significantly overlap, this objective had poor convergence. In this case, the squared concentration residuals are not very sensitive to small adjustments in the conductivity field. An objective based on concentration quantiles is more robust because it avoids penalizing peaks with correct magnitudes and incorrect timing, which would occur when minimizing the squared concentration residuals.

Rather than adjusting the intercept of the a priori relation (5.1), we adjusted the intercept of the relation between log conductivity and the difference between the slowness and the median slowness for each realization, which are listed in Table 5-2.

$$\ln(K) = (a+b S_{\text{median}}) + b(S - S_{\text{median}}) \quad (5.3)$$

where $a = -31.55$ and $b = 0.0411$

$$\ln(K) = c + b(S - S_{\text{median}}) \quad (5.4)$$

where c modified intercept = $(a+b S_{\text{median}})$

This reduces the dependence between the slope and the intercept and thus provides a better parameter set for this inversion. Adjustments in the slope of (5.3) do not require a corresponding change in intercept to maintain a reasonable relation between slowness and log conductivity. Using this approach, we infer both the relation between conductivity and slowness from field data and determine the likely hydraulic conductivity field at the site. For a particular slowness realization, the median slowness is used to calculate the adjusted intercept of the a priori relation (5.1). For example, the median slowness for realization 1 is $571.7 \mu\text{s/m}$, which provides a modified intercept (c) of -8.05 .

Table 5-2. Minimum squared residuals for parameters from Table 5-3.

Realization #	Median Slowness ($\mu\text{s}/\text{m}$)	Drawdown Residual (m^2)	$\Sigma (\tau_{\text{mes}} - \tau_{\text{sim}})^2$ (day^2)	Total Weighted Residual (day^2)
1	571.73	2.94×10^{-5}	40.40	40.72
2	570.38	2.32×10^{-6}	51.95	51.98
3	575.88	8.18×10^{-6}	95.74	95.83
4	573.42	1.86×10^{-4}	15.45	17.49
5	574.55	6.97×10^{-5}	36.10	36.86

KESTERSON RESULTS

The approach detailed above provided reasonable fits to the tracer and drawdown data with only three parameters, the slope and intercept of the seismic slowness to natural log conductivity relation (5.4), and a single value of dispersivity for the region. Five slowness realizations were generated (Figure 5-6) using sequential gaussian simulation, each with the same statistical parameters ($\lambda_h = 9$ meters, $\lambda_v = 0.9$ meters, $\sigma^2=104$). Each realization was then mapped into a natural log conductivity field using the a priori relation in (5.3), providing an initial conductivity field that was used to simulate groundwater flow and tracer transport. The slope and intercept of this relation and the dispersivity are then adjusted to obtain the best fit between measured tracer quantiles and drawdown, and those simulated for each potential conductivity field.

The simulated concentration histories are illustrated in Figure 5-6 for the optimal parameters listed in Table 5-3, along with the observed concentration histories. The simulated concentration histories provide a reasonable match to the observed data, although as expected, the fits differ from one realization to the next (Figure 5-6) due to differences in the estimated hydraulic conductivity fields. The main features of the concentration arrival histories are reproduced in all but a few cases. The drawdown and concentration quantile residuals are listed in Table 5-2 for the five randomly chosen realizations. The best fit to the objective function (5.2) was for realization 4, which also provided the best visual fit of the measured and simulated concentration histories.

Table 5-3. Optimal parameter estimates for the tracer and drawdown data.

Realization*	slope†	Intercept†	modified intercept*	Dispersivity (m)
1	0.032	-26.576	-8.375	0.076
2	0.036	-28.838	-8.145	0.091
3	0.037	-29.595	-8.175	0.091
4	0.058	-41.586	-8.195	0.096
5	0.040	-30.916	-8.145	0.061

* Slowness realizations in Figure 5-6.

† Slope and intercept of slowness ($\mu\text{s}/\text{m}$) to natural log conductivity (m/s) relation [$\ln(K) = a + b * S$].

* Modified intercept = $(a + b S_{\text{median}})$ from equation 5.4

We found that the estimated parameters converged from different starting points to approximately the same objective values. For example, the slope converged to a value of 0.032 for realization #1 from a starting value of 0.061 as well as from the a priori starting value of 0.041. The estimated slope and intercept are similar to the a priori estimates, indicating that pump test and core data can be used in conjunction with seismic tomography to provide valuable information about the relation between slowness and log conductivity.

These equally likely slowness realizations allow us to explore a portion of the likely relations between slowness and log hydraulic conductivity and allow some insight into the uncertainty of the estimated relation. The estimated slope and intercept of equation (5.4), and dispersivity for each realization are listed in (Table 5-2). The differences between realizations allow us to approximate the uncertainty about the parameters. The mean and standard deviation of these parameters are: slope (mean = 0.041, σ = 0.010), intercept with median slowness removed (mean = -8.21, σ = 0.096), and dispersivity (mean = 0.083 m, σ = 0.014 m). The transverse dispersivity was fixed at 0.2 times the longitudinal value for all simulations. To fully characterize the uncertainty in these parameters would involve many more realizations and an analysis of the potential measurement and modeling errors.

At the Kesterson site there was no meaningful correlation between the lab derived hydraulic conductivity and seismic slowness measurements (Figure 5-4), yet the lab derived conductivity measurements are correlated to our tomographic slowness estimates (Figure 5-5). The estimated mean slope and modified intercept (median slowness removed) of the relation between slowness ($\mu\text{s}/\text{m}$) and natural log conductivity (m/s) of 0.041, and -8.21 compare favorably to the a priori estimates of 0.041 and -7.95 (from Figure 5-3, using the median tomogram slowness of 574.2 $\mu\text{s}/\text{m}$). This indicates that the a priori relation between field scale slowness values and core and pump test conductivity values was reasonable. The linear fit of estimates from *Hyndman and Gorelick* [1995] also provided very similar values of 0.041 and -8.33 (from Figure 5-2, using the median slowness of 574.2 $\mu\text{s}/\text{m}$). The estimated dispersivity 0.083 m is slightly larger than the 0.03 m value estimated by *Benson* [1988], who used a one-dimensional analysis of the 1986 tracer test used in this study.

Independent tracer test comparison

To check our parameter estimates, we simulated the concentrations for an independent tracer test that was conducted perpendicular to the 1986 tracer test. *Benson* [1988] conducted this tracer test in 1988 by pumping 5.1 L/s from well LBL-I8a and injecting this water back into well LBL-I4. A steady state flow field was developed by pumping for 24 hours prior to the tracer test. A concentrated fluorescein solution was then pumped into the injection stream for 3825 seconds (1.063 hours) to achieve a total injection concentration of approximately 140 ppm. Concentrations were monitored at seven wells located near the center of the pumping/withdrawal well pair (Wells 1, 2, 3, 4, 5, 7, and 8 – See Figure 5-1 for locations). The coordinates of these wells and the depth of the 1.52 meter screened intervals are listed in Table 5-4.

Figure 5-7 illustrates the simulated and observed concentration histories for the five slowness realizations in Figure 5-6 using the estimated linear relations between seismic slowness and hydraulic conductivity with parameters from Table 5-3. The central tendency of 26 of the 35 illustrated concentration histories were reproduced without adjusting the estimated parameters for the 1986 tracer test. The reproduction of the bulk features of the concentration histories for this independent data set indicates that for this site, our approach provides useful information for aquifer property estimation.

Most of the seismic data were collected in the primary direction of groundwater flow for the 1986 tracer test. The lack of conditioning seismic slowness planes in the direction of the groundwater flow for 1988 tracer test (See site map in Figure 5-1), resulted in much less information about the aquifer properties in this direction. As a result, the hydraulic conductivity estimates varied significantly from one realization to the next near the injection and withdrawal wells (I4 and I8a) for the 1988 test. These conductivity variations resulted in significant differences between the simulated concentration histories for different realizations (Figure 5-7). Realization #2 provided the best overall match, while realization #4 provided the worst match to the 1988 data. This indicates the importance of data acquisition across the entire region of interest, because the simulated tracer concentrations were much closer to the measured values for the 1986 tracer test where densely collected seismic data were available.

Table 5-4. Hydraulic conductivity values from pump tests at the Kesterson site
[after *Benson, 1988*].

Well	North (m)	West (m)	Top of Screen (m)	Bottom of Screen (m)	In K (m/s)
I1	-1.50	2.34	6.10	12.19	-7.98
I2	-0.48	16.12	6.10	12.19	-8.49
I4	14.21	0.00	6.10	12.19	-7.77
I6	-3.40	-13.87	6.10	12.19	-8.89
I8	-16.34	0.06	6.10	12.19	-8.13
I8a	-14.21	0.00	6.10	12.19	-
LBL2	-10.59	3.11	6.50	8.00	-8.76
LBL2A	-11.67	2.10	10.67	12.19	-7.34
HO100	-15.76	-7.54	24.38	30.48	-7.98
HO80	-8.74	-12.80	18.29	24.39	-8.70
HO60	-12.26	-9.44	12.19	18.30	-8.89
ST1	-3.38	0.96	6.10	7.60	-7.42
ST2	-3.43	3.37	7.60	9.10	-7.44
ST3	-0.65	-0.05	9.10	10.60	-8.76
ST4	0.09	0.00	10.60	12.19	-8.35
ST5	-1.36	-0.03	12.19	13.72	-
ST6	-2.17	0.00	4.57	6.1	-
ST7	0.91	0.10	7.62	9.14	-
ST8	-1.83	5.63	10.67	12.19	-

Realization Number:

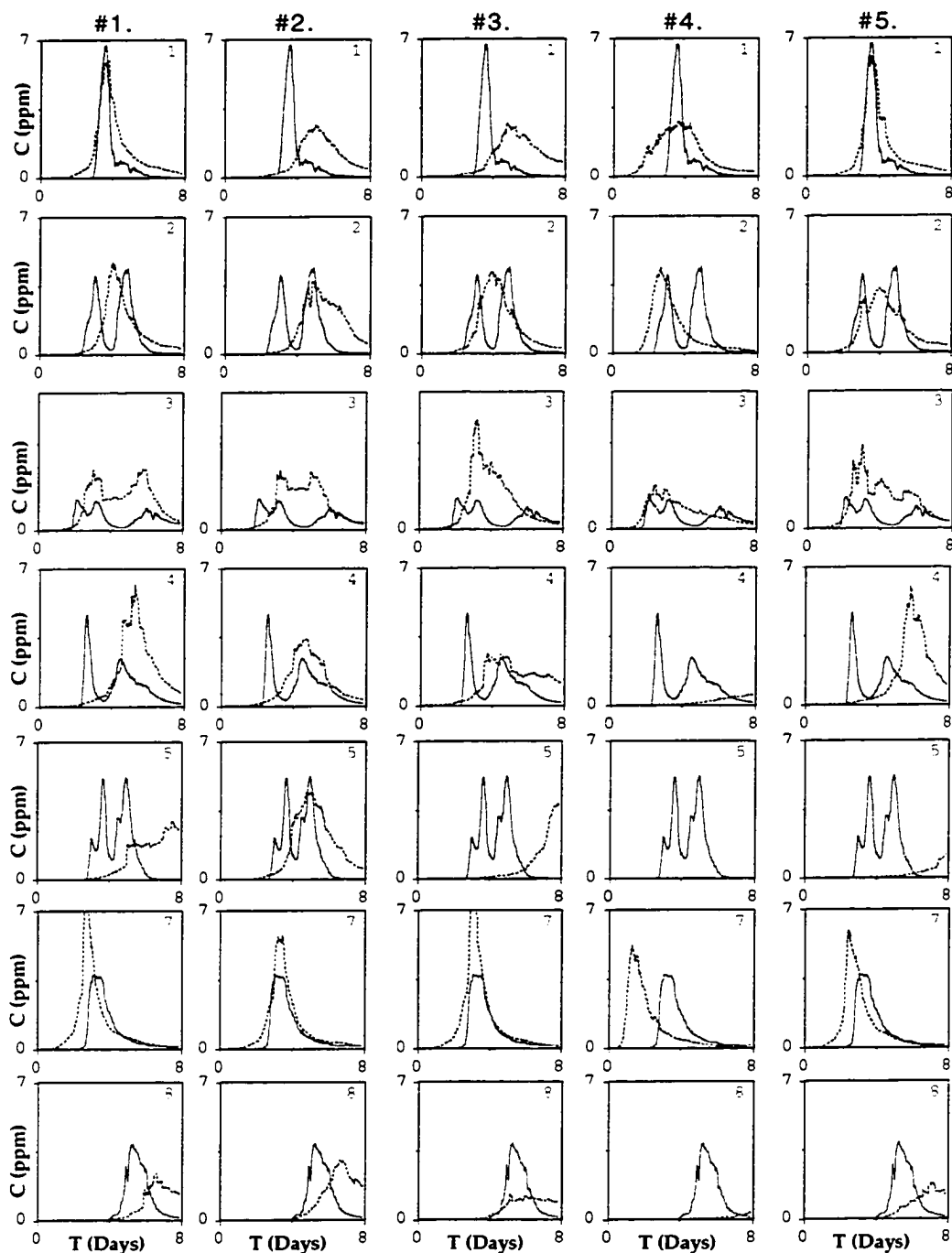


Fig. 5-7. Simulated and observed tracer concentration histories for the 1988 fluorescein tracer test from well 14 to 18a. The well numbers are located in the upper right corner of each graph. See Figure 5-1 for locations.

Incorporation of hydraulic conductivity measurements

Sequential gaussian simulation of conductivity data alone

A large number of conductivity measurements are available at the Kesterson site, enabling us to generate conductivity realizations using these measurements alone. The conductivity measurements are listed in Table 5-4 with the corresponding measurement locations. We assigned the conductivity values to a single cell at the central depth along the screened interval, and generated all other estimates using sequential gaussian simulation. The realization illustrated in Figure 5-8a was generated using the same correlation lengths as used for the generation of slowness realizations ($\lambda_h = 9. \text{ m}$, $\lambda_v = 0.9 \text{ m}$). The mean and variance of this realization match the natural log conductivity measurements ($\sigma^2 = 0.32$, mean = -8.208).

These conductivity measurements, which are mostly at the tracer sampling wells, provide a reasonable representation of subsurface heterogeneities in the region of the 1986 and 1988 tracer tests. A randomly chosen realization is illustrated in Figure 5-8a along with the simulated and observed tracer concentration histories. These simulated concentration histories show similar features to those in Figure 5-6, which indicates that the seismic and tracer data concur about the structure of the hydraulic conductivity field.

Significant differences can be observed between the slowness and log conductivity realizations. The most notable is that the slowness realizations are more heterogeneous than the conductivity estimate in Figure 5-8a, which has a more layered appearance. This higher degree of variability in the seismic estimates is expected since the seismic information provides higher resolution information about inter-well heterogeneities than the more sparsely sampled conductivity measurements. The match between measured and simulated tracer concentration histories was better using the rescaled seismic slowness fields at the withdrawal well (I6) and well 1 than simulated using conductivity data alone. This indicates that the seismic information provides valuable information about the heterogeneous hydraulic conductivity field. The match to the concentration histories are similar at the other wells for both methods.

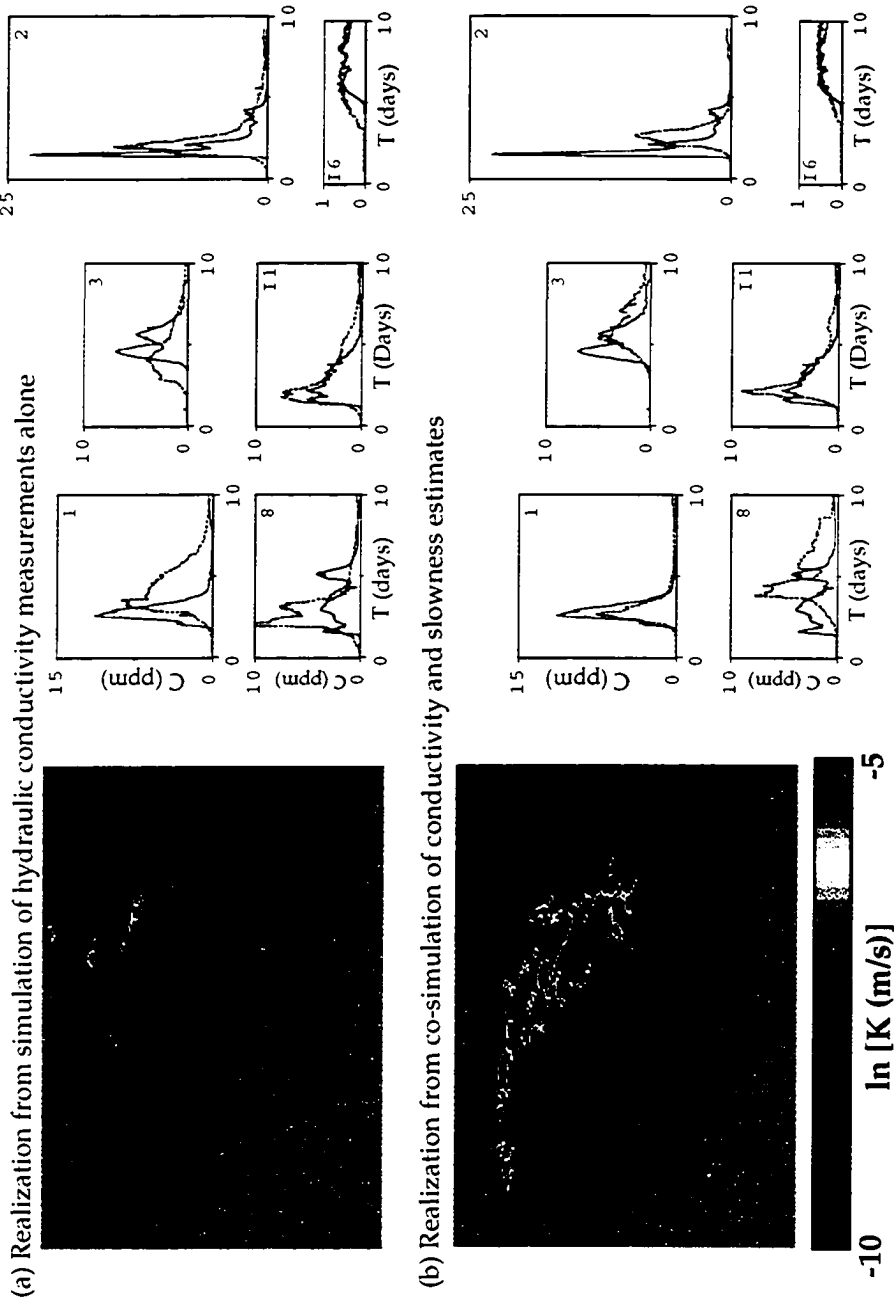


Fig. 5-8. Comparison of tracer concentration histories for the 1986 florencein test simulated through conductivity realizations (a) generated using conductivity measurements alone and (b) generated using sequential gaussian co-simulation with hard conductivity data and soft seismic slowness data from the 4th seismic realization.

Sequential gaussian co-simulation of conductivity and slowness data

For comparison, we also generated a conductivity realization using sequential gaussian co-simulation, using the conductivity measurements as hard data and the slowness estimates as soft data. We used a correlation coefficient of +0.74, as calculated in Figure 5-5, to incorporate the soft data. Figure 5-8b illustrates a randomly chosen realization with the same random number seed as used to generate Figure 5-8a, providing the same random path for both methods. For this realization, we used the entire 4th slowness realization as soft data and conditioned to the hard conductivity data in Table 5-4. We also generated realizations that only used seismic data at the locations of the tomograms and found that the conductivity realizations resulted in poor matches to the measured concentration histories.

In this case, the slowness data improved the concentration histories at all wells except for at well 8, relative to the simulations through the estimate from conductivity data alone (Figure 5-8a). However, relative to the estimate made using our approach of estimating the relation between slowness and log conductivity (Figure 5-6), these sequential gaussian co-simulation estimates provide a poorer match to the tracer data. The least squared tracer quantile residual was 47.2 (day²) for this co-simulation case while it was 15.45 for the case where we estimated the relation between slowness and log conductivity. This is mostly because the fits for the estimated relation case were better for wells 8, I1, and I6. This comparison only marginally illustrates the benefit of the seismic data, because the conductivity measurements describe much of the variability at the site. However, the seismic data also provided useful information for the simulation with conductivity data "alone", because the estimates of horizontal and vertical correlation length were derived from the seismic data.

The benefits of the seismic data were not fully achieved in this study because of computational limitations. Even with the fairly large cells used for the tracer simulations (1.5 meters on a side and 0.45 meters in the vertical direction), individual simulations took approximately 3 hours on a Hewlett Packard 755 workstation. The seismic data appears to have resolution on the order of 0.15 to 0.30 meters, which could provide much more information about the heterogeneities at this site than possible with the limited conductivity measurements.

CONCLUSIONS

We have developed a new approach to integrate seismic and hydraulic information for aquifer property estimation. This approach involves estimating the relation between seismic slowness and aquifer properties of interest, such as lithology and hydraulic conductivity, using field scale measurements. We can thus map three-dimensional slowness realizations derived from densely sampled cross-well tomographic estimates into potential conductivity fields. With this approach, we not only determine the likely conductivity structure of aquifers, but we also explore the range of likely relations between slowness and conductivity at the field scale.

An a priori estimate of the relation between slowness and log conductivity can be derived from a number of data sources, but if field estimates of slowness are available they will likely provide a better correlation to conductivity measurements. Laboratory slowness measurements are weakly correlated to the slowness measurements for longer wavelength cross-well or surface seismic measurements due to factors such as frequency dependent dispersion and sampling differences.

We demonstrate this approach using the Kesterson aquifer, California. At this site, we used cross-well seismic tomography in conjunction with hydraulic property estimates from cores and pump tests, and a multiple-well tracer test to infer the relation between natural log hydraulic conductivity and seismic slowness for an alluvial aquifer. We found that seismic slowness estimates provided valuable information about aquifer properties at the Kesterson site. Slowness is positively correlated to hydraulic conductivity at this site and provides high resolution information about subsurface heterogeneities that is consistent with the hydraulic conductivity measurements at the site.

For the Kesterson site, seismic travel times were used in conjunction with tracer concentration histories and a drawdown measurement during the tracer test to provide estimates of the three-dimensional slowness and hydraulic conductivity fields at the site. Simulation of two multiple-well tracer tests through the region provided reasonable matches to the measured concentration histories for five slowness realizations that were mapped into conductivity realizations using the estimated linear relations between slowness and log conductivity. The estimated relations were similar for these five slowness realizations because of the large number of slowness estimates between the

injection and measurement locations. Conditioning on the slowness estimates in this region is critical for the tracer transport.

Although the method worked well for the Kesterson site, different relations are expected for different depositional environments. In some cases a nonlinear or non-unique relation may exist. If a linear relation does not appear to adequately describe the data, a more complex non-linear relation could be estimated.

Other attributes of the seismic data could also be inverted to provide additional data sets that may correlate to the hydraulic and lithologic properties of interest. For example, seismic attenuation is thought to be better correlated to hydraulic conductivity. The approach we presented could also be used to infer the relation between the dielectric constant and hydraulic conductivity using ground penetrating radar measurements.

The data for combined geophysical and hydrologic inversions needs to be carefully collected to maximize its use. The well field needs to be carefully surveyed because small errors in the measured well locations can have a major impact on the estimated slowness values. The tracer test should be designed with as many wells as possible to provide sufficient sensitivity to the lateral and vertical variability in conductivity. Multilevel samplers with many vertical sampling locations would provide much more information about vertical variations in hydraulic conductivity within the aquifer.

Hydraulic head should be measured at all possible locations during a tracer test to provide sensitivity to the mean conductivity value. Hydraulic head measurements are simple and inexpensive, thus they should be made at all available wells during a tracer test. This provides significant additional information which can be used to constrain the conductivity values. A large amount of hydraulic head data may be sufficient to estimate the conductivity values in conjunction with seismic data, while head measurements alone may not provide information about the spatial patterns of hydraulic conductivity. Another advantage of head measurements is that these data can be used for rapid simulations as opposed to the much more computationally intensive tracer simulations. If possible, tracer concentrations, drawdowns, and seismic travel times should be collected to provide the maximum information about flow and transport properties.

REFERENCES

- Adams, E. E., and L. Gelhar, Field study of dispersion in a heterogeneous aquifer, 2, Spatial moments analysis, *Water Resour. Res.*, 28(12), 3293-3307, 1992.
- Alabert, F., The practice of fast conditional simulations through the LU decomposition of the covariance matrix, *Math Geology*, 19(5), 369-386, 1987.
- Araktingi, U. G., and W. M. Bashore, Effects of properties in seismic data on reservoir characterization and consequent fluid-flow predictions when integrated with well logs, *Society of Petroleum Engineers*, (SPE 24752, presented at 67th Annual SPE conference in Washington, D.C.), 1992.
- Bakr, A. A., L. W. Gelhar, A. L. Gutjahr, and J. R. Macmillan, Stochastic analysis of spatial variability in subsurface flows. 1. Comparison of one- and three-dimensional flows., *Water Resour. Res.*, 14(2), 263-271, 1978.
- Beres, M. J., and F. P. Haeni, Application of ground-penetrating-radar methods in hydrogeologic studies, *Ground Water*, 29(3), 375-386, 1991.
- Belitz, K., S. P. Phillips, and J. M. Gronberg, Numerical simulation of groundwater flow in the central part of the western San Joaquin Valley, California, United States Geological Survey, OFR 91-535, 1992.
- Benson, S. M., Characterization of the hydrogeologic and transport properties of the shallow aquifer under Kesterson reservoir, Ph.D. Thesis, University of California Berkeley, 1988.
- Benson, S. M., A. F. White, S. Halfman, S. Flexser, and M. Alavi, Groundwater contamination at the Kesterson reservoir, California: 1. Hydrogeologic setting and conservative tracer transport, *Water Resources Research*, 27(6), 1071-1084, 1991.
- Boggs, M. J., S. C. Young, L. M. Beard, L. Gelhar, K. R. Rehfeldt, and E. E. Adams, Field study of dispersion in a heterogeneous aquifer 1. Overview and site description, *Water Resour. Res.*, 28(12), 3281-3291, 1992.
- Bourbie, T., O. Coussy, and B. Zinszner, *Acoustics of porous media*, Gulf Publishing Company, Houston, 1987.

- Byers, E., and D. B. Stephens, Statistical and stochastic analysis of hydraulic conductivity and particle-size in a fluvial sand., 47(6), 1072-1081, 1983.
- Cervený, V., The application of ray tracing to the propagation of shear waves in complex media, in *Handbook of Geophysical Exploration*, K. Helbig and S. Treitel ed., pp. 1-124, Geophysical Press, 1985.
- Clifton, P. M., and S. P. Neuman, Effects of kriging and inverse modeling on conditional simulation of the Avra Valley aquifer in Southern Arizona, *Water Resources Research*, 18(4), 1215-1234, 1982.
- Cooley, R. L., A method for estimating parameters and assessing reliability for models of steady state groundwater flow, 1, Theory and numerical properties, *Water Resources Research*, 13(2), 318-324, 1977.
- Cooley, R. L., A method for estimating parameters and assessing reliability for models of steady state groundwater flow, 2, Application of statistical analysis, *Water Resources Research*, 15(3), 603-617, 1979.
- Coptý, N., Stochastic characterization of subsurface flow parameters using geophysical and hydrological data, Ph.D. Thesis, University of California Berkeley, 1994.
- Coptý, N., Y. Rubin, and G. Mavko, Geophysical-hydrological identification of field permeabilities through Bayesian updating, *Water Resources Research*, 29(8), 2813-2825, 1993.
- Dagan, G., Stochastic transport in heterogeneous porous formations, *J. Fluid Mech.*, 145, 151-177, 1982.
- Dagan, G., Statistical theory of groundwater flow and transport: pore to laboratory, laboratory to formation, formation to regional scale., *Water Resour. Res.*, 22(9), 120S-134S, 1986.
- Dalrymple, G. B., K-Ar ages of the Friant Pumice Member of the Turlock Lake Formation, the Bishop Tuff, and the tuff of Red's Meadow, central California, *Isocron/West*, 28, 3-5, 1980.

- Delhomme, J. P., Spatial variability and uncertainty in groundwater flow parameters: A geostatistical approach, *Water Resources Research*, , 1979.
- Deutsch, C. V., The relationship between universal kriging, kriging with an external drift, and cokriging, *Stanford Center for Reservoir Forecasting*, 4, 1991.
- Deutsch, C. V., and A. G. Journel, *Geostatistical Software Library and User's Guide*, Oxford University Press, Oxford, 1992.
- Dines, K. A., and R. J. Lytle, Computerized geophysical tomography, *Proceedings of IEEE*, , 67, 1065-1073, 1979.
- Donaldson, J. R., and P. V. Tryon, Nonlinear least squares regression using STARPAC: The Standards Time Series and Regression Package, National Bureau of Standards, Boulder, CO, 1990.
- Doyen, P. M., T. M. Guidish, and M. de Buyl, Lithology prediction from seismic data, a Monte-Carlo approach, in *Reservoir Characterization*, L. W. Lake, H. B. Carrol Jr. and T. C. Wesson ed., pp. 557-564, Academic Press Inc., San Diego, 1991.
- Dueck, G., T. Scheuer, Threshold accepting: A general purpose optimization algorithm appearing superior to simulated annealing, *Journal of Computational Physics*, 90, 161-175, 1990.
- Eagleson, P. S., and many others, *Opportunities in the Hydrologic Sciences*, National Academy Press, Washington, D. C., 1991.
- Eddy, C. E., B. B. Looney, J. M. Dougherty, T. C. Hazen, and D. S. Kaback, Characterization of the geology, geochemistry, hydrology and microbiology of the in-situ air stripping demonstration site at the Savannah River Site (SRS), Westinghouse Savannah River Company, WSRC-RD-91-21, 1991.
- Elbring, G. J., Using crosswell seismic imaging to monitor in-situ air stripping waste remediation process, *EOS*, 72(44), 295, 1991.
- Freeze, R. A., A stochastic-conceptual analysis of one-dimensional flow in nonuniform homogeneous media, *Water Resour. Res.*, 11(5), 725-741, 1975.

- Freeze, R. A., and J. A. Cherry, *Groundwater*, Prentice-Hall, Englewood Cliffs, N. J., 1979.
- Freyberg, K. M., P. B. Bedient, and J. A. Connor, Modeling of TCE contamination and recovery in a shallow sand aquifer, *Ground Water*, 25(1), 70-80, 1987.
- Gailey, R. M., A. S. Crowe, and S. M. Gorelick, Coupled process parameter estimation and prediction uncertainty using hydraulic head and concentration data, *Adv. Water Resour.*, 14(5), 301-314, 1991.
- Gelhar, L. W., Stochastic subsurface hydrology from theory to applications, *Water Resour. Res.*, 22(9), 135S-145S, 1986.
- Gelhar, L. W., A critical review of data on field-scale dispersion in aquifers, *Water Resour. Res.*, 28(7), 1955-1974, 1992.
- Gelhar, L. W., and C. L. Axness, Three dimensional stochastic analysis on macrodispersion in aquifers, *Water Resour. Res.*, 19(1), 161-180, 1983.
- Golub, G. H., *Matrix Computations*, John Hopkins University Press, Baltimore, 1989.
- Han, D., A. Nur, and D. Morgan, Effect of porosity and clay content on wave velocity in sandstones, *Geophysics*, 51, 2093-2107, 1986.
- Harris, J. M., Initial value raytracing in smoothly varying heterogeneous media, in *Stanford Tomography Project Report*, pp. I1-I14, Stanford University, Stanford, CA, 1992.
- Harris, J. M., S. Lazaratos, and R. Michelena, Tomographic String Inversion, pp. B1-B7, *Stanford Tomography Project Report*, Stanford University, 1990.
- Hess, K. M., S. H. Wolf, and M. A. Celia, Large-scale natural gradient tracer test in sand and gravel, Cape Cod, Massachusetts 3. Hydraulic conductivity variability and calculated macrodispersivities, *Water Resour. Res.*, 28(8), 2011-2027, 1992.
- Hoeksema, R. J., and P. K. Kitanidis, Analysis of the spatial structure of properties of selected aquifers, *Water Resour. Res.*, 21(4), 563-572, 1985.

- Hotchkiss, W. R., and G. O. Balding, *Geology, hydrology, and water quality of the Tracy-Dos Palos area, San Joaquin Valley, California*, U. S. Geological Survey, 72-0169, 1971.
- Hyndman, D. W., and S. M. Gorelick, Mapping lithologic and transport properties in three dimensions using seismic and tracer data: The Kesterson aquifer, *Water Resources Research*, (Submitted), 1995.
- Hyndman, D. W., and J. M. Harris, Travel time inversion for the geometry of aquifer lithologies, *Geophysics*, (Submitted), 1995.
- Hyndman, D. W., J. M. Harris, and S. M. Gorelick, Coupled seismic and tracer test inversion for aquifer property characterization, *Water Resources Research*, 30(7), 1965-1977, 1994.
- Johnson, M., *Multivariate Statistical Simulation*, Prentice Hall, New York, NY, 1987.
- Journel, A. G., W. Xu, and T. Tran, Integrating soft seismic data in reservoir modeling: The collocated cokriging alternative, *Stanford Center for Reservoir Forecasting*, 5, 1992.
- Journel, A. G., and H. Zhu, Integrating soft seismic data: Markov-Bayes updating, an alternative to cokriging and traditional regression, *Stanford Center for Reservoir Forecasting*, 3, 1990.
- Knoll, M. D., F. P. Haeni, and R. J. Knight, Characterization of a sand and gravel aquifer using ground-penetrating radar, Cape Cod, Massachusetts, *Proceedings of U. S. Geological Survey toxic substances hydrology program -- Proceedings of the technical meeting, March 11-15, 1991, Monterey, California*, WRI 91-4034, 1991.
- Koltermann, C. E., and S. M. Gorelick, Paleoclimatic signature in terrestrial flood deposits, *Science*, 256, 1775-1782, 1992.
- Lankston, R. W., High-resolution refraction seismic data acquisition and interpretation, in *Geotechnical and Environmental Geophysics*, S. H. Ward ed., pp. 45-72, Society of Exploration Geophysicists, Tulsa, Okla., 1990.

- Lazaratos, S. K., J.W. Rector III, and J. M. Harris, High-resolution cross-well reflection imaging: Potential and technical difficulties, *Geophys.*, 58, 1270-1280, 1993.
- LBL, Progress Report 2, Kesterson Project, December 1985 through June 1986., Earth Science Division, Lawrence Berkeley Lab., Berkeley, CA, LBL-1188, 1986.
- LeBlanc, D. R., S. P. Garabedian, K. M. Hess, L. W. Gelhar, R. D. Quadri, K. G. Stollenwerk, and W. W. Wood, Large-scale natural gradient tracer test in sand and gravel, Cape Cod, Massachusetts 1. Experimental design and observed tracer movement, *Water Resour. Res.*, 27(5), 895-910, 1991.
- Liu, C. W., and T. N. Narasimhan, Modeling of selenium transport at the Kesterson reservoir, California, U.S.A., *Journal of Contaminant Hydrology*, 15, 345-366, 1994.
- Lucet, N., and G. Mavko, Images of rock properties estimated from a cross-well seismic velocity tomogram., *EOS*, 71(43), 1622, 1990.
- Luthin, J. D., Report on expected seepage into Salt Slough and the San Joaquin River from the Kesterson enhancement area, Western Merced County, Final Report to the Department of Water Resources, September 29, 1966.
- Macmillian, J. R., and A. L. Gutjar, Geologic controls on spatial variability for one-dimensional arrays of porosity and permeability normal to layering., in *Reservoir Characterization*, L. W. Lake and H. B. Carroll ed., pp. 265-292, Academic Press, London, 1986.
- Marion, D. P., Acoustical, mechanical, and transport properties of sediments and granular materials, Ph.D. Thesis, Stanford, 1990.
- Marion, D. P., A. Nur, H. Yin, and D. Han, Compressional velocity and porosity in sand-clay mixtures, *Geophys.*, 57, 554-563, 1992.
- McDonald, M. G., and A. W. Harbaugh, A modular three-dimensional finite-difference ground-water flow model, United States Geological Survey, TWI 6-A1, 1988.

- McLamore, V. R., D. G. Anderson, and C. Espana, Crosshole testing using explosive and mechanical energy sources, in *Dynamic Geotechnical Testing*, pp. American Society for Testing of Materials, 1978.
- McMechan, G. A., J. M. Harris, and L. M. Anderson, Cross-hole tomography for strongly variable media with applications to scale model data, *BSSA*, 77(6), 1945-1960, 1987.
- Miall, A. D., *Principles of Sedimentary Basin Analysis*, Springer-Verlag, Heidelberg, Germany, 1984.
- Miller, D. D., J. G. McPherson, and T. E. Covington, Fluviodeltaic reservoir, South Belridge Field, San Joaquin Valley, California, in *Casebooks in Earth Science: Sandstone Petroleum Reservoirs*, J. H. Barwis, J. G. McPherson and J. R. J. Studlick ed., pp. 109-130, Springer-Verlag, New York, 1990.
- Mualem, Y., Development of methods, tools and solutions for unsaturated flow with application to watershed hydrology and other fields, Technion Israel Institute of Technology, Haifa, Israel, Research Project 442, 1976
- National Research Council (Committee on techniques for assessing ground water vulnerability), *Ground water vulnerability assessment: Predicting relative contamination potential under conditions of uncertainty*, National Academy Press, Washington, D. C., 1993.
- Neuman, S. P., C. L. Winter, and C. M. Newman, Stochastic theory of field-scale fickian dispersion in anisotropic porous media, *Water Resources Research*, 23(3), 453-466, 1987.
- Ohlendorf, H. M., D. Hoffman, M. K. Saiki, and T. W. Aldrich, Embryonic mortality and abnormalities of aquatic birds: Apparent impacts of selenium from irrigation drain water, *Sci. Total Environ.*, 52, 49-63, 1986.
- Parker, J. C., and M. T. Van Genuchten, Flux-averaged and volume averaged concentrations in continuum approaches to solute transport, *Water Resour. Res.*, 20(7), 866-872, 1984.

- Peck, A. J., P. A. Yendle, and F. E. Batini, Hydraulic conductivity of deeply weathered materials in the Darlin Range, Western Australia., *Australian Journal of Soil Research*, 18, 129-138, 1980.
- Prasad, M., and R. Meissner, Attenuation mechanisms in sands: Laboratory versus theoretical (Biot) data, *Geophys.*, 57(5), 710-719, 1992.
- Press, W. H., B. P. Flannery, S. A. Teukolsky, and W. T. Vetterling, *Numerical Recipes - The Art of Scientific Computing*, Cambridge University Press, Cambridge, 1989.
- Pryor, W. A., Permeability-porosity patterns and variations in some Holocene sand bodies., *AAPG Bulletin*, 57(1), 162-189, 1973.
- Raymer, D. S., E. R. Hunt, and J. S. Gardener, An improved sonic transit time-to-porosity transform, Proceedings of 21st Annual Meeting, Paper P, 1980.
- Rehfeldt, K. R., M. J. Boggs, and L. Gelhar, Field study of dispersion in a heterogeneous aquifer, 3, Geostatistical analysis of hydraulic conductivity, *Water Resour. Res.*, 28(12), 3281-3291, 1992.
- Rubin, Y., G. Mavko, and J. Harris, Mapping permeability in heterogeneous aquifers using hydrologic and seismic data, *Water Resour. Res.*, 28(7), 1809-1816, 1992.
- Smart, P. L., and I. M. S. Laidlaw, An evaluation of some fluorescent dyes for water tracing, *Water Resources Research*, 13(1), 15-33, 1977.
- Smith, L., Spatial variability of flow parameters in a stratified sand., 13(1), 1-21, 1981.
- Sun, N.-Z., and W. W.-G. Yeh, Coupled inverse problems in groundwater modeling 1. Sensitivity analysis and parameter identification, *Water Resour. Res.*, 26(10), 2507-2525, 1990.
- Telford, W. M., L. P. Geldart, and R. E. Sheriff, *Applied Geophysics*, Cambridge University Press, Cambridge, 1990.
- Tukey, J. W., *Exploratory Data Analysis*, Addison-Wesley Publishing Company, Reading, Mass., 1977.

- Velleman, P. F., and D. C. Hoaglin, *Applications, Basics, and Computing of Exploratory Data Analysis*, Wadsworth, Inc., Belmont, 1981.
- Voss, C. I., Saturated-Unsaturated Transport (SUTRA): A finite-element simulation model for saturated-unsaturated, fluid-density-dependent ground-water flow with energy transport or chemically-reactive single-species solute transport, United States Geological Survey, 84-4369, 1984.
- Wagner, B. J., and S. M. Gorelick, Optimal groundwater quality management under parameter uncertainty, *Water Resour. Res.*, 23(7), 1162-1174, 1987.
- Williamson, A. K., P. D. E., and L. A. Swain, Ground-water flow in the Central Valley, California, United States Geological Survey, 1401-D, 1989.
- Wyllie, M. R., A. R. Gregory, and L. W. Gardner, Elastic wave velocities in heterogeneous and porous media, *Geophysics*, 21, 41-70, 1956.
- Yeh, W. W.-G., Review of parameter identification procedures in groundwater hydrology: The inverse problem, *Water Resour. Res.*, 22(2), 95-108, 1986.
- Zheng, C., MT3D: A modular three-dimensional transport model, S.S. Papadopoulos & Associates, Inc., 1992.
- Zheng, C., Extension of the method of characteristics for simulation of solute transport in three dimensions, *Ground Water*, 31(3), 456-465, 1993.
- Zhu, H., and A. G. Journel, Formatting and integrating soft data: Stochastic imaging via the Markov-Bayes algorithm, *Stanford Center for Reservoir Forecasting*, 4, 1991.

APPENDIX A: SENSITIVITY OF THE SPLIT INVERSION METHOD TO SAND/CLAY ZONATION

Both seismic and tracer data sample some portion of the same physical environment, so they are both likely to provide sensitivity to the zonation of lithologies. Chapter 2 illustrated the sensitivity of both tracer concentrations and seismic travel times to the geometry of clay zones embedded in a sand aquifer, although the hydraulic conductivity was not constant for different zonations, as described in Chapter 2. In this Appendix, I isolate the effect of zonation on simulated concentrations by fixing the zonal hydraulic conductivities to the optimal values in Table 2-1.

Figure A-1 illustrates the simulated concentrations through time for five potential zonations of the estimated slowness field in Figure A-2. For comparison, the concentration history simulated through the synthetic aquifer is illustrated as a dashed line. This dashed line would thus represent a measured concentration history in a field case.

For small clay zones, the simulated concentration history has a high peak early in time, as illustrated by the blue concentration history. For large clay zones, the peak is much lower and shifted later in time. This is expected for the constant head boundary conditions because the average conductivity of the aquifer is reduced as the clay zones get larger, thus the peak is later in time. The peak concentration is lower because the tracer is forced to flow through multiple sand zones with more irregular geometry as the clay zones get larger, thus dispersing the tracer.

Figure A-2 illustrates how the zonations in Figure A-1 are obtained by splitting the estimated slowness tomogram into high and low slowness zones, as illustrated by the colored lines through the histogram of estimates. The concentration residuals are calculated as the squared difference between "measured" and simulated concentration histories. The minimum squared residual is obtained for the zonation outlined in green in Figure A-1, which thus identifies the best sand/clay zonation. This estimated zonation provides a close match to the "true" synthetic aquifer, which is also illustrated in Figure A-2.

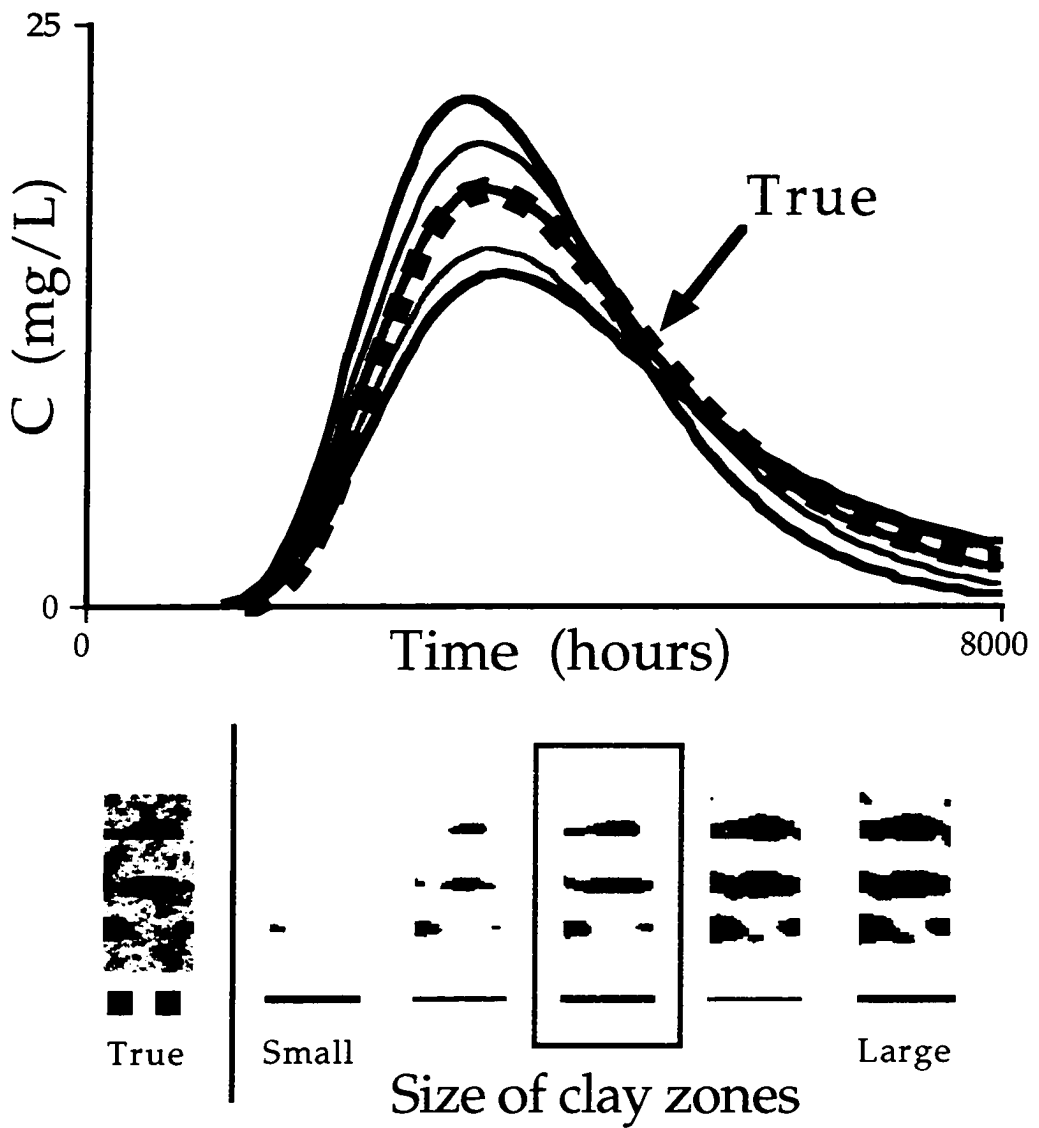


Fig. A-1. Concentration histories for different sand/clay zonations derived from the split inversion method illustrated in Figure A-2. The optimal conductivity and dispersivity values from Table 2-1 were used for the tracer simulations.

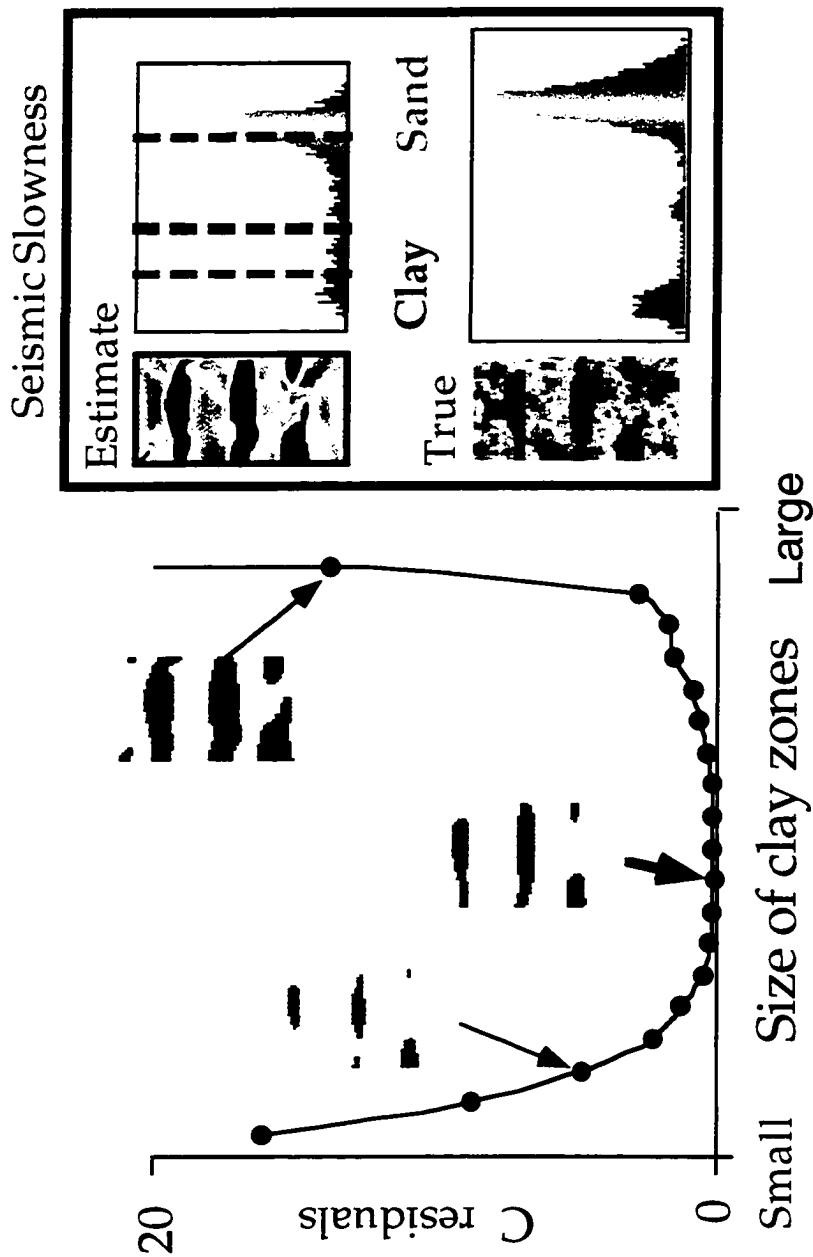


Fig. A-2. Tracer sensitivity to zonation. The residuals between simulated and observed concentration histories from Figure A-1 illustrate the sensitivity of concentrated concentrations to sand/clay zonation. The tomographic slowness estimate in the upper right was split into the illustrated zonation as indicated by the corresponding colored lines on the histogram. The true slowness field is illustrated in the lower right for comparison.

APPENDIX B: SAVANNAH RIVER SITE — SEISMIC AND CORE DATA

OVERVIEW OF THE SAVANNAH RIVER SITE

The Savannah River Site (SRS) near Aiken, South Carolina (Figure B-1), which overlies approximately 300 meters of Atlantic coastal plane sediments, has significant shallow subsurface contamination [Eddy *et al.*, 1991]. Volatile organic compounds (trichloroethylene and tetrachloroethylene) that were used as degreasers in one region of the SRS, infiltrated from a sewer line and a seepage pond into the surrounding sediments and groundwater [Eddy *et al.*, 1991]. This region was designated as an integrated demonstration project to test new remedial technologies, such as horizontal air sparging wells. The sediments in this region are described by Eddy *et al.* [1991] as "layers of sand, clay, and gravel deposited in shallow marine, lagoonal, or fluvial environments". The predominant lithology in the region is sand, but the interbedded clays provide barriers to groundwater flow and solute transport. The clays are only identified at the available wells and the lithologies are unknown between wells. This common data limitation leads to significant uncertainty about potential solute transport paths and barriers.

Although monitoring of contaminant remediation was the primary goal of the data collection during the Integrated Demonstration Project at the SRS, the data can be used to estimate some heterogeneous aquifer properties at this site. The SRS data set was used as an initial test location for estimating aquifer properties using geophysical and hydrologic data because of the wide variety of collected measurements and the expected large scale lithologic zonation. In this Appendix, I infer the lithologies in a vertical cross section using the seismic travel times and core measurements from wells.

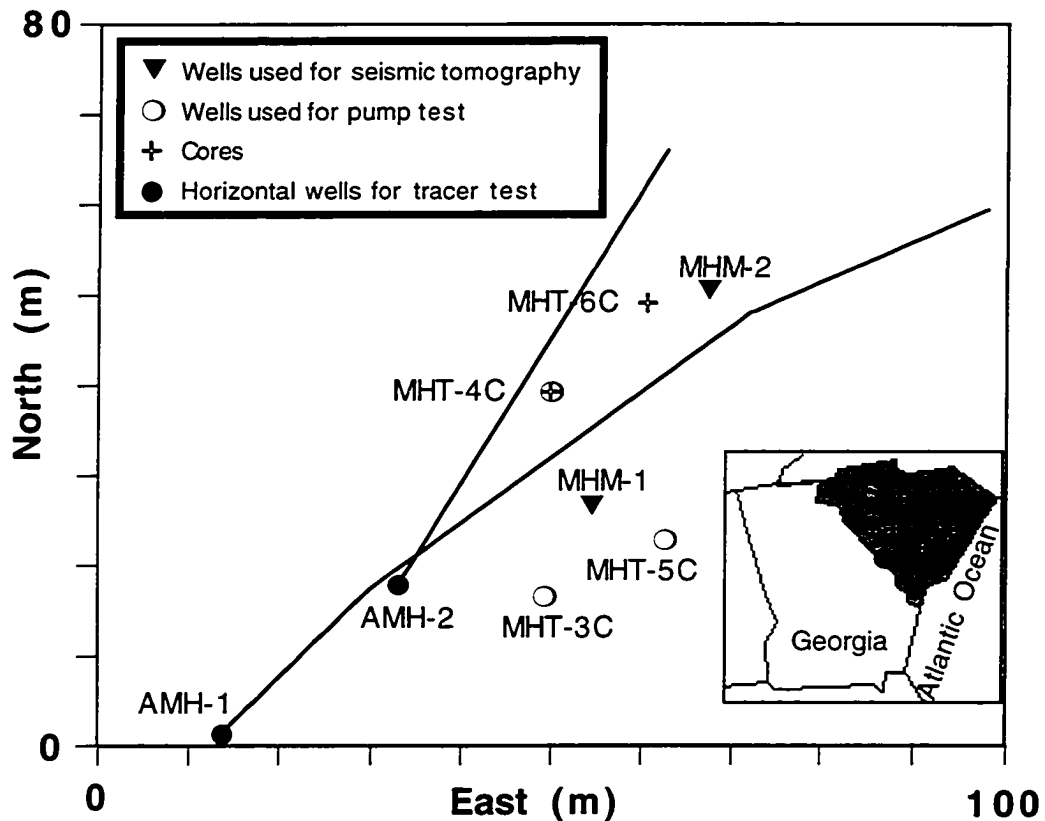


Fig B-1. Savannah River Site (SRS) map showing the location of wells used for the cross-well seismic survey (MHM-1 and MHM-2), wells with core data near the seismic section (MHT-4C and MHT-6C), the pump test wells (MHT- 5C pumping, MHT-3C and MHT-4C – measured response), and the horizontal wells used for the tracer experiment (AMH-1 and AMH-2) [after Eddy, et. al, 1991].

Shear-wave travel times were collected between two wells (MHM1 and MHM2) in the Integrated Demonstration Project region of the SRS (Figure B-1). These travel times were collected to characterize subsurface heterogeneities before a scheduled air sparging test (injection of air below a region of contaminated groundwater), and to determine if seismic tomography could be a useful tool to measure changes in saturation during the air sparging test [Elbring, 1991]. I use the pre-sparging travel times to infer subsurface lithologies and hydraulic properties in conjunction with core data.

Our approach is to invert the seismic data to determine the likely zonation of lithologies at the site, since traditional tomographic inversions do not find the zonation. I first use SIM to estimate the slowness zonation for the cross-section between two wells. I then infer the lithology for each of the estimated slowness zones using the core data from a pair of nearby wells. For each inferred lithology, estimates of hydraulic properties are then made based on laboratory and field measurements of hydraulic conductivity for this type of lithology from nearby wells.

In the following section, I describe the methodology and results for the inversion of seismic travel times collected by Elbring [1991] at the SRS. The seismic data provide a preliminary field test of the split inversion method (SIM) [Hyndman *et al.*, 1994] with seismic data alone. The SIM was developed to determine the geometry of lithologic zones using all available data that are sensitive to variability in lithology. The SIM is thus used to extract the lithologic zonation from the seismic travel times at the SRS.

INVERSION METHOD AND RESULTS - SAVANNAH RIVER CASE

The split inversion method (SIM) [Hyndman *et al.*, 1994] is a flexible approach to determine the zonation of aquifer properties using data that are sensitive to the lithologic geometry. These data could include geophysical measurements from seismic and electromagnetic methods and hydraulic measurements from pump tests and tracer tests. The philosophy of this approach is that these different data types have sampled regions of the same physical environment and thus can be combined to provide more detailed information about aquifer properties compared to using these data sets alone.

The objective of this implementation of the SIM is thus to adjust the zonation of the seismic slowness image to minimize the average travel time residual from each source to each receiver. The first step of the SIM is to estimate a seismic slowness field (Figure B-2a) using cross-well seismic tomography with a curved ray simultaneous iterative reconstruction technique [McMechan *et al.*, 1987]. This iterative inversion used a homogeneous starting model with a slowness of 3095 $\mu\text{s}/\text{m}$, which was determined by minimizing the least squared slowness residuals for straight ray paths. This tomogram was smoothed using one iteration of a Hanning smooth [Tukey, 1977] over two cells up and two cells down in the vertical and horizontal directions to reduce inversion artifacts. This unconstrained tomographic inversion provides an initial estimate of the lithologic structure between the wells.

I then use the SIM to estimate the geometry of three seismic slowness populations for the region. Three populations appeared to adequately describe the histogram of estimated slowness values (Figure B-2b) at the SRS. The histogram illustrated in Figure B-2b exhibits a dominant slowness population with two extended limbs that I describe with additional slowness populations. These three populations are separated by two values of separation slowness, which I estimate by minimizing seismic travel time residuals. For this case, the SIM iteratively estimates two separation velocities: one above the dominant slowness mode and the other below the dominant mode. The mode of the estimated seismic slowness values is used to describe the predominant population, while the maximum and minimum smoothed seismic velocities describe the other two estimated populations as was done by Hyndman *et al.* [1994].

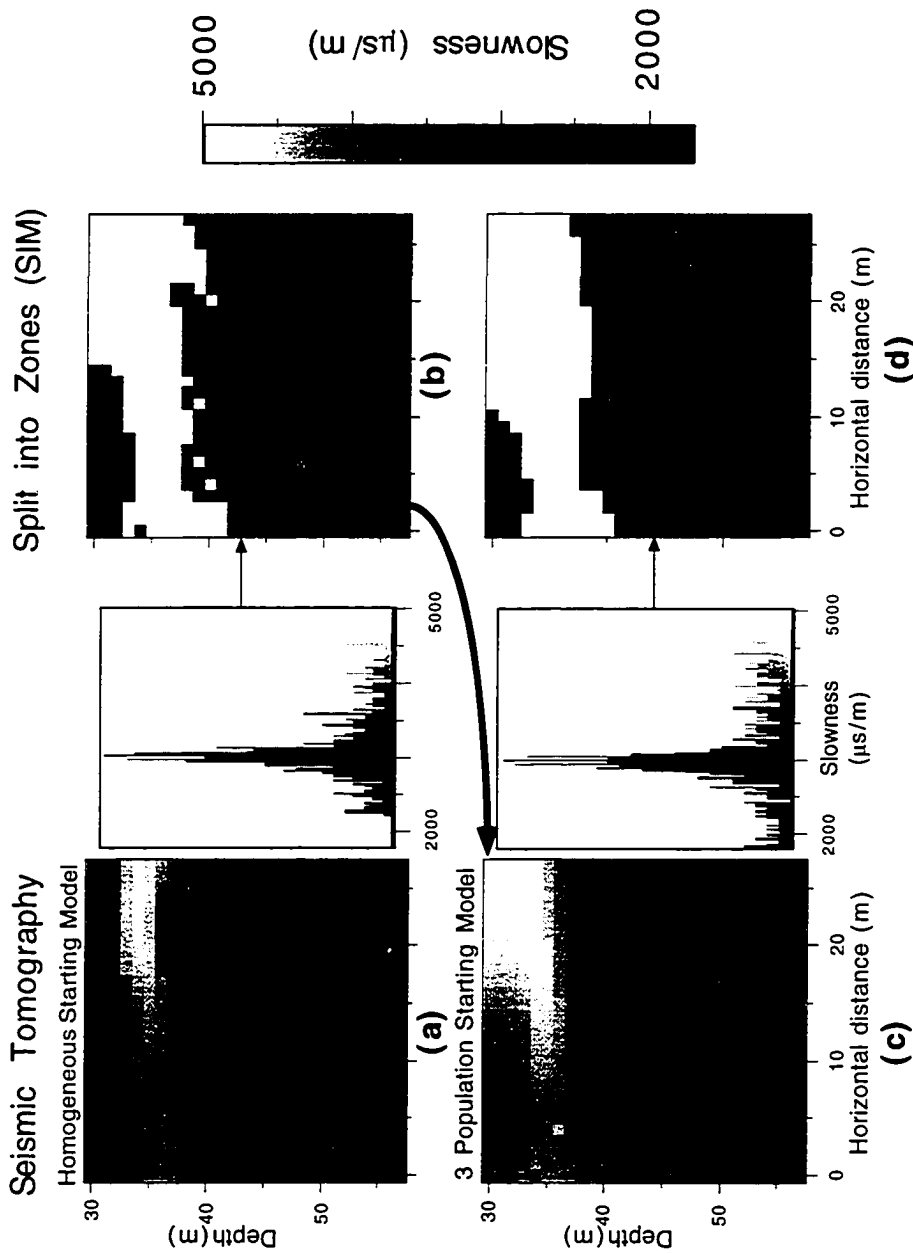


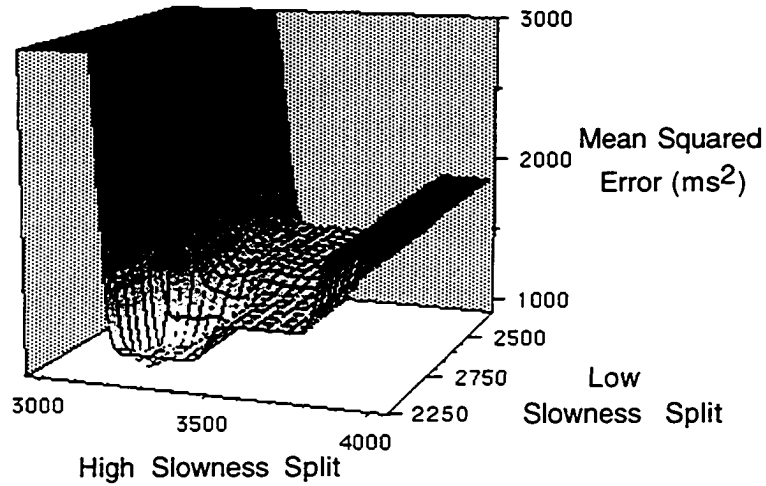
Fig. B-2 Seismic slowness tomograms obtained by inverting shear wave travel times. (a) Tomogram estimated using unconstrained tomography using a homogeneous slowness model with corresponding histogram. (b) Tomogram estimated using the split inversion method (SIM) to divide (a) into three slowness populations. (c) Unconstrained update of (b) with corresponding histogram. (d) Final tomogram obtained by splitting (c) into three populations.

I used the SIM to split the smoothed slowness tomogram (Figure B-2a) into three populations. One slowness split was maintained above the mode and the other was maintained below the mode to describe the three slowness populations observed in the histogram. The first slowness split was estimated to be above the mode, so all pixels with slowness less than the split value were assigned the slowness of the mode (2923. $\mu\text{s}/\text{m}$) and all pixels above the split slowness are assigned the maximum smoothed slowness (4849. $\mu\text{s}/\text{m}$). The second split was then estimated below the mode, and the pixels in this population were assigned the minimum smoothed slowness (1735. $\mu\text{s}/\text{m}$) providing the tomogram illustrated in Figure B-2b. Rather than estimating both separation velocities concurrently, I iteratively determined each separation slowness value while holding the previously estimated value constant.

A second SIM iteration was used to refine the slowness zonation and reduce the travel time residuals. For this iteration, the three population slowness model from Figure B-2b was used as the starting model for a second unconstrained tomographic inversion (Figure B-2c). The potential three-population slowness fields were again smoothed for ray tracing, but for this iteration I only smoothed with a moving window that extended one cell in the horizontal and vertical directions. The histogram shows a broader distribution of slowness values for this unconstrained inversion, since the starting model was more complicated than the homogeneous model used for the first iteration. The second estimate from the SIM (Figure B-2d) provided similar zonation to the first estimate from the SIM, but fewer isolated high slowness cells exist for this iteration.

The convergence of the objective function of minimizing the mean square residual between measured and simulated travel times is illustrated in (Figure B-3). These plots illustrate that a well defined minimum is located at split values of 2805 $\mu\text{s}/\text{m}$ and 3291 $\mu\text{s}/\text{m}$. For the second iteration these splits were adjusted to 2382 $\mu\text{s}/\text{m}$ and 3608 $\mu\text{s}/\text{m}$, because the slowness values assigned to the cells in each population are more extreme due to the broader distribution in Figure B-2d. I counted the number of simulated rays that arrived at the receivers for each possible geometry since the huge slowness contrasts at this site reduced the number of simulated rays arriving at receivers for particular smoothing criteria. The three-population SIM rapidly converged for the presented SRS case despite the huge slowness contrast.

a) First SIM Iteration



b) Second SIM Iteration

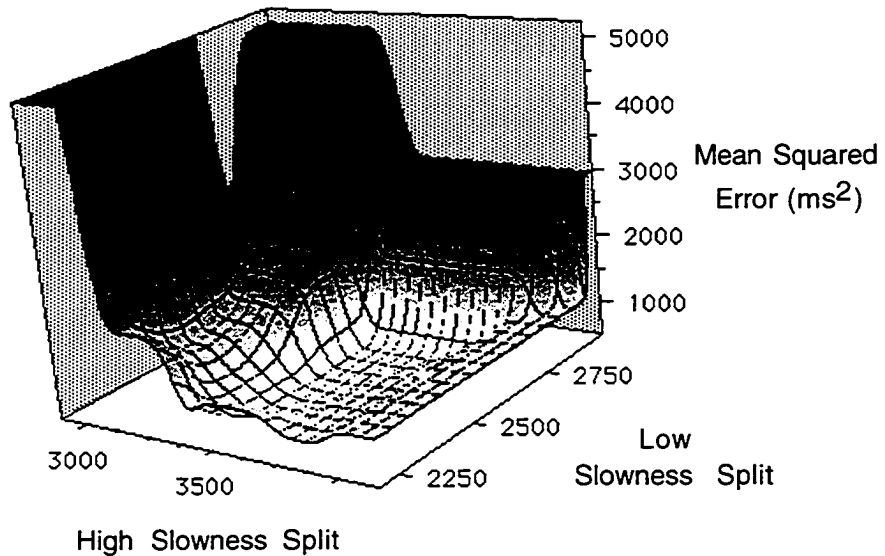


Fig. B-3 Objective value surfaces showing the optimal high and low slowness splits for the first (a) and second (b) iterations of the split inversion method (SIM). For (a), the SIM was used to split Figure B-2a into Figure B-2b and the optimal split values were 2805 and 3291. For (b), the SIM was used to split Figure B-2c into Figure B-2d and the optimal split values were 2382 and 3608.

HYDROGEOLOGIC INTERPRETATION OF ZONAL TOMOGRAMS

The water table is approximately 42 meters deep at the SRS, and thus intersects the estimated slowness field as indicated in Figure B-4. According to *Bourbie* [1987], partial saturation due to capillary effects should increase the stiffness of unconsolidated sediments (relative to dry sediments) and thus reduce seismic slowness. Slowness should increase when the saturations are insufficient to create significant cohesive forces. Unfortunately, very few slowness measurements are available for variable saturations in unconsolidated sediments.

If slowness increases by a significant amount due to some threshold of reduced saturation, this threshold could be imaged using seismic methods. The moisture content of several silty sands sharply declines from 1 to 2 meters above the water table [*Mualem*, 1976] and then stabilizes at shallower depths, with no significant recharge or evaporation. The clayey sand zones of the SRS are likely to have similar characteristics, which would indicate that this zone of greatly reduced saturations is approximately at the location of the significant estimated slowness contrast (Figure B-4).

The geometry of subsurface heterogeneities is a critical piece of information for the design and operation of contaminant remediation systems. As illustrated in Figure B-4, the inversion accurately inferred the locations of the main clay zones. Thus with seismic data and limited core measurements, a rough image of the subsurface lithologies can be developed. The average conductivity of the "green clay", which is the large imaged clay in well MHT4C, is 1.0×10^{-8} m/s based on lab tests [*Eddy et al.*, 1991]. The average conductivity for this semiconfined aquifer is 2.5×10^{-5} m/s based on calibration of a groundwater flow model [*Eddy et al.*, 1991]. With these limited data, this would be the best possible estimate for the conductivity of the estimated mid-slowness region.

In addition, the method imaged a region of the unsaturated zone with much higher slowness, which is likely to be the region where saturation declines rapidly with shallower depths. The difference in elevation of the bottom of this zone could be explained by lithology differences from one end of the tomogram to the other. Figure B-4 illustrates that a clay is located just above the water table on the right side of the image, and the capillary fringe appears to be thicker than on the left side of the tomogram. This is consistent with the interpretation of the geologic logs at wells MHT4C and MHT6C (Figure B-4). The thickness of the zone with significant saturation should be thinner for a cleaner sand, which the seismic inversion indicates is toward well MHT4C.

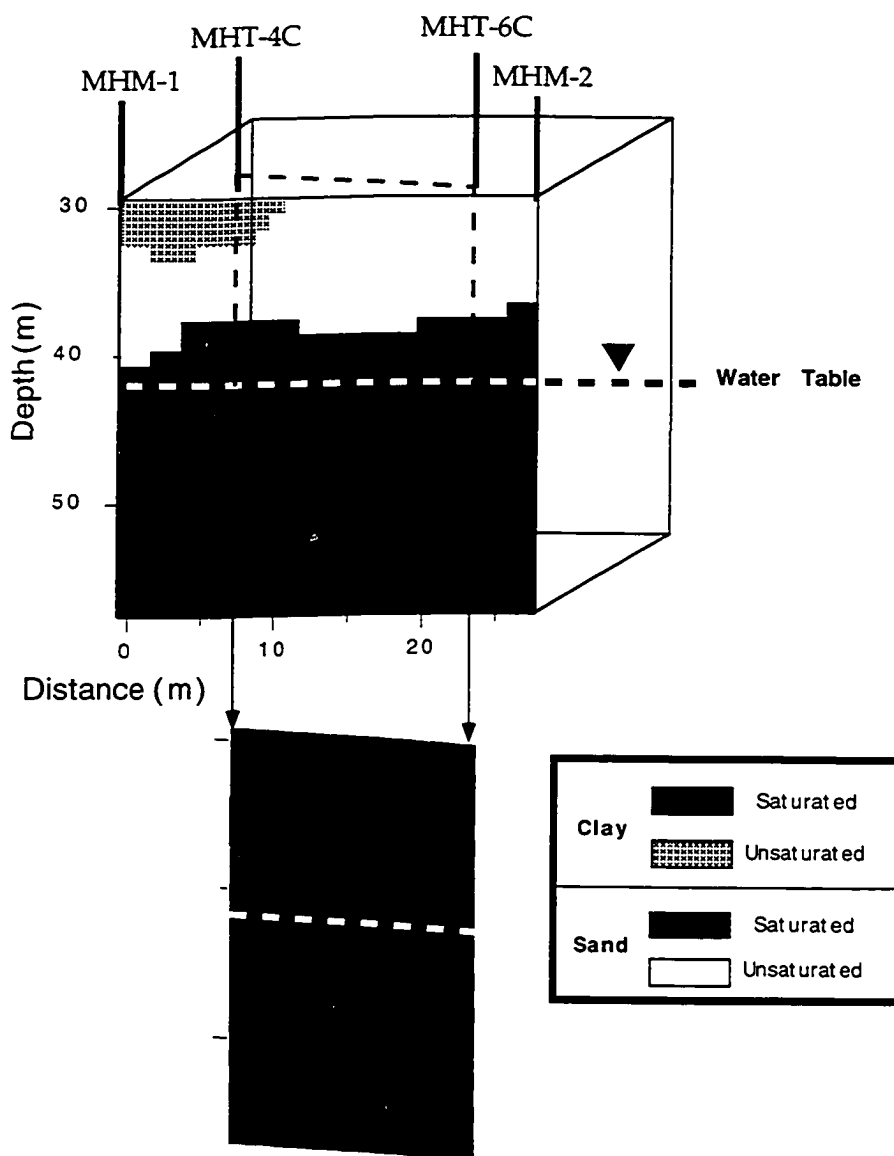


Fig. B-4 Interpretation of the final zonal slowness estimate from Figure B-2d in terms of lithologies and degree of saturation. The top of the saturated clay approximates the capillary fringe at this site, thus on the right side the capillary fringe is shallower because a clay zone is present just above the water table. The image on the right represents a geologic section based on well log and cutting information two wells approximately 3 meters to the NE and nearly parallel to the seismic section.

For the Savannah River Site, a zonal seismic inversion identified the main clay zones that were measured in well cores. The slowness of the saturated clays were significantly lower than the slowness of the sands, indicating a positive correlation between these parameters. The seismic inversion also imaged a region of significantly higher slowness a few meters above the water table, which is likely due to reduction in saturation. If travel time tomography can accurately image saturation changes through time for a transient hydraulic experiment, the estimates could be used for high resolution estimation of the saturated hydraulic conductivity.